Pore-Scale Modelling of *In Situ* Geochemical Reactions

Kelechi Sabinus Eze

Submitted for the Degree of Master by Research

Institute of Petroleum Engineering

School of Energy, Geoscience, Infrastructure and Society

Heriot-Watt University

August, 2017

ABSTRACT

The key objective of this work is to develop a framework to predict, design and interpret the chemistry and physics relating to rock geochemistry and scale precipitation in porous media. The interest is to understand the impact of mineral scale deposition on the produced reservoir fluid compositions and on the petrophysical properties of the rocks they occur in. In the bid to achieve these aims, the first step adopted is to account for the propagation/transport of chemical species within a pore network model used in modelling the reservoir rock. Afterwards, chemical interactions amongst the species are incorporated into the model. Subsequent steps look at mechanisms of the fluid flow at the pore scale and the impact of mineral deposition on subsequent flow distribution and on composition of chemical species downstream of the flow.

A pore network simulator capable of predicting mineral scale deposition in various conditions was developed to achieve the goals of this study. Transport of tracers is incorporated into the simulator and the improved model is validated by comparison with related observations in the literature and other sensitivity studies. The sensitivity studies also provide valuable insights into the physics of scale deposition on pore walls of reservoir rocks.

Furthermore, *in situ* reactions and permeability decline due to barite scale deposition were investigated using the developed model. Raw and de-sulphated seawater injections were simulated. The pattern of permeability impairment with time was monitored.

Additionally, the effluent chemical concentration profile was analysed. A novel 'Delay Factor' was developed to help understand the retardation of the breakthrough of chemical species at the production well due to ion stripping taking place *in situ*.

Finally the impact of rock heterogeneity on the process of in situ reaction and mineral scale deposition was explored. The degree of accuracy in scale prediction hinges partly on

sound understanding of rock structural parameters and their corresponding controls on fluid flow.

Results underscore the fact that the damage deep in a reservoir due to one pore volume displacement of formation water with seawater is negligible. The reduction in permeability only becomes significant when several pore volumes of brine containing barium are flowing *simultaneously* and mixing with the sulphate rich brine. Results also suggests that rock parameters, such as pore connectivity, may impact on the extent of stripping taking place *in situ* when they are considered in networks with narrow pore size distributions. In addition, analysis of the saturation ratios suggests that risk of downstream scaling may be higher in rocks with permeability heterogeneity.

DEDICATION

This work is dedicated to Chinwe (my wife), Kobi and Ola (my kids) for giving me all the reasons to keep on living and to keep on loving.

This work is also dedicated to the memory of my late dad, Mathias Eze, who sowed but did not live to reap.

ACKNOWLEDGEMENTS

My sincere appreciation goes to my supervisors Prof Eric MacKay and Dr Steven McDougall for their guidance and support throughout this work. Prof MacKay was also committed in seeing that this work comes to a logical conclusion, a gesture which I forever remain grateful.

I wish to express heartfelt gratitude to the FAST research group of the Institute of Petroleum Engineering and to Foundation CMG for sponsoring this work.

Above all, I am grateful to my family for their love, support, thoughts and prayers at all times.

HERIOT WATT UNIVERSITY

ACADEMIC REGISTRY
Research Thesis Submission

Name:	Kelechi Sabinus Eze		
School:	EGIS		
Version: *(i.e. First, Resubmission, Final)*	Final	Degree Sought:	MSc (by Research) in Petroleum Engineering

Declaration

In accordance with the appropriate regulations I hereby submit my thesis and I declare that:

1) the thesis embodies the results of my own work and has been composed by myself
2) where appropriate, I have made acknowledgement of the work of others and have made reference to work carried out in collaboration with other persons
3) the thesis is the correct version of the thesis for submission and is the same version as any electronic versions submitted*.
4) my thesis for the award referred to, deposited in the Heriot-Watt University Library, should be made available for loan or photocopying and be available via the Institutional Repository, subject to such conditions as the Librarian may require
5) I understand that as a student of the University I am required to abide by the Regulations of the University and to conform to its discipline.
6) I confirm that the thesis has been verified against plagiarism via an approved plagiarism detection application e.g. Turnitin.

* *Please note that it is the responsibility of the candidate to ensure that the correct version of the thesis is submitted.*

Signature of Candidate:	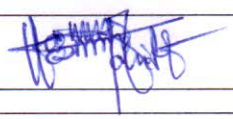	Date:	20/Aug/2017

Submission

Submitted By *(name in capitals):*	
Signature of Individual Submitting:	
Date Submitted:	

For Completion in the Student Service Centre (SSC)

Received in the SSC by *(name in capitals):*			
Method of Submission *(Handed in to SSC; posted through internal/external mail):*			
E-thesis Submitted ***(mandatory for final theses)***			
Signature:		Date:	

Please note this form should be bound into the submitted thesis.
Academic Registry/Version (1) August 2016

TABLE OF CONTENTS

LIST OF TABLES

LIST OF FIGURES

LIST OF EQUATIONS

NORMENCLATURE

DF	Delay factor
SR	Saturation Ratio
Ksp	Solubility Product
ppm	Parts per million
SW	Sea water
FW	Formation Water
$[C_{i,T}]$	Average of all the tracer concentrations at point i and time T
[Ba]	Barium Concentration
$[SO_4]$	Sulphate Concentration
[PPT]	Barite precipitate concentration
PSD	Pore size distribution
PV	Pore volume
R_o	Original bond radius
R_h	Hydraulic radius
V_{PPT}	Volume of the bond occupied by precipitating barite
Z	Cordination Number

1 INTRODUCTION

1.1 Background

Hydrocarbon fluid is known to exist in porous reservoir rocks. For production purposes, the fluid is extracted from its *in situ* location using various recovery techniques. This, inevitably, leads to diverse rock-fluid flow interactions. Examination of thin sections of the rock (Figure 1-1) reveals how challenging the modelling of fluid flow through porous fluid-bearing formations could be. The formation is made up of complex network topologies consisting of a tortuous path of interconnected pores. As the reservoir fluid is transported (through the porous rock) to the wellbore, the aqueous chemical species (i.e. the mineral elements) in the fluid will interact with other species present in the system.

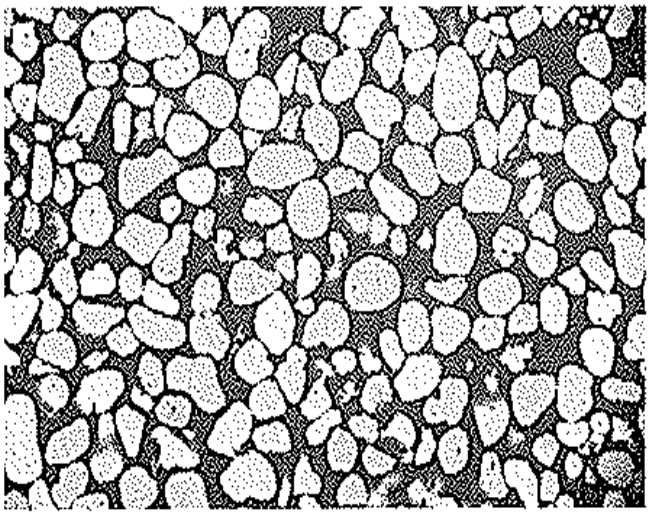

Figure 1-1: A thin section of well-rounded loose sand (the sand grains in light grey and the pore in darker area) (Field of view 5mm across) [Source HWU Petroleum Geoscience MSc Note]

Geochemical reactions (involving aqueous species and mineral compounds) are known to take place in oil and water bearing formations (Frenier & Ziauddin, 2008). Over geological time frames, the formation brine will have equilibrated with the reservoir rocks. However, this chemical equilibrium may be disturbed by alterations to the pressure and temperature conditions of the pore fluids or by mixing with brine, as may occur during water flooding. Water flooding is a secondary recovery technique frequently used in the industry to recover more hydrocarbon fluid. As depletion continues with hydrocarbon production, water flooding is also used to maintain reservoir pressure above bubble/dew point.

The equilibrium disturbance within the rock-brine system may result in ion exchange reactions, dissolution of the primary minerals or precipitation of secondary minerals.

Some processes in particular are known to result in *in situ* mineral scale precipitation;

(a) Brine mixing, i.e. the mixing of injection water with formation water, may lead to the precipitation of sulphate scales, such as $BaSO_4$, $SrSO_4$ and $CaSO_4$ (Barium Sulphate, Strontium Sulphate and Calcium Sulphate respectively). This typically occurs where seawater, rich in SO_4 ions, is injected into reservoirs where the formation water contains Ba, Sr and/or Ca ions.

(b) Pressure depletion, especially in the vicinity of production wells, may lead to the precipitation of carbonates scales, such as $CaCO_3$ (calcium carbonate). As pressure declines, CO_2 is evolved from the brine resulting in an increase of pH value. Since carbonate solubility varies inversely with pH, the solubility of $CaCO_3$ decreases and precipitation may occur.

The mineral scale may eventually get deposited on the pore walls of reservoir rocks, thereby plugging the pores (Figure 1-2). In some other cases scale deposition may occur inside production tubing. As such, it reduces the area open to fluid flow. Scale deposition acting alongside other *in situ* phenomena such as fines migration, may eventually lead to formation damage and decreased productivity.

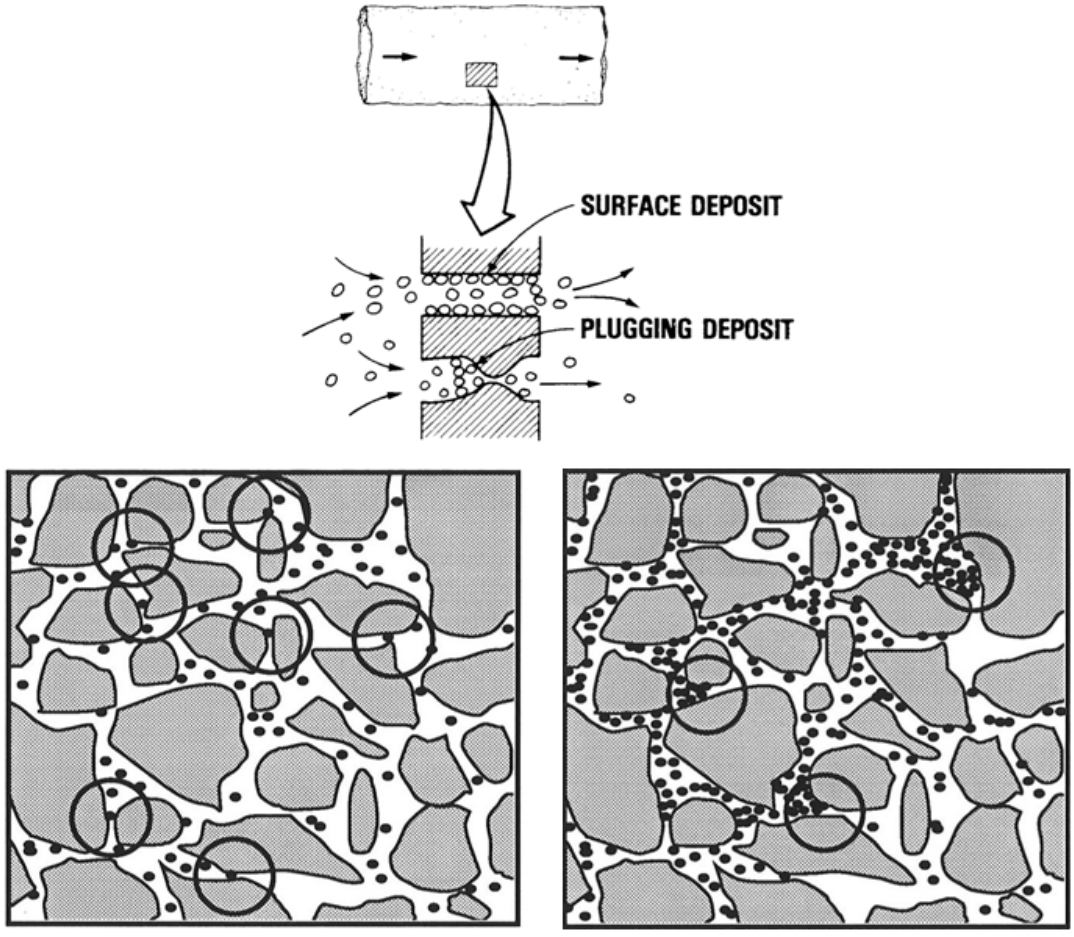

Figure 1-2: Scaling leading to plugging of pores thus constituting flow assurance problem. Particle straining (left) and log jamming (right) [Sources: Gruesbeck & Collins 1982, E. Mackay & K. Sorbie, 1992]

1.2 Aims and Scope of Work

Inorganic/mineral scaling refers to the process whereby scales from brines or other aqueous solutions deposit on a surface when such aqueous solutions become supersaturated. Elaborate research work has been performed on mineral scale precipitation, and many researchers have postulated means of scale precipitation, removal and inhibition (Wang, et al, 2005); (Zhang, et al, 2001); (Yuan, 1994); (Yuan, 1989). Most of this research was undertaken in a bulk fluid configuration. To gain an understanding of geochemical reaction *in situ* within the reservoir, it is useful to adopt a technique that will reflect the porous network topology of the reservoir rock. Hence the use of a pore-scale network model in investigating the physics and chemistry of geochemical reactions becomes very desirable. It allows for the investigation of geochemical reactions within the original environment (i.e. the interconnected pore network that constitutes the rock). It is on this premise that the study 'Pore-Scale Modelling of *In Situ* Geochemical Reactions through Porous Media' was motivated. *The ultimate objective of the study is to develop a framework within which to predict, design and interpret the chemistry and physics relating to rock geochemistry and scale precipitation in porous media*. Geochemical reactions involve interplay between different scientific disciplines. Thus, to ensure accurate investigation of geochemical phenomena, mass transfer, thermodynamics and fluid mechanics need to be included in the model to be used for the study. Such complete modelling can then be used to investigate the physical and chemical processes that accompany geochemical interactions and perhaps mineral scale precipitation. Consequently, one of the aims in this study is to develop a pore-scale simulator that can account for the steps in geochemical reactions and mineral scale precipitation, viz;

i. transportation of chemical species,
ii. reaction between chemical species,
iii. precipitation and deposition of insoluble chemical compounds on the pore walls,
iv. alteration of rock petrophysical properties due to scale deposition,
v. alteration of flow behaviour downstream due to *in situ* stripping.

This simulator will be able to account for rock geochemistry at the pore scale. As such, the impacts of scale deposition on the pores walls of reservoir rocks will become better understood. Results, observations and insights gained from this pore-scale study could also help inform larger core and reservoir-scale studies.

1.3 Thesis Chapter by Chapter Summary

This thesis is structured in five chapters.

Chapter 1 is the introductory chapter setting the background of the work. The concept of rock-fluid interaction is briefly discussed. The scope and significance of the studies are all highlighted here in chapter 1; the need to accurately study reservoir flow phenomena using a pore network model is discussed.

Chapter 2 discusses conservative transport of chemical species within the porous medium i.e. no reaction occurs as the components are displaced within the medium. The transport of the species (as ideal tracers) is modelled based on a single phase flow calculation. Sensitivity studies are then conducted to validate the model.

In Chapter 3, reactions taking place between the chemical species travelling within the porous medium are introduced. Effects of the reaction, such as mineral scale precipitation on the pore wall, are discussed. All processes presented in Chapter 3 take place *in situ*.

Chapter 4 extends the study of the impact of chemical species reactions by looking at the downstream flow configuration. Effluent profiles are used to analyse how *in situ* stripping could delay breakthrough of ions into the production tubing. Chapter 4 also discusses the concept of delay factor which links the retardation in transport of chemical species to the concentration of the species present *in situ*.

Chapter 5 is the conclusion of the thesis and includes recommendations for future work.

2 PARTICLE/TRACER TRANSPORT

2.1 Modelling Transport of Chemical Species

Oilfield tracers are special chemical species introduced in injection fluid to measure flow paths and to track the injected fluid (Zemel, 1995). In other words, tracers could be seen as some sort of chemical markers used in tagging waters. The use of tracers in the oilfield has helped in advancing the understanding of reservoirs and underlying geological structures. Tracers have helped give further insights into the nature of flow paths and boundaries existing within a reservoir formation. Consequently, tracers have found useful application in the area of flow assurance both down-hole and top-side. One such application is the use of different tracers in distinguishing between waters from different injectors.

Zemel in his work (Zemel, 1995), has pointed out that chemical species used in tagging must travel at the same speed as the water itself. Hence, the movement of ideal tracers must reflect the movement of injected waters (Lake, 1989). Both the water and the associated tracers should have the same frontal advance rate and should break through to the producing well at the same time. To achieve this, chemical species used as tracers are expected to be inert while travelling through the reservoir rock. In real cases, however, tracers do not always remain chemically inert while travelling *in situ*. Some chemical species may undergo some form of reactions and suffer some degree of retardation with respect to injection water.

In this chapter, we study the transport of tracers in their ideal form with the use of a pore scale simulator. The ideal form (as identified in the paragraph above) is that the tracer remains inert at all times.

The pore-network model used for the purpose of this study is a network of *bonds* (where bonds are actually cylindrical capillary tubes). The bonds are connected at junctions known as *nodes*. The number of bonds meeting at a given node is characterized by a parameter known as the *coordination number, z.* A fully connected 3D network will have a coordination number of 6 and a fully connected 2D network will have coordination number of 4 (Figure 2-1). Coordination number could be one of the vital parameters governing flow processes at the micro-scale. This is because it impacts such things as residual saturation and fluid breakthrough during *in situ* mixing.

In a 3-dimensional model network, the interconnection of these capillaries forms a scaffold-like structure (Figure 2-2).

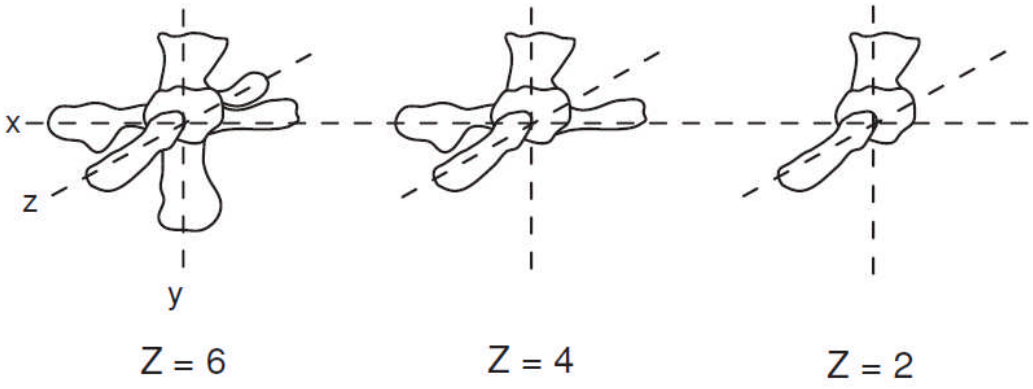

Figure 2-1: Illustration of coordination number [Source: S. McDougall Thesis 1994]

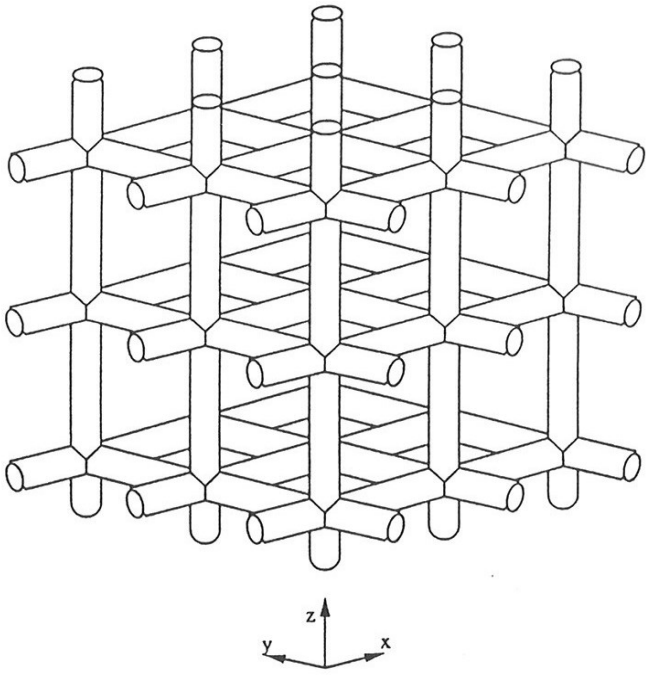

Figure 2-2: A 3-D pore network model with nodal dimension 3 x 3 x 3 [Source: S. McDougall Thesis 1994]

A pore size probability distribution function (pdf) is used to assign a radius to each capillary tube in the network. Properties of the network (e.g. permeability) are controlled by the shape, range and type of the distribution function used. Uniformly distributed bond radii are used for all simulation results presented in this thesis. In general, pore size distribution may take other forms such as log-normal; however, uniform distribution has been used in this thesis for simplicity. Since this work demonstrates that the order of

blocking pores is affected by the pore sizes (as seen in section 3.6.1), it is recommended that while it was considered best in this initial study to use a simple (uniform) distribution, future work should consider the impact of other distributions. Having gained a good understating of the processes being modelled using this simplest of pore size distributions, future work should consider the impact of other pore size distributions, including analytical forms such as Gaussian and Log-Normal. Single phase flow calculations can then be used to calculate the cumulative flow across the entire network as a function of pressure gradient, and so calculated permeabilities can then be correlated to the various types of pore size distribution for various ranges of pore sizes. The distribution of pore sizes will impact the order in which pores block during injection of scaling ions, with there being a balance between smaller pores requiring less precipitate to fill, but larger pores having a greater volume throughput and therefore potentially greater mass flux of scaling ions. Also, 3D image-based morphological analysis of microstructures has been used in the prediction of the macroscopic properties of porous media (Jiang, et al., 2017), and thus a pore size distribution derived from analysis of physical systems could be used, the permeability of the entire network calculated and compared with the value predicted by the 3D reconstruction approach, and then the impact of scale deposition and reduction in pore conductivities on permeability assessed.

In order to establish flow direction within the network, different pressure values are imposed at the inlet and outlet bonds of the network. This will allow for fluid to flow under an induced pressure gradient from left to right, say. In addition, to ensure that fluid flowing out of the lateral edges flows back in at the opposite edge, periodic boundary conditions are applied top and bottom and back and front of the model.

For each capillary element the single phase fluid flow rate Q in the capillary is given by Poiseuille's law;

$$Q = \frac{\pi R^2}{8\mu L}\Delta P \qquad \textbf{2-1}$$

where L and R are the length and radius of the capillary element, respectively, μ is the viscosity of fluid on the capillary element and ΔP is the pressure drop along the capillary element.

To solve for the pressures at each node in the network, a set of linear equations is obtained by assuming no fluid accumulation at the node, thus:

$$\sum Q = 0 \qquad \text{2-2}$$

Equation 2-2 is the application of the conservation of flow principle and it can be calculated for each node in the network. Thus for all the nodes, a set of equations with the same number of unknowns can be generated. In this regard, the unknowns are the pressure differences ΔP across each capillary tube. The set of linear equation is solved numerically to obtain a distribution of ΔP for all element within the network. Once the nodal pressures are obtained from Equation 2-2, they are substituted into Equation 2-1 to obtain the flow through each capillary element.

After identifying the flow in each capillary element and the pressure at each node of the network, the transport of any chemical species can then be tracked, at all times, within the network. The three steps below describe how tracers of given concentration at the inlet bonds is tracked as it propagates through the network to the outlet bonds.

1. Total flow in and out of each node, Q_{in} and Q_{out}, are computed as in Equation 2-3. Assuming flow remains incompressible within the network, the flow into each node should be the same as the flow out of each node.

$$Q_{in} = Q_{out} = 0.5\{(Q_{xin} + Q_{xout}) + (Q_{yin} + Q_{yout}) + (Q_{zin} + Q_{zout})\} \qquad \text{2-3}$$

where Q_{xin}, Q_{yin} and Q_{zin} are the flows into a given node through the respective X, Y and Z upstream bonds connected to the node. Likewise Q_{xout}, Q_{yout} and Q_{zout} are the flows out of the given node through the respective downstream bonds.

2. The total mass of each chemical component going into each node is calculated according to Equation 2-4. Here, the direction of flow is taken into account to ensure that the correct mass of tracers is flowing into each node over time interval ΔT

$$Mass_{in} = \sum \left(Q_{in} \times [C] \times \Delta T\right) \qquad \text{2-4}$$

where [C] is the concentration of the component.

3. At each time step ΔT, the mass of each component in a given bond after flowing from time T to T+ΔT is calculated as

$$Mass_{T+\Delta T} = Mass_T + Mass_{in} - Mass_{out} \qquad \text{2-5}$$

where $Mass_T$ is the mass of the tracer component at time T; $Mass_{T+\Delta T}$ is the mass of the tracer after flowing from time T to time T+ΔT.

To ensure mass conservation at all times during the simulations, appropriate time steps sizes have to be determined. The time taken for the flowing fluid to fill each of the bonds in the network is evaluated and taken into account. The minimum of these evaluated times is set as the time steps size to be used for the entire simulation (see Equation 2-6);

$$\Delta T = MIN\left(\frac{\pi R^2 L}{Q}\right) \qquad \text{2-6}$$

where all terms in Equation 2-6 have been defined earlier in Equation 2-1. This criterion ensures that in any given time step, the volume throughput in each of the bonds is smaller than the volume of the smallest bond.

2.2 Sensitivity Studies

The network model was set up to track the transport of two chemical species, say X and M. The chemical components 'X' and 'M' flow through the model without any reaction. Thereafter, various sensitivity studies were conducted to validate the model. In each of the sensitivity studies the initial conditions set in the model are as follows;

1. Component M is at a maximum concentration (=1) in every bond of the network, while the concentration of component X is zero throughout.

2. Component X is then continuously injected from the inlet bonds (at maximum concentration of 1) to displace tracer component M out of the network.

In the first set of the sensitivity studies, the maximum and minimum values of the uniformly distributed bond radii are varied with the nodes fully connected.

These sensitivity studies are used to validate the model and gain further insights into the impact changes in the bond radii variance will have on flow dynamics within the network. If the model is valid, the tracers are expected to flow favourably along the direction of reducing pressure gradient. Simulations were conducted both under constant pressure gradient and under constant tracer injection rate.

Simulations were also conducted where the normally regular structure of the cylindrical bonds is distorted by varying a network parameter called *distortion factor.* This parameter is varied from 0 (a case of no distortion) to 0.5 (a case where each node may be moved by up to half a bond length). In real reservoir rocks pore lengths vary, so varying the distortion factor makes the network model more realistic.

As the mineral scale precipitates and is deposited on the pore walls of the reservoir rocks, some of the pores will become blocked. To gain an insight on the flow configurations as

the pores become blocked, the network's *co-ordination number* is varied from z = 4 (cylindrical bonds fully connected) to z = 2.67 (bonds partly connected).

2.3 Results and Discussion

2.3.1 Constant Pressure Gradient Simulation

The minimum and maximum values of the uniformly distributed pore radii (Rmin and Rmax) were varied as follows;

1. Rmin to Rmax = 1 to100 μm (can also be interpreted as a heterogeneous porous medium)

2. Rmin to Rmax = 10 to 90 μm

3. Rmin to Rmax = 40 to 60 μm and

4. Rmin to Rmax = 49 to 51 μm (can also be interpreted as a homogeneous porous medium)

For each set of radii, simulations were conducted with the inlet and outlet pressures fixed so that there is a 20 Pa pressure gradient across the model. Each of the simulations was run for a time of 100 s. Profiles of the tracer concentrations along the length of the network were computed and plotted at different times. This gives detailed information on the concentration distribution of aqueous chemical species *in situ* in a given porous reservoir rock. The value of pore network modelling is that it provides these detailed pressure information at all positions and at all times while flowing through the system. Such information cannot be obtained (in such detail) from laboratory experiments.

To obtain the tracer concentrations profile along the length of the network, the concentrations are averaged using Equation 2-7 below;

$$[C_{i,T}]_{in} = \frac{\sum_{j=0}^{n_y}\sum_{k=0}^{n_z}\left\{\left([C_{Xijk}]V_{Xijk}\right)+\left([C_{Yijk}]V_{Yijk}\right)+\left([C_{Zijk}]V_{Zijk}\right)\right\}}{\sum_{j=0}^{n_y}\sum_{k=0}^{n_z}\left\{\left(V_{Xijk}\right)+\left(V_{Yijk}\right)+\left(V_{Zijk}\right)\right\}} \qquad \text{2-7}$$

where $[C_{i,T}]$ is the average of all the tracer concentrations at location i bonds from the inlet and at time T; $[C_{Xijk}]$, $[C_{Yijk}]$ and $[C_{Zijk}]$ are tracer concentrations going into node ijk from the X, Y and Z oriented bonds respectively; V_{Xijk}, V_{Yijk} and V_{Zijk} are the corresponding volumes of the bonds in the direction of X, Y and Z respectively (see Figure 2-2).

It has been pointed out earlier (Section 2.1) that the properties of the pore network are controlled by the pore radius distribution function used for the bond elements. The ranges of maximum and minimum radii used (Rmax & Rmin) and the calculated abd input corresponding network properties are summarized in Table 2-1.

Table 2-1: Summary of parameters computed for each of the Four networks used for the study

Network Properties	Rmin:Rmax (μm)			
	1:100	10:90	40:60	49:51
Permeability k (D)	5.498	7.361	20.066	22.104
Porosity (%)	9.08	9.85	13.43	13.88
Pore Volume PV (m^3)	8.55e-9	9.27e-9	1.26e-8	1.31e-8
Flow Rate (m^3/s)	3.6e-11	4.80e-11	1.31e-10	1.44e-10
Inlet Pressure P_{in} (Pa)	20			
Outlet Pressure P_o(Pa)	0			
Nodal Dimensions	50 x 50			
Bond Length (μm)	333 μm			
Coordination Number (z)	4			

The concentrations of tracers X and M were averaged along length of the network and plotted (line plot on the top left corner) at three different stages of the simulation, as presented in Figure 2-3 (for the 1-100 μm network) and Figure 2-4 (for the 49-51 μm network). The three stages are: the early time (just at the commencement of the simulation, with line plots for components X and M denoted by CONCX0 and CONCM0), the intermediate time (after the simulations have run for 50 s with line plots denoted by CONCX50 and CONCM50) and the late time (at the end of the 100 s simulation period with line plots denoted by CONCX100 and CONCM100). In addition, a graphical display was used to visualize the propagation of the tracer components within the network. Different colours have been used in the tracer graphics to denote the concentration of tracer components present in each bond. For the graphics of component X, bonds with maximum concentration are coloured red and those with minimum concentration are coloured white. For component M, the colour code for the maximum concentration is green and that of the minimum concentration is white. Yellow has been used to denote the bonds where components X and M are present at finite concentration,

and hence have a high probability of reacting with each other (i.e. the region where the saturation ratio is expected to be greater than 1 if X and M are scaling ions and the product of their activities is high enough).

At the top left corner of Figure 2-3 and Figure 2-4 are line plots of the concentration averaged along the length of the network. The top right and bottom corners are the graphics of such plots for the two components (X and M) at different times of the simulation. As the simulations progresses from time 0 towards 100 s, the graphics show that both components become spread out within the network. This dispersion is reflected on the plot as the concentration gradient becomes less steep. A similar trend is observed when looking at the corresponding plots and graphics for the bond radii range 49 to 51 μm (i.e. Figure 2-4).

To further understand the effects of decreasing the bond radii variance by changing the range from 1-100 μm through 49-51 μm, we present the plots of the concentrations along the length of the network (without the graphics) in Figure 2-5. It is observed, from the plots, that the tracer concentration profiles become less steep as the range of bond radii are varied from 1-100 μm through to 49-51 μm. This suggests that the flow of tracers becomes more dispersed as the variance in bond radii decreases.

This suggestion is physically plausible. With a decrease in the bond radii variance (i.e. for the 49-51 μm network), there will be a predominance of flow in the direction of pressure gradients. As a result, the tracer components will be easily transported, in the direction of principal pressure, but tracers orientated perpendicular to the primary flow direction will be displaced very slowly, and as such be subjected to higher dispersion. In cases where there is high variation in bond radii (i.e. the 1-100 μm scenario), flow is not favoured in any particular direction. Higher variation in bond element radii means that flow in the direction of pressure gradient will become less dominant. Due to this constraint, the tracers are less likely to be propagated in slow moving bonds and as such become less dispersed within the network.

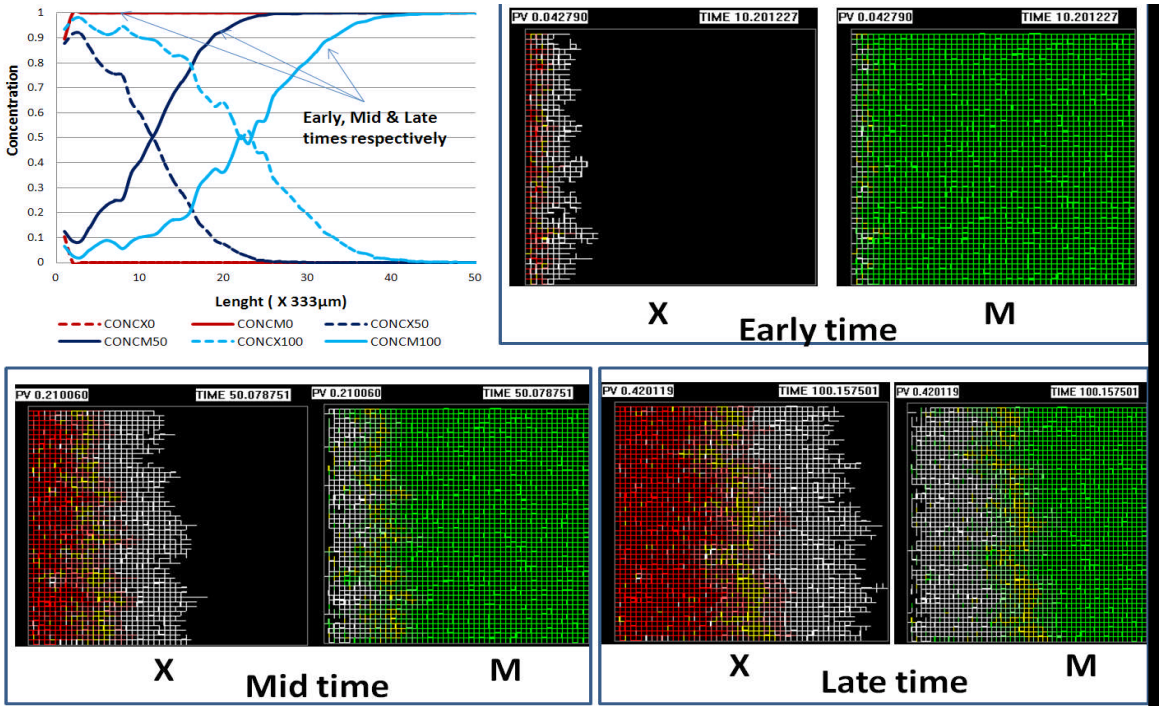

Figure 2-3: Line plot and graphical display of tracer concentration along the length of the network for minimum and maximum bond radii of 1 µm and 100 µm respectively. The plot and the graphics are captured at three different stages of simulation viz the early, mid and late times. In the line plot, at early time (0 s) CONX0 is in red dotted line, CONCM0 in red solid line. At mid time (50 s) CONCX0 is in dark blue dotted line CONCM0 in dark blue solid line. At late time (100 s) CONCX0 is in light blue dotted line, CONCM0 in light blue solid line

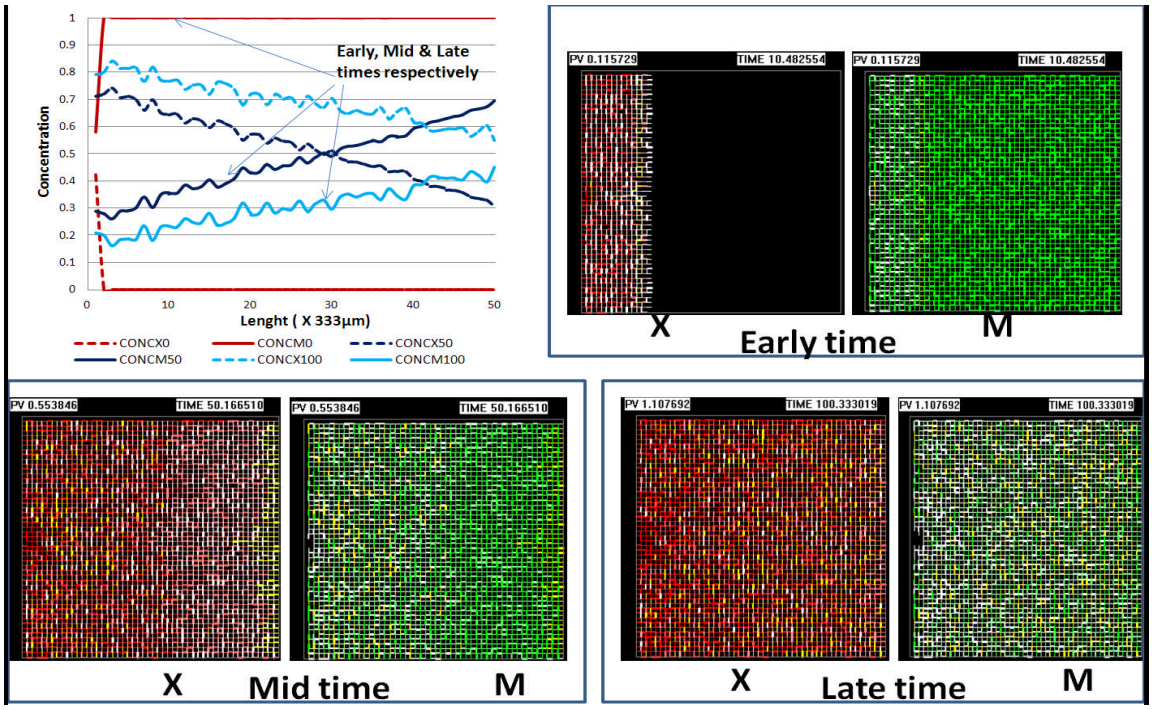

Figure 2-4: line plot and graphical display of tracer concentration along the length of the network for minimum and maximum bond radii of 49 µm and 51 µm respectively. In the line plot, at early time (0 s) CONX0 is in red dotted line, CONCM0 in red solid line. At mid time (50 s) CONCX0 is in dark blue dotted line CONCM0 in dark blue solid line. At late time (100 s) CONCX0 is in light blue dotted line, CONCM0 in light blue solid line

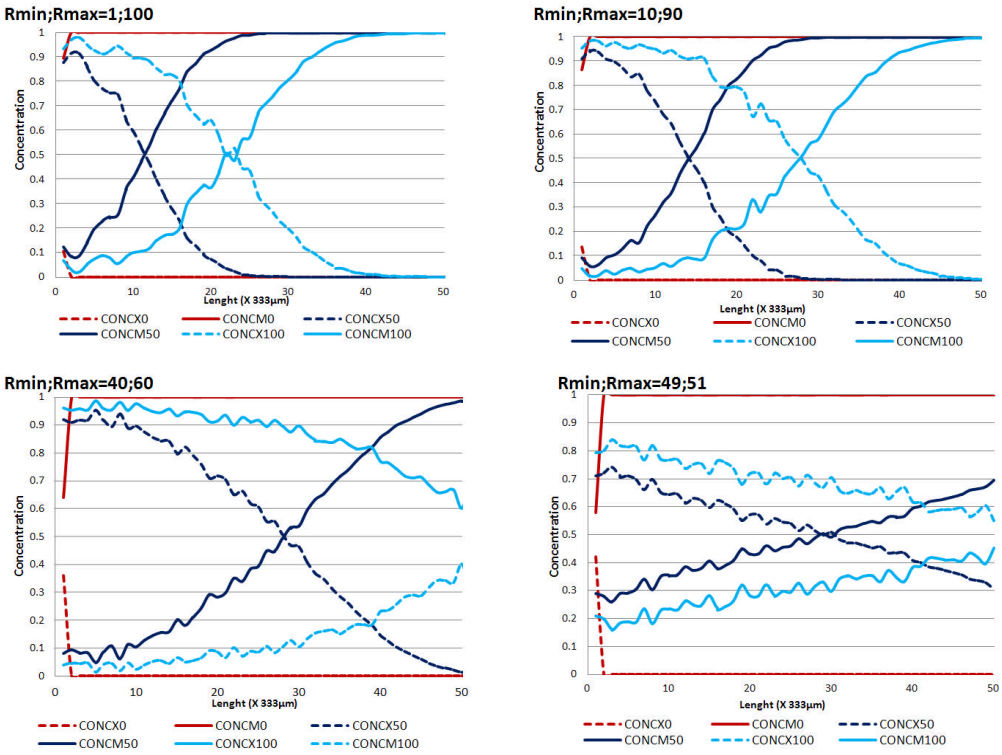

Figure 2-5: Line plots of tracer concentration along the length for the Four different networks studied i.e. for minimum and maximum bond radii of 1-100; 10-90; 40-60 and 49-51 µm. As before, in each plot are captured curves at three different stages of simulation, viz the early, mid and late time

It is acknowledge that straight cylindrical bonds are an over-simplification of the actual structures of real porous media. However, the bonds can be distorted to make the network reflect, more realistically, the structure of an actual porous medium. Thus we incorporate some degree of bond distortions into the network by increasing the *distortion factor* from 0 to 0.5 (see Figure 2-6 and Table 2-2). This will alter the positions of all other nodes in the network while keeping the inlet and outlet nodal positions fixed. As a result, some degree of distortions will be established within the network without generally changing the connectivity of the network.

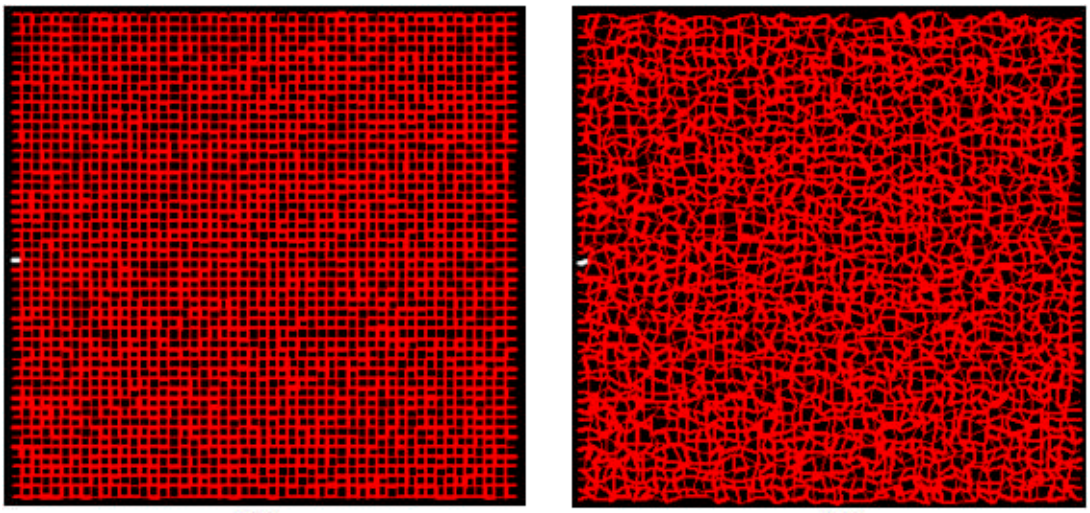

Figure 2-6: A 50x50 network (a) without distortion (b) with distortion

Table 2-2: Summary of parameters for the distorted network

Network Properties	Rmin:Rmax (µm)			
	1:100	10:90	40:60	49:51
Permeability k (D)	4.889	6.544	17.745	19.569
Porosity (%)	10.61	11.52	15.74	16.28
Pore Volume PV (m^3)	9.99e-09	1.08e-08	1.48e-08	1.53e-08
Flow Rate (m^3/s)	3.20e-11	4.28e-11	11.6e-10	1.28e-10
Inlet Pressure P_{in} (Pa)	20			
Outlet Pressure P_o(Pa)	0			
Nodal Dimensions	50 x 50			
Bond Length (µm)	333			
Coordination Number (z)	4			

When a distortion factor of 0.5 is set in the network, the dispersion of the tracer components in the network is expected to behave differently given that the network parameters are different in both cases (compare Table 2-2 and Table 2-1).

Figure 2-7 suggests that as the variance in the bond element radii is decreased (by varying range of bond radii from 1-100 µm to 49-51 µm) the differences in dispersion become less pronounced for the distorted network (compare Figure 2-7 and Figure 2-5). Figure 2-8 compares the dispersion of the tracers between the networks with no distortion and

the network with distorted bonds. All four networks were presented together (ie. 1-100 µm, 10-90 µm, 40-60 µm and 49-51 µm). Each of the plots displays information for all networks at the time stages of the simulation described earlier (i.e. Figure 2-8a and b for mid and late time stage in network without distortion respectively Figure 2-8c and d for mid and late time stages in network with distortion respectively).

At early time of the simulation, the curves are expected to overlay each other as the tracer component M is at maximum concentration of 1 (reflecting the initial conditions set in the network). As the flow simulation progresses further, the curves separate. This is due to the varying degree of tracer dispersion in the respective networks. Separation, however, is less pronounced for the distorted networks (as highlighted with the green arrow in Figure 2-8c and Figure 2-8d). Incorporating distortion into the network leads to less uniform alignment of the bond elements in the axial direction. Thus tracer components flowing through the network have to take a more tortuous route as they propagate from the inlet towards the outlet bonds. In addition, distortion of the bonds leads to a decrease in the permeability of each of the networks (compare Table 2-1 and Table 2-2). The overall effect of these changes is that fluid flow in the direction of pressure gradient will become less dominant for distorted network cases compared with cases when the distortion factor is 0.

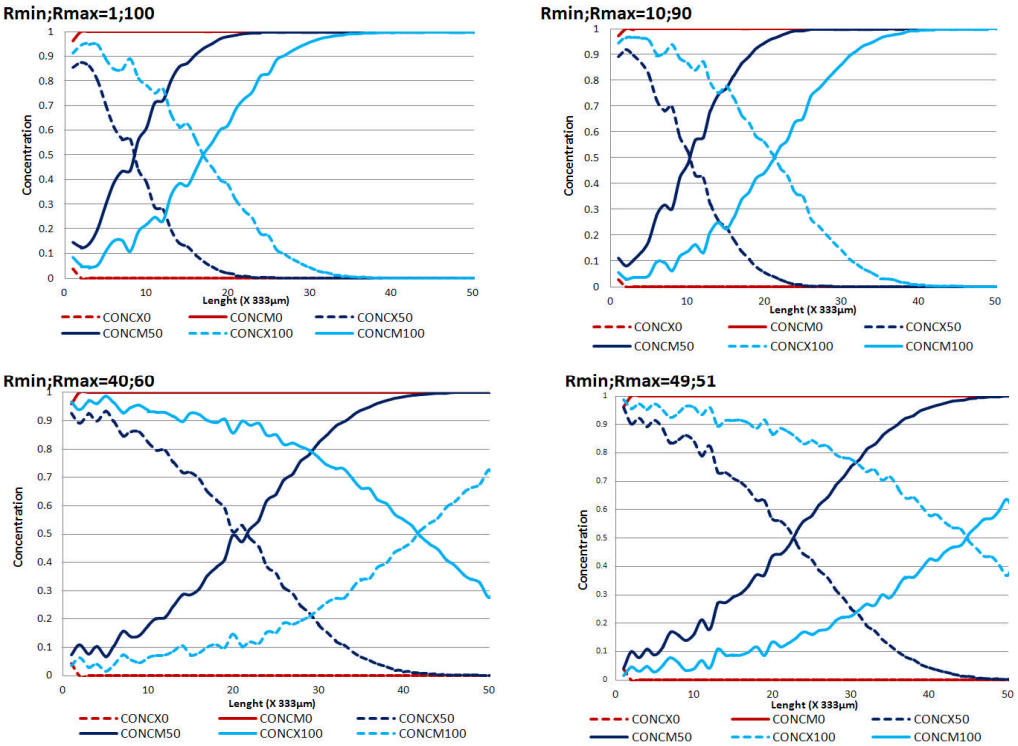

Figure 2-7: Tracer concentration along the length for the 4 networks studied with the bonds distorted

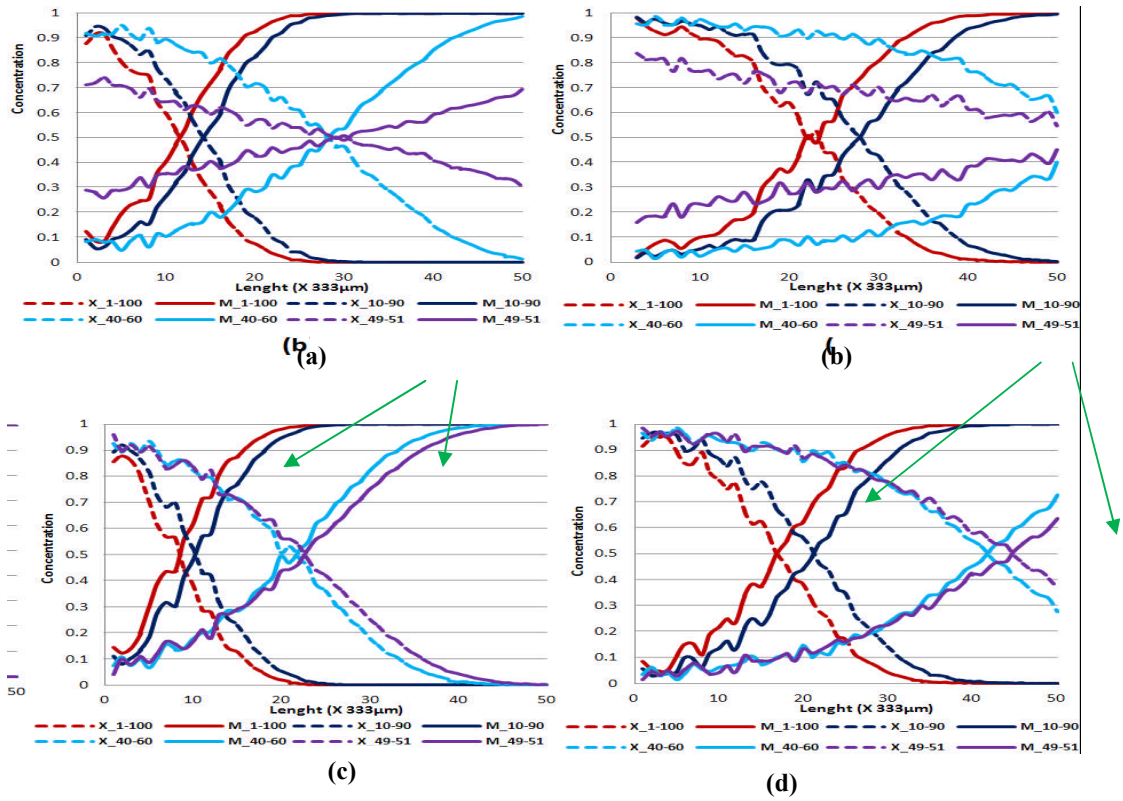

Figure 2-8: Comparing the tracer concentration (at 50 s and 100 s time stages of simulation) along length of the 4 different network without distortion (a, b) and with distortion (c, d)

Similar inferences can be drawn when the effluent profile of the tracer concentration is analysed. Figure 2-9a is a plot of tracer concentration leaving the network after 1,000 s of flow simulation. In order to obtain the effluent profile, the simulation was allowed to run for 1,000 s to allow enough time for the displacement of the tracers out of the network.

Here, we observe that as the variance in bond element decreases, tracer component X breaks through to the network outlet at earlier times as it displaces tracer M. Thus, in a system devoid of reactions, chemical species are expected to flow with fewer restrictions in a homogeneous porous medium as opposed to a heterogeneous porous medium. This is because the flow will be predominantly in the axial direction as discussed earlier.

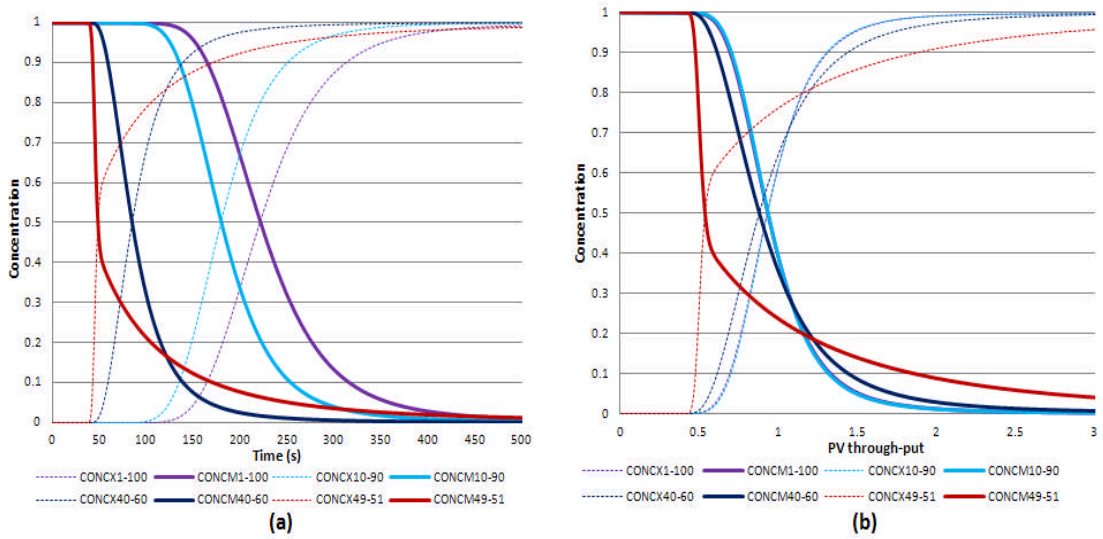

Figure 2-9: Effluent tracer concentration for the four different networks (i.e. the concentration of tracers X and Y at the exit bonds after 1,000 s)

The effluent profiles plotted against the pore volume throughput (Figure 2-9b) suggest that in the region of 0.5 pore volume throughput, tracer X breaks through as it displaces tracer M (for all networks). However, for the lower bond radii variance, it takes a lower pore volume throughput for X to displace M down to 50% of the initial concentration. To explain this result further, we take a look at the flow averaged concentration separately along the length for the horizontal and vertical bonds in the network (Figure 2-10 and Figure 2-11, respectively). Each graph, as before, has line plots showing the concentration at time 0 s, 50 s and 100 s of simulation. Top graph is concentration for the entire network. Bottom left graph considers only the bonds in the principal direction of flow within the network. Bottom right graph considers just the bonds perpendicular to the principal direction of flow. Figure 2-11 shows that when the bond radii in the network are homogeneous, flow will be mostly through the bonds in the X (horizontal) direction. Consequently, there is high probability of displacing tracer components in the X bonds first before those in the vertical direction (Y bonds). Compare Figure 2-11 with Figure 2-10 where bonds in both directions contribute almost evenly to the flow through the network. As such, I conclude that it will take about half the pore volume throughput to displace up to 50% of the initial concentration (as seen in Figure 2-9a). This early displacement can be seen to be mostly coming from the X-bonds. Afterwards, it takes longer to displace the remaining components out of the network since flow through the Y bonds contributes less to the flow through the entire network.

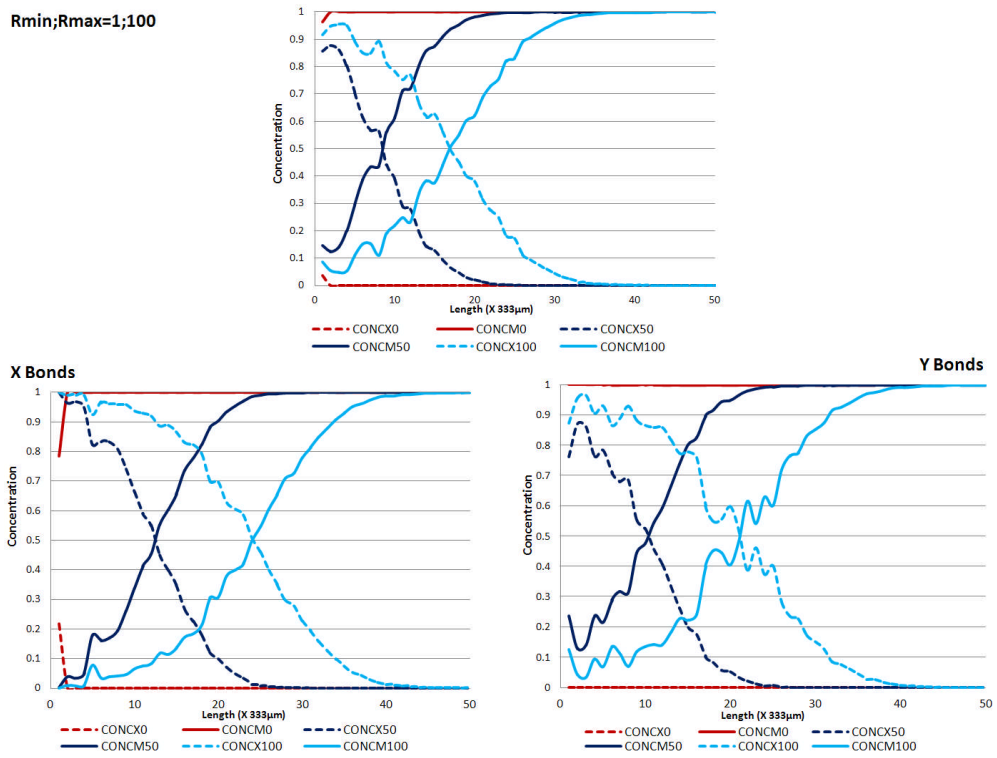

Figure 2-10: Comparing the horizontal (X) and vertical (Y) bonds for 1-100 µm network at 0 s, 50 s and 100 s. Top graph is concentration for the entire network. Bottom left graph (i.e. X-Bonds) considers only the bonds in the principal direction of flow. Bottom right graph (i.e. Y-Bonds) considers the bonds perpendicular to principal direction of flow

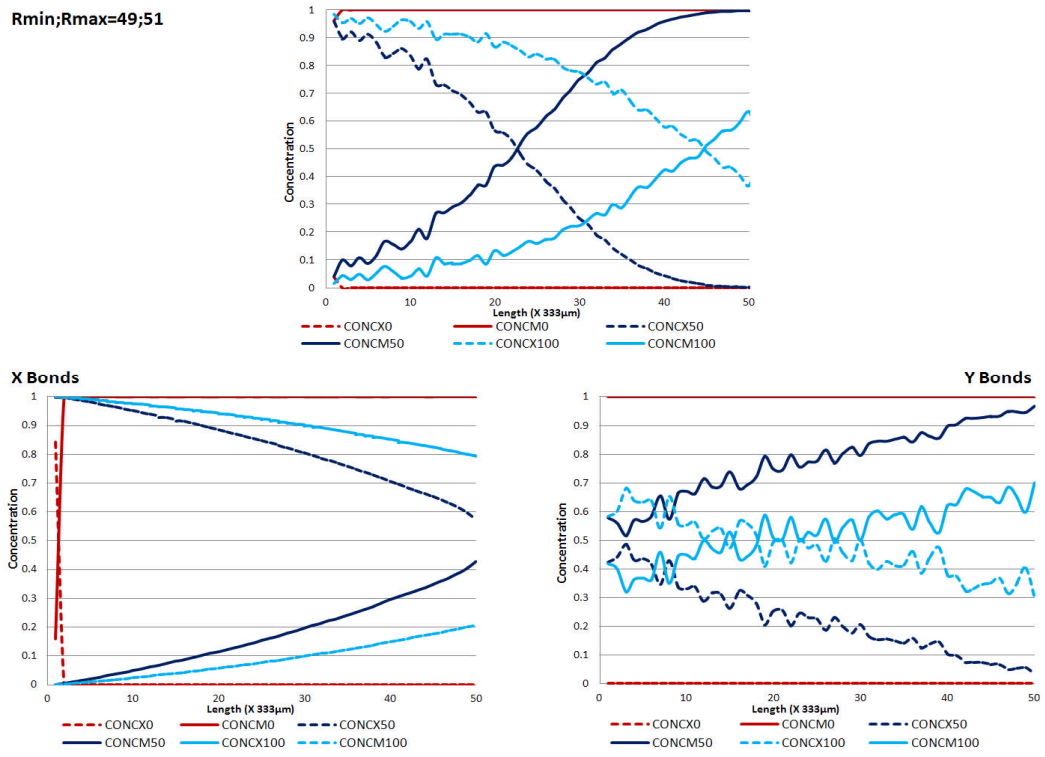

Figure 2-11: Comparing the horizontal (X) and vertical (Y) bonds for 49-51 µm network at 0 s, 50 s and 100 s. Top graph is concentration for the entire network. Bottom left graph (i.e. X-Bonds) considers only the bonds in the principal direction of flow. Bottom right graph (i.e. Y-Bonds) considers the bonds perpendicular to principal direction of flow.

2.3.2 Constant Flow Rate Simulations

When the bond radii variance is changed by altering the ranges of the pore size distribution from 1-100 μm to 49-51 μm, the permeability of the respective networks will change as well. This happens because the pore size distribution controls properties of the network (as pointed out earlier in Section 2.1). As a result, constant pressure simulations will result in different flow rates in each of the four networks used for the studies presented in Section 2.3.1 (see flow rate values in Table 2-1 and Table 2-2). Typical laboratory experiments motivating this study are conducted under constant flow rate conditions; as such it will be desirable to model such conditions in the network. In order to achieve constant flow rate simulations, the inlet and outlet pressures must be adjusted throughout simulations. The actual pressures to be used at the inlet and the outlet of each network have to be case specific. The pressures are adjusted while taking the changes in permeability into account. For each of the four networks being studied, the pressure difference used for the simulations, ΔPnew, is determined by Equation 2-8

$$\Delta P_{new} = \Delta P_{old} \frac{Q_{new}}{Q_{old}} \qquad \text{2-8}$$

where ΔPold and Qold are the parameters used in a previous (non-constant rate) simulations; Qnew is the new constant rate desired.

Equation 2-8 was used to compute the network pressure difference that will result in a constant network flow rate of 3.6e-11 m^3/s. Other network parameters remain as given in Table 2-1 earlier.

The result (Figure 2-12) shows that when the bond radii variance is decreased, it takes longer time for tracer X to break through network while displacing tracer M. Compare this result with that observed with constant pressure simulations (Figure 2-5 above). Observations made here are more or less the opposite of what was observed in the constant pressure flow conditions. The network parameters (Table 2-1) suggest that pore volume of the network increases as the bond radii variance is reduced (i.e. as the range of the bond size distribution is altered from 1-100 μm through 49-51 μm). As such, maintaining a constant rate flow implies that it will take longer to fill those networks with lower variance in bond radii.

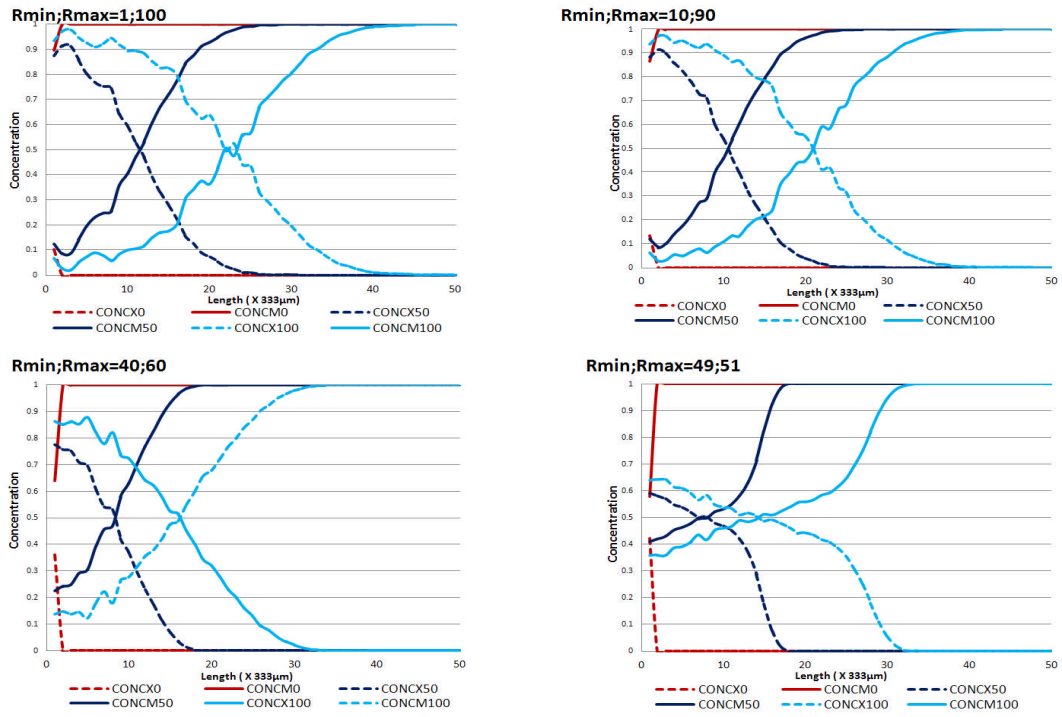

Figure 2-12: Tracer concentration along the length for the four different networks (for constant flow rate simulations). Each plot captured the curve at three different stages of simulation, at 0 s, 50 s and 100 s

Interestingly, however, the difference in concentration gradient along the length of the network is even less pronounced for constant rate simulations compared with the constant pressure cases. In Figure 2-13, we look at these two simulation conditions side by side. At mid-time and for constant pressure simulation (Figure 2-13a and b) we observe widening differences in the slope representing the concentration gradient of the four different networks. This is less pronounced for the constant flow simulations (Figure 2-13c and d). In other words, when the flow rate is kept constant, changes in pore radii variance have a lesser effect on the dispersion of the tracer component within the network.

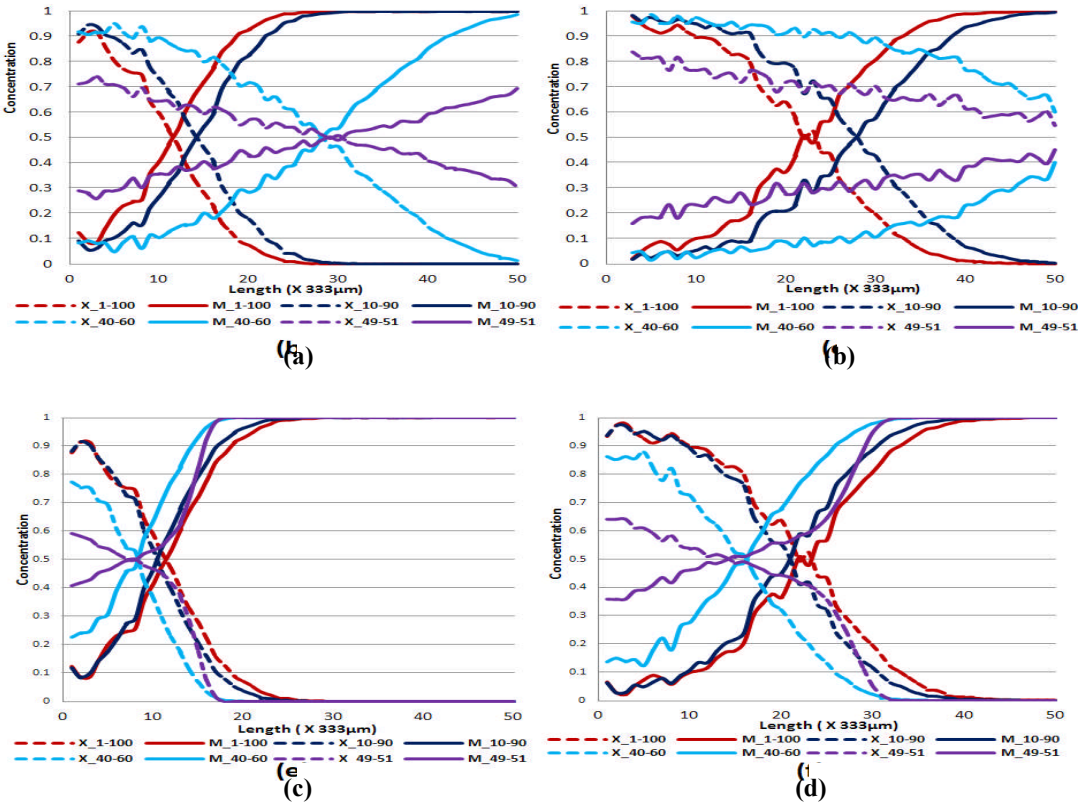

Figure 2-13: Comparing the tracer concentration along length of the 4 different networks for constant pressure (a, b) and constant flow rate (c, d)

The effluent profile against time and against pore volume through-put shows similar trends. In Figure 2-14a we observe that in the network with the lowest pore volume (i.e. network of bond radii between 1-100 µm), tracer X exits the network at the earliest time while displacing tracer M.

There appears to be no difference between the effluent profiles plotted against pore volume through put for both the constant volume and constant pressure cases (compare Figure 2-14b below and Figure 2-9b above). This observation is explicable. Irrespective of the rate of flow through a given porous medium, it should take the same volume of solvent to propagate chemical species within the network provided there is no reaction taking place within the network. The statement is valid when all network parameters are the same and there is no reaction that may lead to retention of the chemical components within the network.

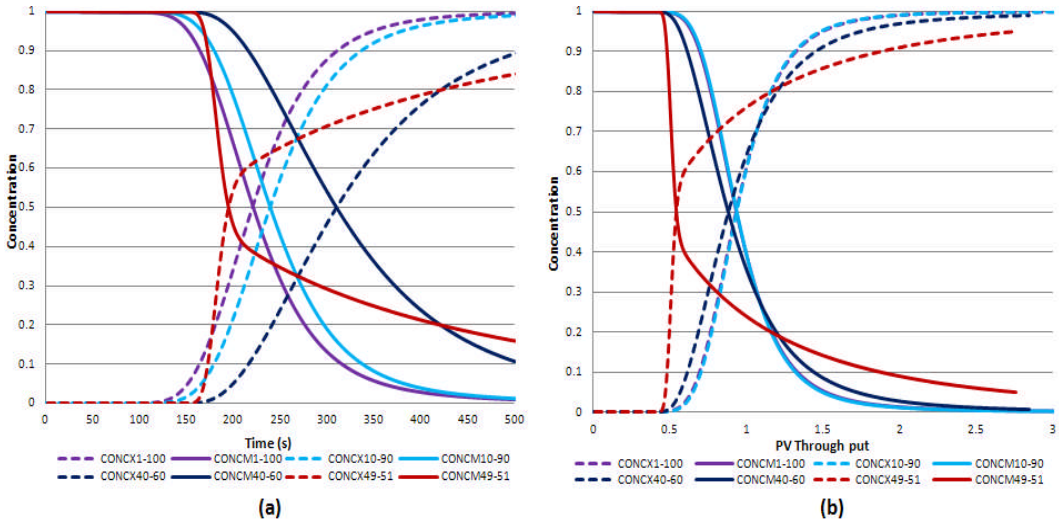

Figure 2-14: Effluent tracer concentration for the four networks (flow constant for all networks)

2.3.3 Decreasing the Coordination Number

As pointed out in Section 2.1, the connectivity between the bond elements of a pore network model is characterized by a parameter known as the *coordination number*, z.

Sensitivity results presented above were performed with the coordination number set to 4 thereby ensuring that bonds within the 2D networks are fully connected. Here, the coordination number is set to a lower value of 2.67 and similar studies as presented above were performed. At this lower z value, some of the bond elements will become disconnected from the surrounding bonds. As such, they will become dead-end pores. Studies with a network having dead end pores will be useful in advancing the knowledge of pore scale geochemistry. As reactions take place among the chemical species in a reservoir rock, deposition of scales may lead to eventual plugging of the pores. As such, the surrounding pores will become dead end pores.

For the non-fully connected network, studies of the impact of varying bond radii were conducted by changing the range of bond radii from 1-100 µm to 49-51 µm as before. Comparing the results between each of the networks (having the same value for z = 2.67), the trends observed is the same as the result for fully connected network presented earlier. As such, the results have not been presented here since adequate discussions have been made on the results earlier.

However, it is desirable to compare what the trend will be as the network changes from being fully interconnected to minimally connected. We made a comparison of the results between 3-D networks of coordination number = 6 (fully connected network) and

coordination number = 4 (non-fully connected network). Figure 2-15 shows that decrease in bond connectivity increases the time it takes for tracer X to propagate across the network while displacing tracer M. The result validates the conclusion that with less connectivity of the bond elements, there are fewer pathways in the network open to fluid flow.

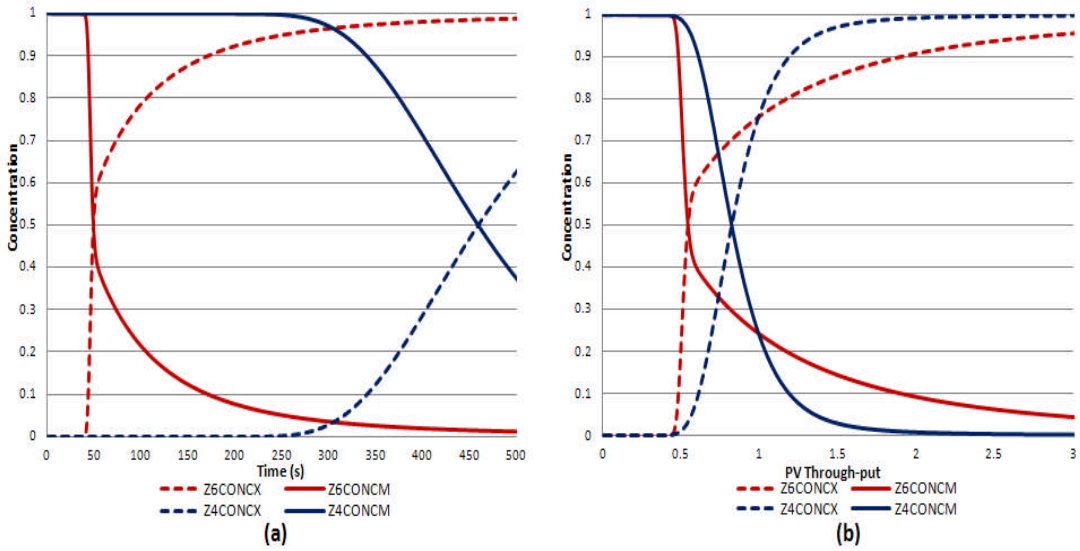

Figure 2-15: Comparing effluent profile at different connectivities

2.3.4 Varying Tracer Injection Rate

For coordination number of 6 and distortion factor of 0, the rate of injection of tracer X (or the rate of displacement of tracer M) was varied. This was achieved by changing the pressure differences imposed between the inlet and the outlet bonds of the network. The pressure differences were varied to achieve high flow rate in one set of simulations and low flow rate in another. The aim here is to compare the trends of effluent concentration profile at a higher and lower flow rate.

The result (Figure 2-16) is a plot of the concentration profiles for high and low flow rates. The set of simulations with higher flow rates consistently shows early displacement of tracer M by tracer X. This confirms that if other parameters of the network are kept constant, the higher flow rates is expected to transport the tracers faster relative to the lower flow rates. The effluent profile plot against the pore volume throughput shows no difference between both conditions. For networks of the same parameters, it will take the same pore volume throughput to fill the networks irrespective of the flow rates.

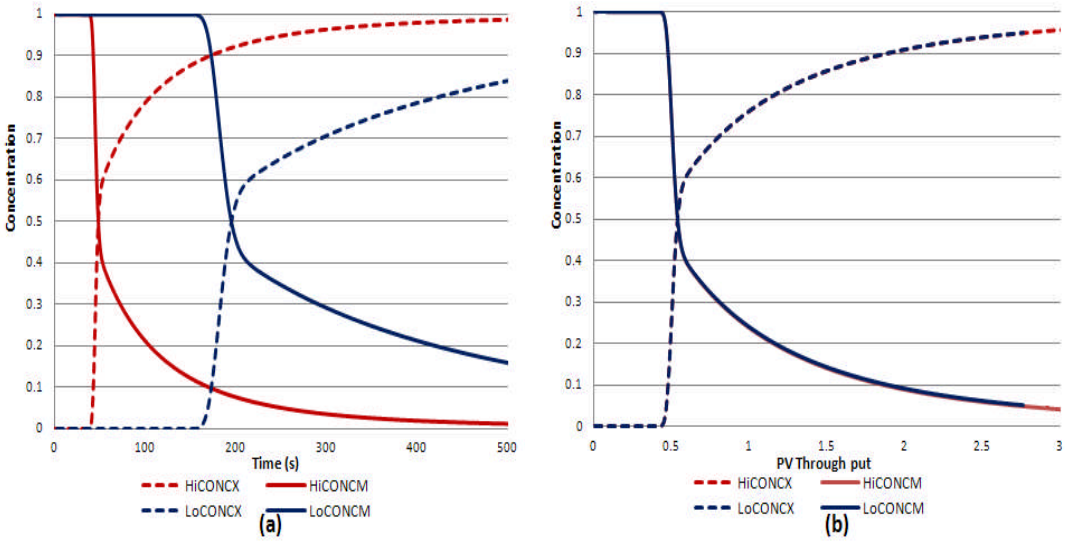

Figure 2-16: Comparing effluent tracer profiles for high and low flow rates

2.4 Summary

Sensitivity studies have been conducted to validate the pore network model and also gain further insights on the transport of two aqueous chemical species (X and M) within a pore network model. During the initial studies, components X and M were set up to flow through the network with no reactions i.e. inert tracers.

Further studies (as described in subsequent chapters) will now concentrate on what happens when the aqueous species X and M react.

3 CHEMICAL SPECIES REACTION AND EFFECTS

It has been discussed in Sections 1.1, 1.2 and 2.1 that studying geochemical reaction using pore network models helps provide an understanding of geochemistry *in situ* reservoir rock. In this chapter we study the phenomenon of chemical reactions taking place between the chemical species present in pore spaces of reservoir rocks. The rocks contain mineral elements that have attained chemical equilibrium with the formation water over geological time frames. Yet some production activities (like waterflooding) might induce reactions that alter thess equilibrium conditions. The reactions between the mineral elements could lead to dissolution of the reacting compounds and/or precipitation of insoluble compounds. Formation of these chemical compounds itself is not a flow-assurance problem. The problem lies in the tendency of the compounds to deposit on the pore walls of the reservoir rock (Wang, et al, 2005).

Inorganic/mineral scaling refers to the process whereby scales from brines or other aqueous solutions deposit on a surface when these aqueous solutions become supersaturated. Supersaturation could be as result of chemical reactions leading to alteration in the thermodynamic state or chemical equilibria existing in the system. The problem of mineral scale precipitation occurs very frequently in reservoir management. Scale deposition could lead to low water injectivity and/or low hydrocarbon productivity. It could also lead to formation damage, which in turn affects oilfield recovery efficiency. Hence it will be helpful to have a convenient and accurate way of quickly predicting scaling potentials and severity in reservoir fluid flow systems. This will be useful when planning water flood schemes and/or in the selection of effective scale prevention techniques.

The pore network modelling technique has been adopted here to seek better insights into the coupled physics and chemistry of geochemical interactions. This is needed because conventional laboratory tests, used in studying/evaluating the scaling potentials of the reservoir flow configurations (Wang & Others, 2005); (Dawe & Zhang, 1997); (Ghaderi, 2009) are susceptible to difficulties, since it is not easy to replicate field conditions in the lab. Besides, software is available that is capable of calculating the amount of scale one may expect from a mixture of incompatible waters at different pHs, temperatures and concentrations; while these codes may make accurate predictions, they provide no information about the impact such scale deposition will have in a given porous medium [(Read & Ringen, 1982)] (see Figure 1-1). The approach of pore network modelling is to

take a microscopic network representation of the porous medium, impose various assumptions of brine mixing/ion interactions and calculate the effects of these interactions on petrophysical properties such as porosity and permeability. Adopting a technique that will reflect the porous network topology of the reservoir rock is useful in achieving an accurate understanding of the impact of geochemical reactions *in situ* the reservoir. This is because the approach facilitates investigations of geochemical interactions within the interconnected pore body-to-pore throat framework that actually constitutes the reservoir rocks.

3.1 Pore Network Model for In Situ Reactions

The background to pore network modelling was introduced in Section 2.1 , and will be re-capped here as follows;

- Porous medium is modelled with network of cylindrical capillary tubes that are interconnected (see Figure 2-2).

- Probability distribution function (pdf) is used to assign random radius from a given distribution to each capillary tube. Properties of the network (e.g. permeability) are, to some extent, controlled by the shape, range and type of the distribution function used.

- Different pressure values are imposed at the inlet and outlet bonds of the network to establish flow under the applied pressure gradient (see Figure 3-1).

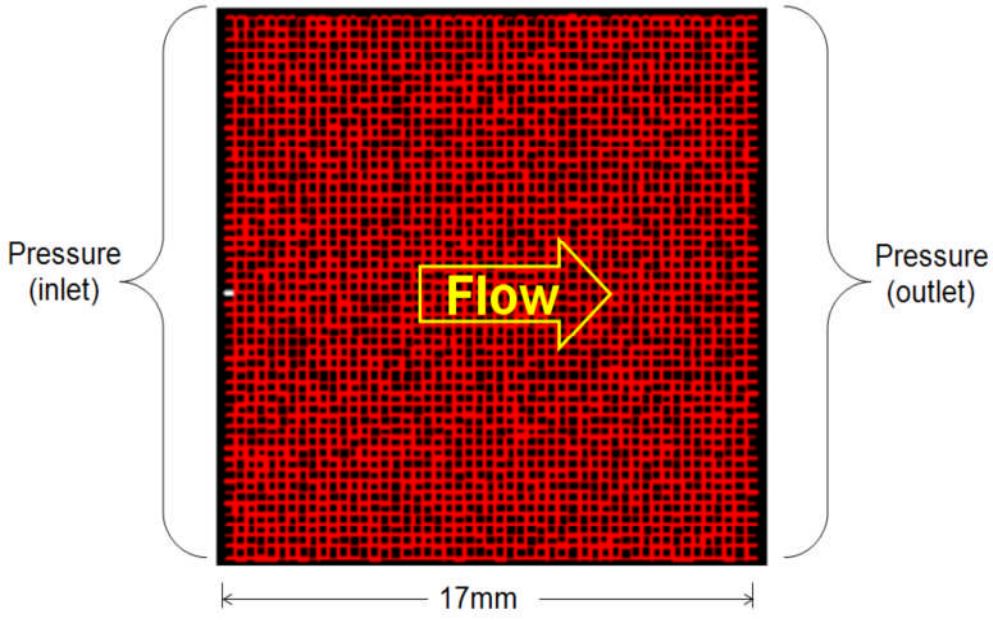

Figure 3-1: A 2-D example 50 x 50 network

- Periodic boundary conditions are used within the network to ensure that fluid flowing out of the topmost bonds is fed into the corresponding bonds located at the bottom row, and vice versa.

- Fluid flow rate Q in each capillary is given by Poiseuille's law; (equation **3-1**)

$$Q = \frac{\pi R^2}{8\mu L}\Delta P \qquad \textbf{3-1}$$

where L and R are the length and radius of the capillary element, μ is the viscosity of the fluid in the capillary element and ΔP is the pressure drop across the capillary element.

- Assuming incompressible fluids, conservation of fluid flow is applied at each node; this generates sets of linear equations with the pressure at each node as the unknowns. These equations are solved numerically to obtain the distribution of pressure fields in the network.

- The propagation of chemical species can then be tracked at all times within the network. The following steps describe how components of a given concentration [C] at the inlet bond are tracked as they propagate through the network.

1. The total mass of each chemical component going into each node, $Mass_{in}$, is calculated according to equation 3-2

$$Mass_{in} = \sum \left(Q_{in} \times [C] \times \Delta T \right) \qquad \textbf{3-2}$$

2. At each time step ΔT, the mass of each component in a given bond after flowing from time T to T+ΔT is calculated as shown in equation 3-3

$$Mass_{T+\Delta T} = Mass_T + Mass_{in} - Mass_{out} \qquad \textbf{3-3}$$

where Q_{in} is the total flow to the node; $Mass_T$ is the mass of the chemical component at time T; $Mass_{T+\Delta T}$ is the mass of the component after flowing from time T to time T+ΔT.

- To ensure mass conservation at all times during the simulations, appropriate time steps sizes have to be determined. The time taken for the flowing fluid to fill each of the bonds in the network is evaluated and taken into account. The minimum of these

evaluated times is set as the global time-step size to be used for the simulations (see equation 3-4)

$$\Delta T = MIN\left(\frac{\pi R^2 L}{Q}\right) \qquad \textbf{3-4}$$

3.2 Preciptation/Dissolution Reactions

Study of mineral scale precipitation in an oilfield system, be it in the reservoir rock, downhole completions equipment or topside facilities, involves two important aspects

1. It is necessary to ascertain *if* the scaling problem could possibly occur within the system.

2. It is also necessary to estimate the severity of such scale problem, should it occur.

Consequently, the prediction of a system's scaling tendency involves the calculation of two parameters: the saturation ratio(s) of the insoluble salt(s) and the mass(es) of salt(s)' precipitation that could result from the supersaturated brines (Yuan, 1989).

3.2.1 Saturation Ratio SR

Saturation ratio, SR, is a useful quantity employed in precipitation/dissolution reaction modelling to determine the possibility of scale formation in a given aqueous solution. Consider the simple reaction between barium and sulphate to produce barite mineral (equation 3-5), multiplying the concentration of the reacting ions [Ba] and [SO_4] gives a quantity known as *ion product*.

$$Ba^{2+}(aq) + SO_4{}^{2+}(aq) \leftrightarrow BaSO_4(s) \qquad \textbf{3-5}$$

SR is the ratio of the ion product to the solubility product of the barite mineral, $K_{SP,BaSO_4}$. It is defined mathematically as shown in equation 3-6.

$$SR = \frac{[Ba][SO_4]}{K_{SP.BaSO_4}} \qquad \textbf{3-6}$$

where [Ba] and [SO_4] are the concentrations (strictly, activities) of barium and sulphate ions, respectively.

With the value obtained from equation 3-6 one could say if it is thermodynamically possible to precipitate barite mineral or not. When the SR is less than 1, the aqueous

solution is undersaturated and any solid barite present could re-dissolve into the solution. When it is equal to 1, the solution is in equilibrium with its mineral salts. However, when it is above 1, the solution is supersaturated. Mineral scaling is only possible in a supersaturated solution.

Another parameter that is often used to identify the possibility of scaling is the *saturation index SI*. SI is the logarithm of the saturation ratio. A positive SI value indicates that the solution is supersaturated.

The important thing to note is that both SR and SI are only indicators. When these parameters indicate that a solution is supersaturated, that does not mean that there must be scale formation in the system. Scales only form when the kinetics and other conditions of the flow configurations, such as residence time, are favourable.

3.2.2 Amount of Precipitation

The severity of a mineral scale problem is quantified by the amount of the scale (say in mg/L) thermodynamically possible for a given brine mixing ratio.

In an equilibrium reaction, the precipitation/re-dissolution event progresses instantly to an equilibrium state between the ions and its mineral salt. Therefore, in order to calculate the amount of scale mineral (barite in this case) that could possibly drop out in a given brine (where temperature and pressure are fixed and the ion composition is known) the first step is to determine the concentrations (activities) of the reacting ions at equilibrium. In the model developed for this work, we have adopted a simple mathematical method for deducing these equilibrium concentrations, as described by equations 3-7 and 3-8.

At equilibrium SR is 1, and as such equation 3-6 can be written as;

$$[Ba]_e.[SO_4]_e = K_{SP.BaSO4} \qquad \textbf{3-7}$$

where $[Ba]_e$ and $[SO_4]_e$ are the unknown equilibrium concentrations of barium and sulphate respectively.

Equation 3-7 presents the relation between the equilibrium concentration of sulphate, barium and the barite solubility product $K_{SP.BaSO_4}$. We maintain the actual (molar) concentration of barium and sulphate ions as [Ba] and $[SO_4]$ respectively. [Ba] and $[SO_4]$ are known since they can be measured from the analysis of the given brine. A parameter PPT is used to define the amount (in molar concentrations) of barite that will precipitate

(or dissolve) in a supersaturated (undersaturated) solution. Equation 3-7 can then be re-written in terms of PPT as below;

$$([Ba]-[PPT]).([SO_4]-[PPT]) = K_{SP.BaSO4} \qquad \textbf{3-8}$$

The quadratic equation 3-8 is solved for [PPT] which is the only unknown. This relatively simple approach has been implemented in the model to derive the possible amount of barite to precipitate or re-dissolve in the solution at any given time.

In realistic cases, barium is not necessarily the only ion in the formation water. Other ions, such as strontium and calcium, could be present to compete with barium for reaction with the sulphate ion in the seawater. This is the *common ion effect*. This phenomenon was not modelled in the study presented in this thesis. It will be an interesting area of future study to expand the model in order to accommodate this *common ion effect* and some other physico-chemical processes that are not modelled at this time.

3.3 Scale Deposition and Pore Plugging

A number of investigators have described the scale-formation mechanisms by studying the complex scaling process (Crabtree, 1999; Nancollas, 1985; Naono, 1967). For a scale to form, unstable particles of the mineral have to agglomerate out of the supersaturated solution. This formation of unstable clusters is the first step in scale formation mechanism and it is termed *homogeneous nucleation*. Homogeneous nucleation is controlled by two free energy terms relating to the release of supersaturation and the creation of crystal surfaces. These two enthalpy terms oppose each other. Details of the interaction of the opposing energy and the eventual scale nucleation have been discussed in the references stated earlier in this section.

In oilfield systems, mineral precipitation is likely to occur in the presence of external surfaces such as completion tubing, pore-walls of a reservoir formation, etc. As a result, *heterogeneous nucleation* on the external surfaces would be more likely, as the energy required to form a crystal surface homogeneously may not be attained.

Once the scale has nucleated, the crystals of the mineral continue to grow until the supersaturated solution in the system returns to equilibrium. The mechanism of scale formation has been summarised in Figure 3-2.

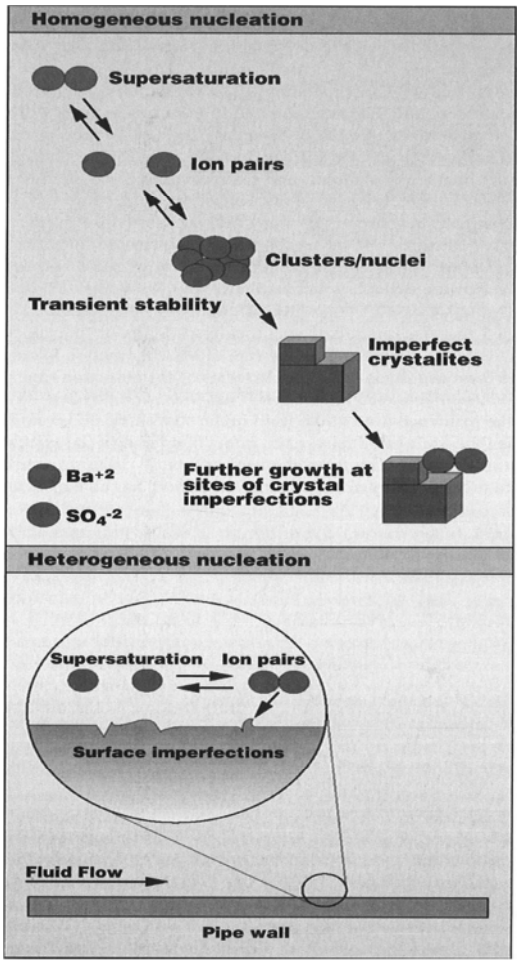

Figure 3-2 Summary of Barite Scale Formation Process (Source: Crabtree, et al, 1999, as reproduced by Frenier, W. W. and Ziauddin, M., 2008)

Consequently, deposition of unstable clusters (and the subsequent crystal growth) will lead to some form of reduction in the pore volume open to fluid flow. For the purpose of numerical calculations, the basic challenge is to ascertain (at all times) the volume occupied by the mineral adsorbing on the pore wall. In order to calculate this, a simple heterogeneous nucleation process has been implemented in the code and is being referred to in this thesis as *bond blocking*. The main assumption made in developing this bond blocking process is that the scales will evenly lodge along the entire length of the respective pore.

Below is a descriptive list of how the scale deposition is implemented in the code;

- At every time step, the network is scanned for unblocked bonds.
- For all unblocked bonds, the SR and amount of barite likely to precipitate are calculated, as described in sections 3.2.1 and 3.2.2.

- In bonds where SR is greater than 1, the precipitate coming out of the solution is assumed to deposit evenly along the length of the respective bond (see Figure 3-3).
- The volume occupied by the scale deposits is calculated using equation 3-9
- The new bond radii are calculated by taking off part of the pore volume now occupied by the scale (equation 3-10).

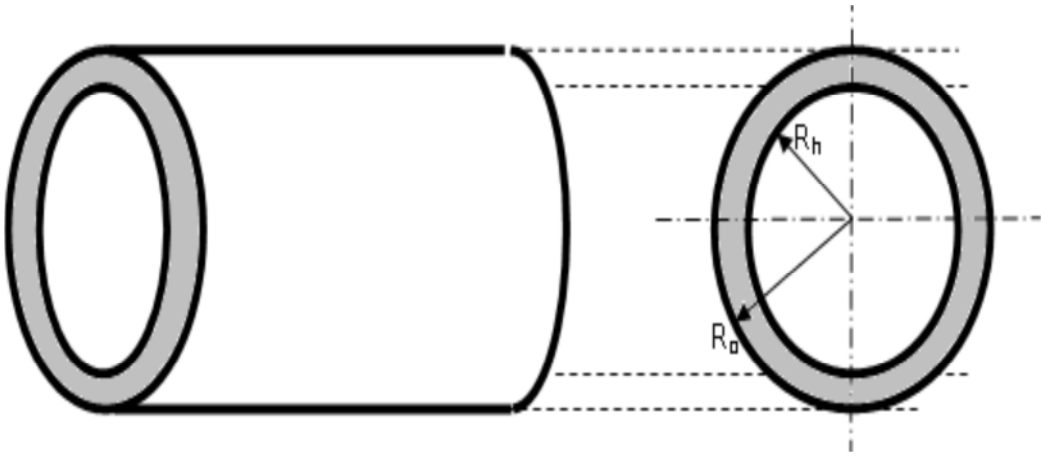

Figure 3-3: Front and side view of a bond with scale deposits. The area shaded in gray colour depicts the scale deposit. The front view shows the original and hydraulic radii (R_o and R_h, respectively)

The code keeps track of two forms of radius for each bond in the network; the original radius R_o and the hydraulic radius R_h. The original radius is the property of the bond prior to the deposition of scales on the pore walls. The hydraulic radius is the actual radius as scales keep depositing on the pore walls with time and reaction. As a result, the hydraulic radius changes as long as scale deposition is taking place in the bond.

The hydraulic radius R_h of each bond is calculated and updated after the scaling event of each time step. Assuming V_{PPT} denotes the volume of the bond occupied by the precipitating barite, Equations 3-9 and 3-10 below describe how the hydraulic radii of all bonds are derived in the code.

$$V_{PPT} = \pi R_o^2 L - \pi R_h^2 L \qquad \textbf{3-9}$$

$$R_h = \sqrt{R^2 - \frac{V_{PPT}}{\pi L}} \qquad \textbf{3-10}$$

Note that V_{PPT} can be calculated using the mathematical relation between density, mass and volume of the barite. The mass of the barite precipitate is derived from equation 3-8.

Scaling continues until the barite plugs off the bond. When a bond is plugged, all aqueous species in that bond are trapped. The flow in the bond ceases, and as such the pressure fields and flow distributions in the network have to be recalculated.

3.4 In Situ Reaction and Permeability Decline

3.4.1 Previous Work on this Area

One of the *in situ* processes that contribute to permeability reduction is particle migration. Particle mobilisation, transport, deposition and resulting formation damage have been the subject of some study for quite some years now. These studies cut across various engineering domains and the findings have been used in petroleum and environmental applications. Examples of such applications include water flooding for enhanced oil recovery and pollutant transport.

Jones (Jones, 1965) reported the reduction in permeability due to clay dispersion and expansion due to changes in water salinity. Mungan (Mungan, 1965) undertook work on permeability reduction with changes in pH and salinity. He concluded that permeability reduction is always observed when fines are entrapped, irrespective of the type of clay. Around the mid-1970s, Maly (Maly, 1976) presented a paper on how best to minimize formation damage due to fines transportation. Maly's work came at a time when formation damage due to fines migration was posing a serious challenge in the petroleum industry.

By late 1970s, Muecke (Muecke, 1979) and Almon and Davies (Almon & Davies, 1978) undertook independent studies of fines transportation. Muecke used both micro-models and sand packs to investigate the effects multiphase fluid flow has on the movement of fine particles through porous media. He reported that wettability and interfacial tension also influence fines mobility when there are multiple fluid phases present; this is because particles move preferentially in the fluid that wets them. Almon and Davies carried out an investigation into the different clays capable of causing formation damage during well stimulation. They concluded that the knowledge of smectite location, if present in a reservoir, is of importance in designing a well stimulation program.

Khilar, in 1981, conducted experiments clearly illustrating the phenomenon of formation damage due to fines movement (Khilar K. , 1981). He observed a dramatic reduction in permeability when saturated sandstone was flushed with distilled water. Khilar and Fogler (Khilar & Fogler, 1983) also observed that reversing the direction of flow leads to a

momentary recovery of the lost permeability. Thus they concluded that the migration and subsequent entrapment of fines is the mechanism responsible for the dramatic decline in the permeability. This result corroborated the findings by Mungan and by Gray and Rex (Mungan, 1965); (Gray & Rex, 1966).

The dependence of permeability reduction on salt concentration (salinity) was studied and established by Khilar and Fogler (Khilar & Fogler, 1984), following the previous works of Jones (Jones, 1965) and Mungan (Mungan, 1965). These studies concluded that there exists a critical salt concentration below which the permeability of a sandstone varies with salinity.

Gruesbeck and Collins (Gruesbeck & Collins, 1982) investigated particle entrapment and fine deposition with the use of cores and unconsolidated bead packs. They reported the existence of a critical flow velocity below which reduction in permeability was not observed. Above this critical velocity, the permeability decreases linearly with the fluid velocity. To provide further insights, Gabriel and Inamdar (Gabriel & Inamdar, 1983) conducted some experimental work using Berea sandstone cores. They established from their work that permeability reduction due to fines migration is caused by physico-chemical and mechanical effects. They concluded that damage due to fines migration *could* be mechanically induced below a critical flow velocity and chemically induced below a critical salt concentration. Thus Gabriel and Inamdar's work linked and contrasted with the studies by Khiller and Gruesbeck.

Sharma et al (Sharma & Yortsos, 1986) also investigated the dependence of fines deposition on the fluid velocity distribution within the porous medium. The rates of release and deposition were estimated using a mathematical model known as the Effective Medium Approximation (EMA). The fines entrapment and subsequent permeability reduction was modelled using population balance equations. The equations were solved analytically for several cases. The solution of the equations relates the sensitivity of fines migration to the concepts of release and capture coefficients. Sharma's work also shows that the permeability reduction is a function of the coordination number and the size of the fines particles.

In summary, we can deduce from the previous studies, as presented above, that permeability decrease results from a complex set of combined effects involving rock and fluid parameters, and that it can be linked to mobilization and entrapment of fines particles. There are two parts to the mobilization and entrapment mechanisms: one is

related to chemical effects such as overall salinity, specific ionic composition, pH and temperature; the other is related to fluid motion and associated hydrodynamic effects.

3.4.2 Models for Permeability Decline

Over the years, mathematical models have been developed to simulate decline in permeability due to *in situ* entrainment of solid particles. The early models developed were based on empirical relationships between porosity and permeability and the resulting porosity decrease by particle entrapment (Hertzig, Leclerc, & Le Goff, 1970) (Ives, 1975). Subsequently, there have been models based on Gruesbeck and Collins' and Khilar and Fogler's experimental work discussed earlier under the subheading 'Previous Work in this Area' (section 3.4). These models consider the phenomenology of particles release and capture. The limit of such models is that they require experimental inputs as adjustment parameters.

Permeability decline models based on pore network theory has been developed as well. In 1977, while studying Particles Transport in Sandstones, Donaldson et al (Donaldson & Baker, 1977) developed a statistical random walk model using Poiseuille's capillary flow equation. Solid particles are selected at random, based on the particle's size, and a probable passage through a capillary tube is solved for. If the particle passes, another particle is randomly selected. When the particle is entrained, pressure is re-calculated, and each capillary is tested for particle breakout with the new pressure. This process is continued until a plugging pressure is attained or a maximum number of particles pass through the core. In 1984, Todd et al (Todd, Somerville, & Scott, 1984) conducted studies on permeability impairment and how it impacts on water injectivity. Part of their studies involved a pore network model generated using lab-derived pore size distribution data. Impairment in permeability was simulated through reduction in pore diameters caused by the lodging of solid particles in the pore. This deposition of solid particles is determined randomly with the use of statistical functions just as in the work of Donaldson et al. Both Todd and Donaldson reported good agreement of their permeability models with experimental values. The random walk model for simulating permeability has since been modified by Rege and Fogler (Rege & Fogler, 1987); Imdakm and Sahimi (Imdakm & Sahimi, 1987); and Sahimi (Sahimi, 1994). These modifications were necessary to account for the physico-chemical and mechanical processes that lead to particle mobilization and entrapment. In the work of Sharma discussed earlier (section 3.4) (Sharma & Yortsos, 1986), the permeability decrease model was developed based on population balanced equations solved for simple homogenous media. Ochi and Vernoux

(Ochi & Vernoux, 1995) went further to develop a model that could be applied to homogenous and heterogeneous porous media.

From the above literature review, significant work has been performed on permeability reduction due to particle transport and entrapment. A handful of such investigations were conducted with the use of pore network models. However, less progress has been reported on permeability impairment resulting from *in situ* geochemical reactions. In this study, the quantitative changes in the permeability of a given porous medium after the on set of geochemical reactions are presented. The study at the moment is restricted to the reaction between barium and sulphate species and the eventual deposition of barite on the pore walls. The scaling of the pore walls is modelled using the approach described in section 3.3 (see Figure 3-3). Thereafter, the Extended Mean Radius Model developed by McDougall (McDougall S. , 1994) is used to work out the radius of the bonds in the network while calculating the permeability. This is repeated for all bonds in the network at each time step. The pore network medium therefore provides permeability as a function of time. In other words, it provides information on the extent of damage due to the scaling in the pores. Such information will be valuable in not just predicting formation damage but also in designing appropriate stimulation and/or squeeze jobs after damage has occurred.

3.4.3 The Model Set-up and Input Parameters

The pore network model was set up to model equilibrium reactions of barium and sulphate components as described in section 3.2 above. A network of 100x100 nodal dimensions was used in all the studies. A two-dimensional network was used in order easily visualise the underlying porous media structure and the flow of aqueous species. A uniform pore size distribution in the range of 10 μm to 90 μm was used to assign radius to all bonds in the network. Bond length of 333 μm was used, arbitrarily, for all the bonds in the network. In the studies the initial conditions set in the model are as follows:

1. All bonds contain brine with barium at uniform concentration.

2. Sulphate rich brine is then continuously injected from the inlet bonds (at uniform concentration) to then mix with and displaces the barium-containing brine.

The concentration levels of sulphate used were varied from 50 mg/L to 3,000 mg/L. These sulphate concentration levels represent de-sulphated and sea water concentration levels, respectively.

The actual concentration of sulphate ion in seawater varies around the world. This depends on the specific conditions of the sea water. However, raw seawater could be generically said to contain about 2,800 mg/L of sulphate. In the late 1980s, Marathon Oil and Dow Chemical Company developed membranes that could selectively remove sulphate ions from raw seawater based on nanofiltration (Marathon Oil & Dow Chemical Company). Originally, the membrane was designed to remove all but 100 mg/L of sulphate from raw seawater. This has since been improved to as low as 20-50 mg/L (Vu, Latapie, & Davis, 1999). This informs the choice of concentration values used in the studies presented in this report.

3.5 Results and Discussion

For each of the 50 mg/L and 3,000 mg/L concentration level of sulphate, the barium concentration level was increased in the magnitude of 20 mg/L to 200 mg/L to 2,000 mg/L. This gives six different scenarios as shown in Table 3-1 below.

Table 3-1: Concentration Matrix Used for Permeability Decline Study

[SO4] (in mg/L)	[Ba] (in mg/L)
50	20
	200
	2,000
3,000	20
	200
	2,000

Flow simulations were performed for each of the six different scenarios. The network was set up with initial conditions as described in Section 3.4.3 above. The changes in permeability with time and with PV through-put were investigated to understand how permeability declines with barite deposition in the pores.

Results for one of the two different sulphate concentration (and the corresponding barium concentration) are presented in Figure 3-4 below. In the figure (and for all cases) we observe a decline in permeability less than 1% of the original permeability. The result suggests that for geochemical reactions involving the displacement of formation water with sea water, the damage in permeability due to the reaction between the brines is negligible. Although there is deposition taking place on the pore walls, the amount of

barite being deposited is very low. As such the volume occupied by the scale is very small relative to the pore volume of the network model.

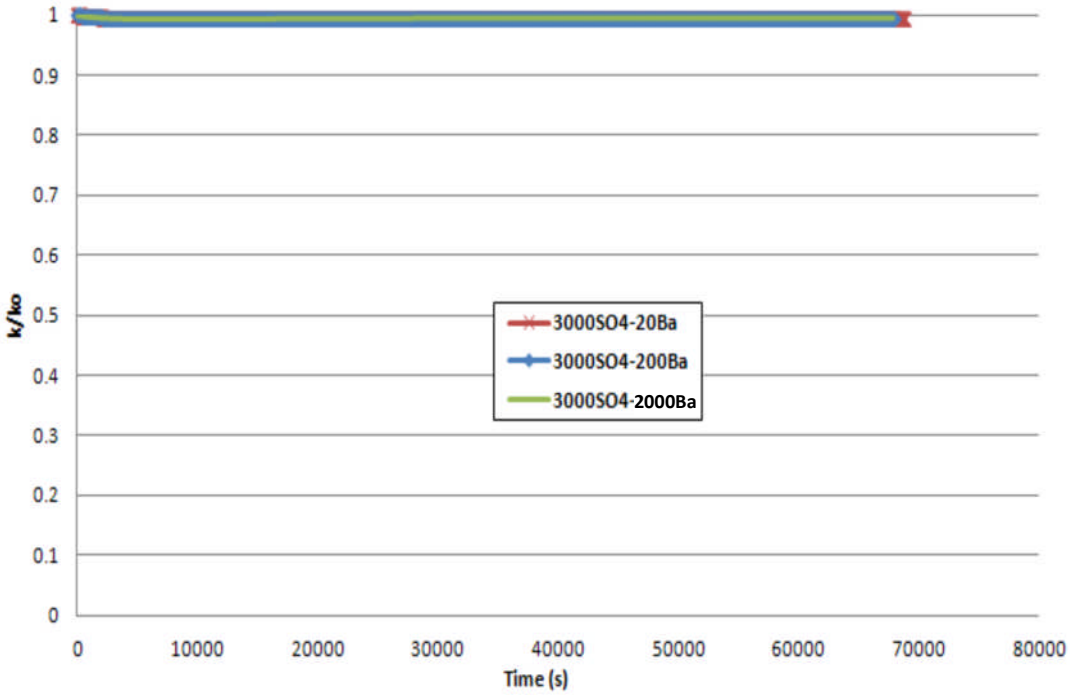

Figure 3-4 Permeability ratio against pore volume throughput for full sulphate seawater and different barium concentrations. Note that there is negligible change in permeability, even when full sulphate seawater is injected into a system containing one pore volume of barium rich brine.

It seems paradoxical that even at the high concentrations experienced in the oilfield, the displacement reaction of two incompatible brines does not necessarily result in damage to permeability. As such it was pertinent to investigate this result further analytically. We consider the worst case scenario i.e. the case involving the highest concentration levels of sulphate and barium (3000 mg/L and 2000 mg/L, respectively). We assume that at all times the two ions react instantaneously, leading to the maximum amount of barite possible being precipitated. This maximum amount is dictated by the limiting ion (which is barium in this case). Table 3-2 shows the maximum amount of barite that could possibly precipitate with time for such a reaction. The table indicates that within 1 PV throughput of injecting the sulphate-rich fluid (see the row highlighted with a red boundary), the precipitating barite constitutes less than 1% of the pore volume. This analytical calculation corroborates the results obtained from the numerical simulations.

Table 3-2: Manual Calculation Assuming Maximum Barite is Precipitated

PPT Conc (mg/L)	PPT Conc (mol/m3)	Pore Vol. (m3)	Density (kg/m3)	Molar Wt (kg/m3)	Rate (m3/s)	Time (s)	PPT Mass (kg)	PPT Vol (m3)	Vol Ratio PPT Vol/Pore Vol
3000	31.25	6.8E-10	4500	0.233	4.94E-12	1	1.54E-10	3.431E-14	5.04271E-05
						10	1.54E-09	3.431E-13	0.000504271
						20	3.09E-09	6.861E-13	0.001008542
						30	4.63E-09	1.029E-12	0.001512813
						40	6.18E-09	1.372E-12	0.002017084
						50	7.72E-09	1.715E-12	0.002521355
						60	9.26E-09	2.058E-12	0.003025626
						70	1.08E-08	2.401E-12	0.003529897
						80	1.24E-08	2.744E-12	0.004034168
						90	1.39E-08	3.088E-12	0.004538439
						100	1.54E-08	3.431E-12	0.00504271
						110	1.7E-08	3.774E-12	0.005546981
						120	1.85E-08	4.117E-12	0.006051252
						130	2.01E-08	4.46E-12	0.006555523
				Time to flow 1 Pore Vol		138	2.13E-08	4.734E-12	0.00695894
						140	2.16E-08	4.803E-12	0.007059794
						150	2.32E-08	5.146E-12	0.007564065

3.6 When Does a Pore Become Blocked?

Section 3.5 has indicated that at the concentrations usually experienced in the oilfield, geochemical reactions resulting in deposition of barite scales are insufficient to cause blocking of the pores of the reservoir rocks. That notwithstanding, it is possible to have blocking of pores due to barite scaling given different circumstances.

3.6.1 Injecting Ultra High Concentration of SO_4^{2-} to Displace Ultra High-Ba^{2+}

One of the possibilities of blocking the pores is by theoretically flooding an ultra-high concentration of sulphate to displace an ultra-high concentration of barium. In this report, unrealistically high concentrations of barium and sulphate ions (about 1000 times higher than normally observed in the oilfield) are used to demonstrate this fact.

We model a 2-D regular network with nodal dimensions of 50 by 50. The pore radius is uniformly distributed with a range of 1 μm to 100 μm. Uniform bond length of 333 μm is maintained for all pores. The pores are fully connected. All bonds in the network are filled with brine containing barium at 2,000,000 mg/L at the start of simulation. Brine containing sulphate at 3,000,000 mg/L is then injected from the inlet bonds to displace the barium rich brine. Equilibrium reaction (as described in section 3.2) is coded up to take place at each bond where, and each time when, barium and sulphate are both present (see Figure 3-5 and Figure 3-6).

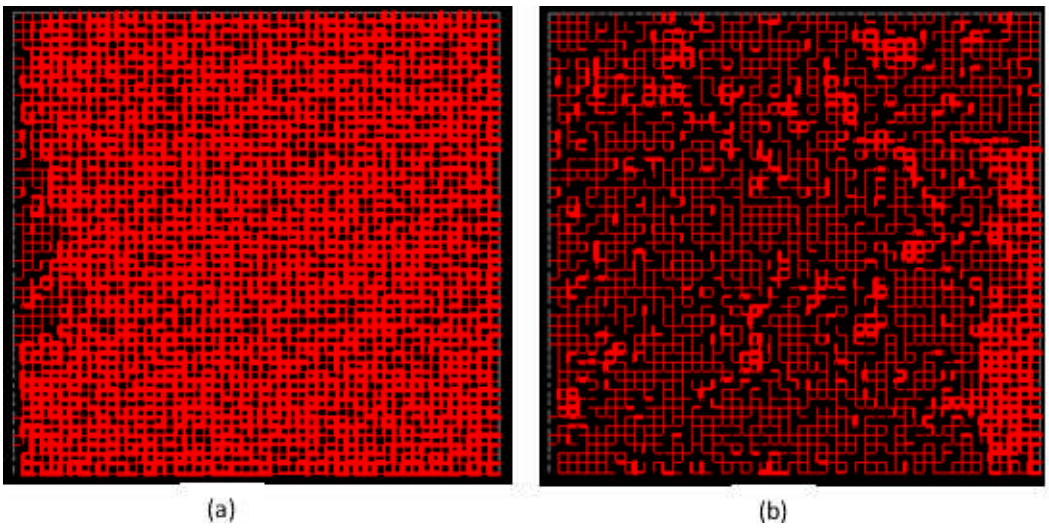

Figure 3-5: The pore network model used for Injecting Ultra-High Concentration of SO_4 to displace Ultra High concentration of Ba. (a) is at the commencement flow; (b) is at the end of flow

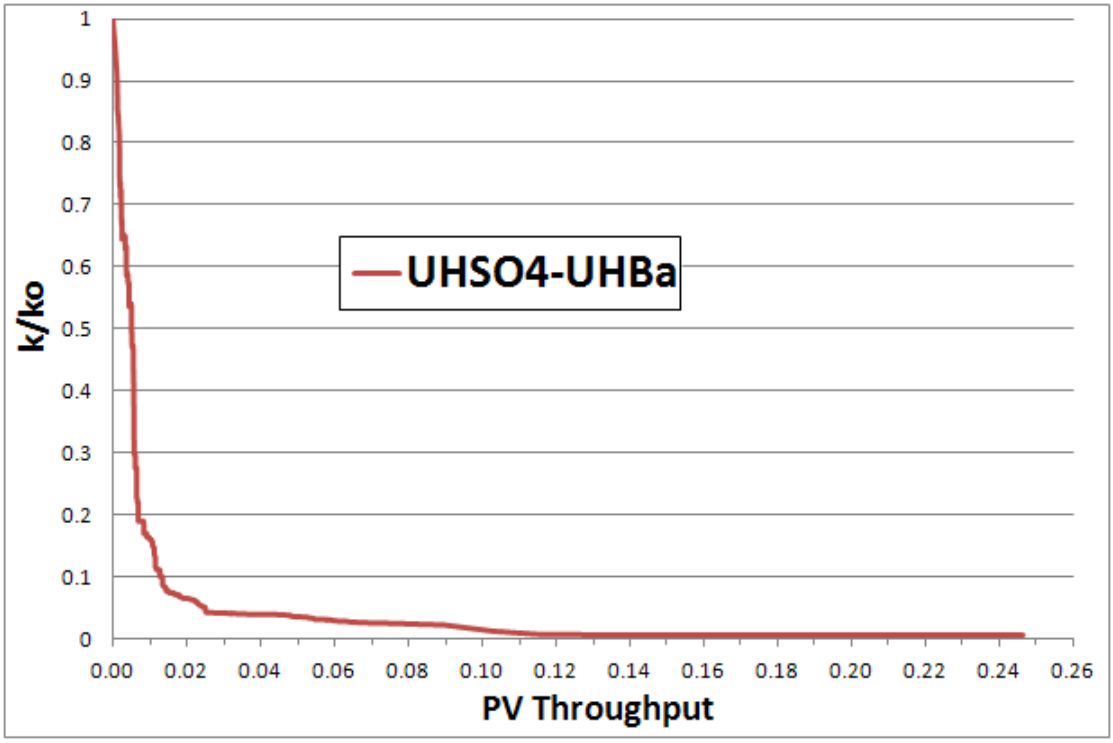

Figure 3-6: Permeability ratio against Pore Volume throughput for the case of injecting Ultra-High (UH) concentration of SO_4 to displace Ultra High (UH) Concentration of Ba

Furthermore, to understand the pattern of blocking that could be taking place in the porous medium we looked at the histogram of the pore size distribution (PSD). This is the PSD of the model described in the paragraph above. Figure 3-7 compares the PSD of the original radii before reaction, the hydraulic radii after reaction and the original radii of the

blocked bonds due to the reaction. The comparison of the original and hydraulic radii before and after reaction aids the understanding of how the radii change with the reactions. We see clearly, that with reactions, the pore radii distribution changes from uniform to something more like a truncated normal distribution. This is true because as the barite deposits on the pore walls, most of the big pores becomes smaller. This result is very interesting when we consider how scale deposition could relate to other processes such as fines migration. This result suggests that *in situ* scale deposition, when it does occur, could lead to severe fines entrapment problems due to the fact that most of the radii in the porous medium will become smaller, and there will no longer be a connected pathway of larger pores linking the inlet to the outlet of the system.

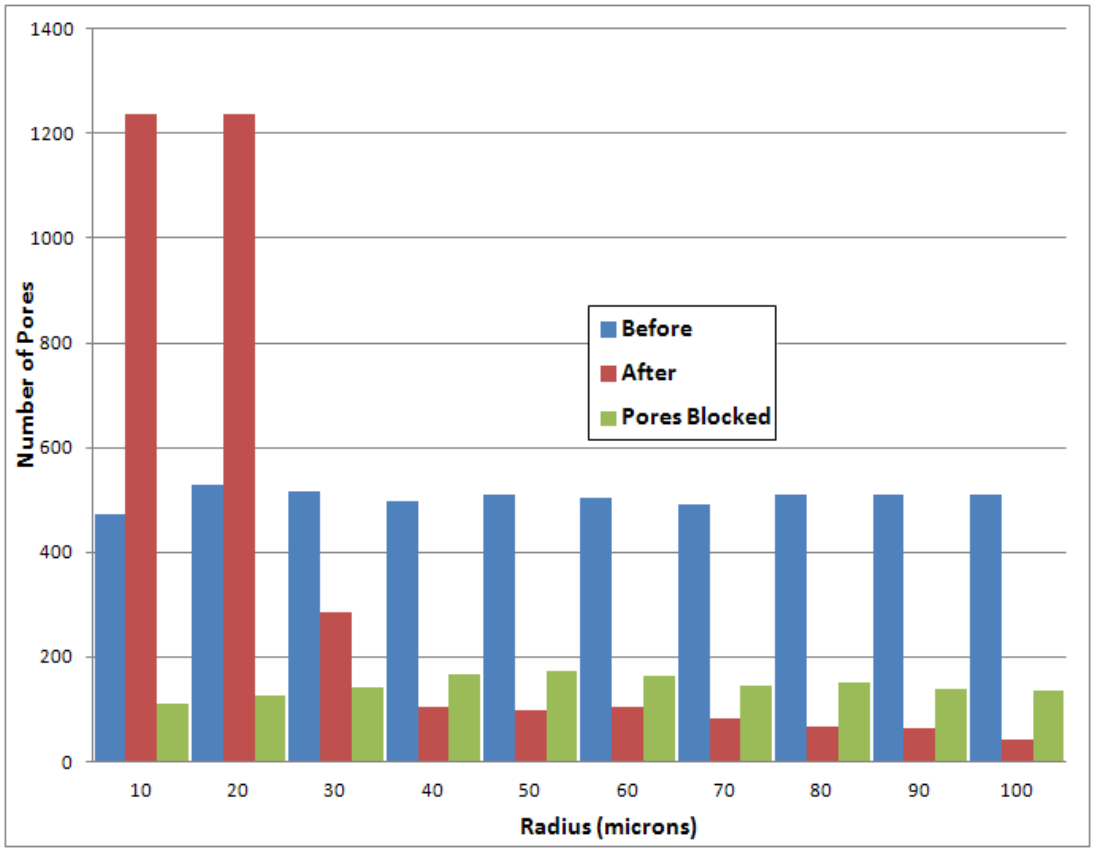

Figure 3-7 Histogram of the radii distribution before reaction (in blue); the hydraulic radii after reaction (in red) and the original radii of the blocked pores (in green)

Next, we take a closer look at the bonds that were blocked due to the barite scale deposition (i.e. the bars in green colour in Figure 3-7). To understand the order of blocking of the different sizes of the bond, the green histogram of Figure 3-7 has been re-presented in Figure 3-8. For each of the radii ranges, the bars have been divided up according to the sequence of blocking. For instance the first 200 bonds to block have been presented in blue, the second 200 in red and so on. This result suggests very interestingly

that the majority of bond blocking at the early stages does not come from the smallest pores. In fact, at each of the 200th pores that get blocked, those that come exclusively from the smallest pores are the least. The pores that have radius within the median of the distribution account for more of the blocked pores than do the largest or the smallest pores.

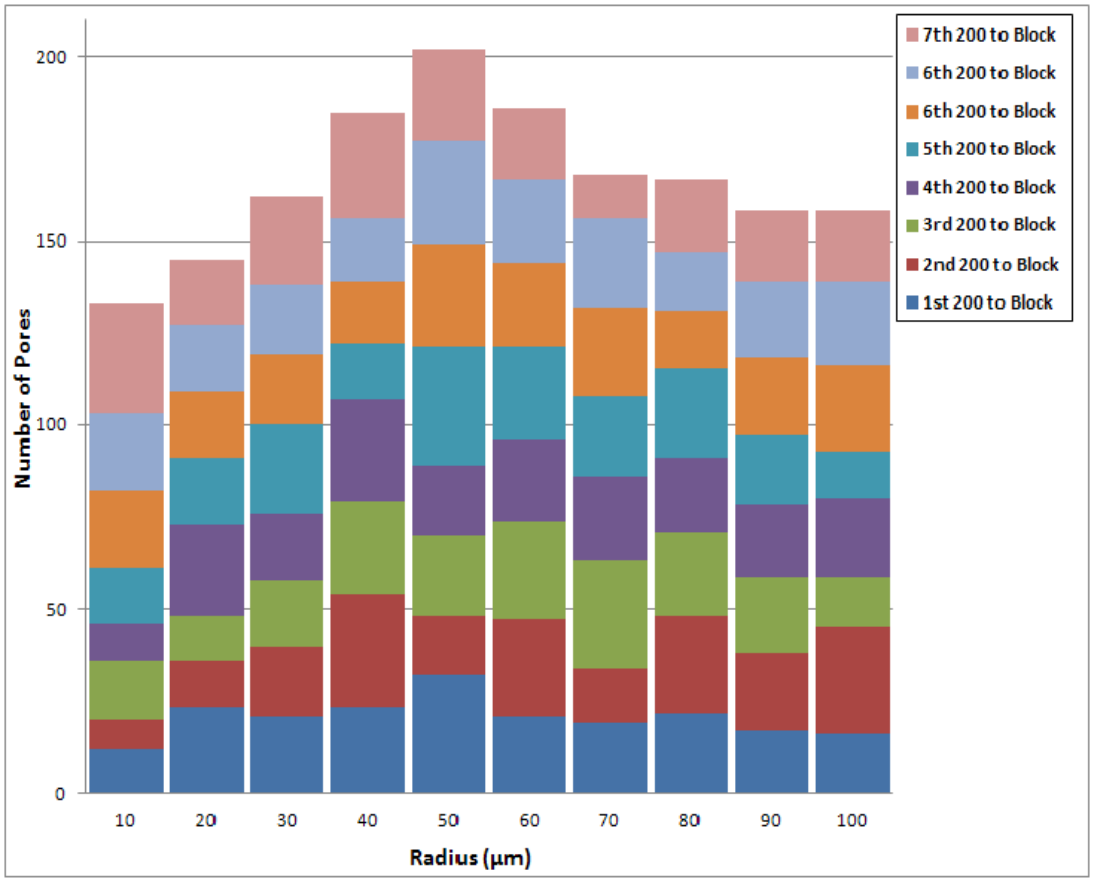

Figure 3-8 Bond blocking pattern

This suggests that the greatest amount of mixing and therefore the greatest mass of scale precipitate occurs in the median sized pores. However, the impact on the resulting effective pore size distribution is that most unblocked pores will eventually have a small hydraulic radius, and hence be very susceptible to the effects of fines migrations, and it will in fact eventually be fines that stop flow altogether, not scale.

3.6.2 Continuous Injection of 3000mg/L SO_4^{2-} and 2000mg/L Ba^{2+}

Another possibility of having blocked pores due to geochemical reaction is a scenario where there is continuous supply of sulphate and barium species. This would occur during mixed sea water injection and produced water re-injection. Here, the permeability is

observed to reduce over time and eventually the inlet pores become blocked (see Figure 3-9 and Figure 3-10).

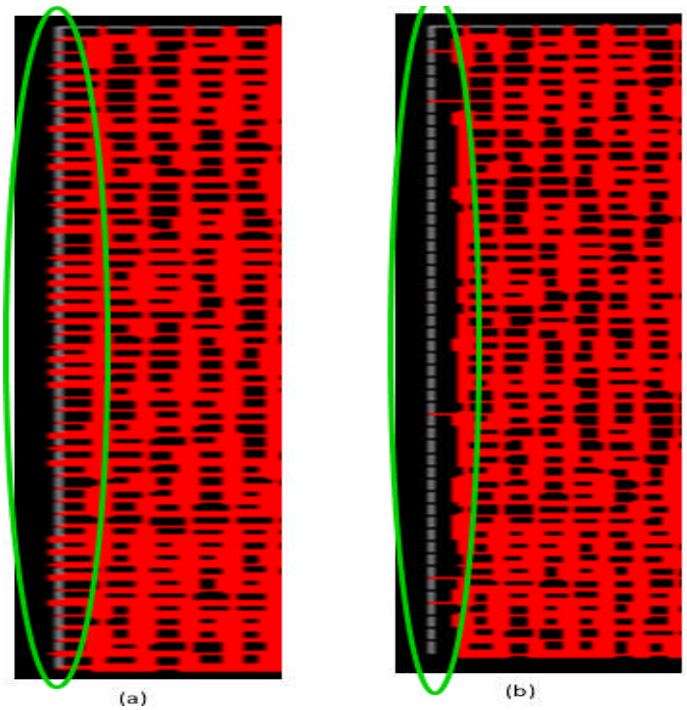

Figure 3-9: The inlet side of the pore network model used for continous injecting of SO_4 and Ba. (a) is at the commencement flow; (b) is at the end of flow (X pore volumes)

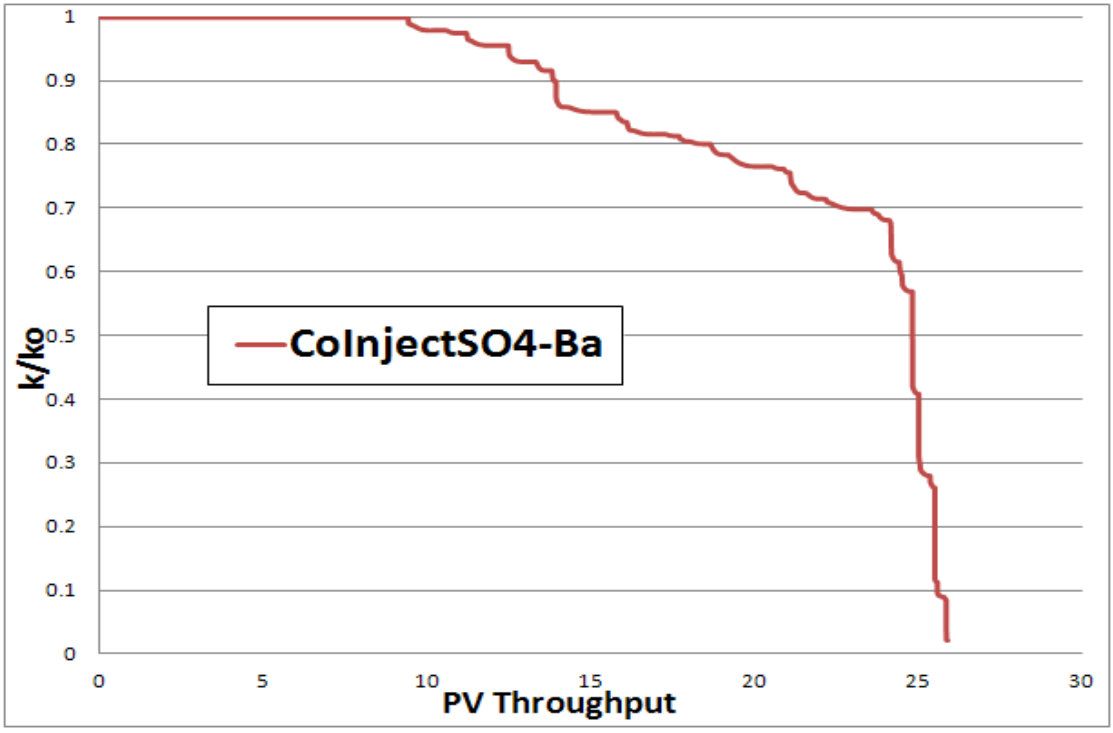

Figure 3-10: Permeability ratio against Pore Volume throughput for the case of co-injecting SO_4 and Ba

3.7 Summary and Conclusions

Pore network modelling has been used for studies of permeability impairment with scale deposition. Some of the studies have been carried out by previous researchers as pointed out in the literature review of section 3.4. In the work presented here, however, the objective is to demonstrate that the pore network model could be used as a tool for investigating geochemical reaction processes, and their impact on flow redistribution.

In all the studies presented here, a 2D regular lattice with 100x100 nodal dimensions was used. Various concentration levels were used to determine the extent of formation damage attributed solely due to *in situ* reaction of barium sulphate

Based on the results presented in section 3.5, the following conclusions could be made:

- Scale deposition due to incompatible brine mixing involving displacement of formation water with seawater does not lead to significant reduction in the permeability of the formation. The permeability damage due to *in situ* scale deposition remains less than 1% of the original permeability at all the ion concentration levels generally observed in the industry. This result is only valid when there is no trace of the barium ion present in the injection sea water.

- Findings in previous studies (see section 3.4) have indicated that permeability reduction in actual reservoir systems may be due to a combination of various processes such as fines migration and entrapment, clay mineral expansion, scale deposition etc. However, the permeability impairment contributed by the scale deposition process only is negligible.

The studies presented here have been achieved with a simple equilibrium reaction model. The actual concentration of the species, rather than the activity of the species, has been used in the reaction model. The solubility product value used in the reaction is that of barite at room temperature. Thus, the reaction model did not consider the pressure and temperature dependence of the solubility products. All these limitations notwithstanding, there is still reasonable confidence in the results obtained from this study being representative of the behaviour that occurs in the subsurface.

The reaction model of the PHREEQC geochemical software has now been linked to the network model, to perform reaction calculations in each pore at each time step, instead of the simple equilibrium reaction developed in this work. PHREEQC is a fully developed

open source code that takes into account all the variable parameters of a geochemical reaction. The results from linking the network code to PHREEQC show that reservoir permeability after damage did not decrease below 99% of the original permeability.

Furthermore, in some calculations, when both sulphate and barium ions are co-injected (the situation when co-injecting produced water and seawater), it was observed that the inlet pores become plugged with barite scale deposition after flowing over twenty pore volumes throughput. Therefore, having barium present in the injection brine could pose a threat to the reservoir formation adjacent to the injection wells. This contrasts with the results presented in this thesis where there is no barium in the injected brine, and under normal oilfield conditions no significant *in situ* permeability damage occurs. As pores begin to block due to in situ mixing, the flow rate through them decreases meaning that the mixing and delivery of scaling ions to them decreases. Thus there is a negative feedback effect which reduces the rate of overall blockage. While the overall permeability of the system declines to the point where in practical terms flow is very much restricted, the individual pores themselves do not block completely. However, in the case of mixed seawater and produced water re-injection, the mixing has already taken place upstream of the porous medium under investigation and so the extent of mixing is not affected by deposition. Hence the pore blocking is more extensive.

4 IN SITU REACTIONS AND IMPACT ON EFFLUENT CONCENTRATIONS

When barium and sulphate are co-produced, it can lead to barite deposition in the production tubing. Therefore, a flow assurance problem could arise from the scaling of the tubing. The extent of the problem depends on the amount of scale deposition taking place upstream in the reservoir. Various researchers have used different tools, such as reservoir simulators (Boak, et al., 2005); (Mackay, et al., 2006); (Daher, et al., 2005); (Bertero, et al, 1988) (Mackay, et al., 2005) and core flooding (McElhiney, et al, 2001) to investigate how *in situ* deposition impacts flow assurance.

In this thesis, we will demonstrate that the pore network model can be used as a tool for evaluating *in situ* reaction processes as well.

One of the values of pore network modelling is that it provides detailed information on species concentrations at all positions and at all times while flowing through a network system. This has been utilised extensively to provide insights on *in situ* deposition.

In the work presented here, the concentration profile, for barium and sulphate, downstream at the effluent is evaluated. This is achieved by flow-weighted averaging of the concentrations in the last column of horizontal x-pores in the network, i.e. the effluent of the system (discussed in section 2.1).

Just as we did in the permeability decline study (sections 3.4 and 3.5), here we seek to understand the extent of *in situ* reactions when displacing formation water with seawater. We have studied the cases of both raw and desulphated seawater injection. The model for *in situ* study has been set up just as was done in the permeability-decline study (see Section 3.4.3). In all the six different scenarios (see section 3.4.3), we interrogate the effluent profiles to deduce the retardation experienced by the reacting ions. In the *in situ* reaction results presented here, we have normalised the concentration of the aqueous chemical species (i.e. C/C_o). This is to allow for effective comparison among different scenarios. The value used to normalise the concentrations C_o is different for sulphate and barium. For sulphate, we normalised with the concentration value that is being injected (i.e. C_o = 3000 or 50 mg/L, as the case may be). For barium we normalised with the maximum barium concentration value in the network prior to the start of the flow simulation (see Table 3-1 in section 3.5).

We first consider the effluent profile for high sulphate (3,000 mg/L) and intermediate barium (200 mg/L) case. The effluent profile against pore volume throughput and time is presented in Figure 4-1 and Figure 4-2, respectively. In each case the profile involving reactions of the ion is presented side-by-side with that of no reaction. The obvious curve separation for barium suggests that a greater fraction of barium is consumed *in situ*. Here barium is the limiting ion; as such, more of it is consumed relative to sulphate. The less obvious separation in the sulphate curves shows that at high sulphate concentrations, where barium is the limiting ion, sulphate is not consumed to the same relative extent.

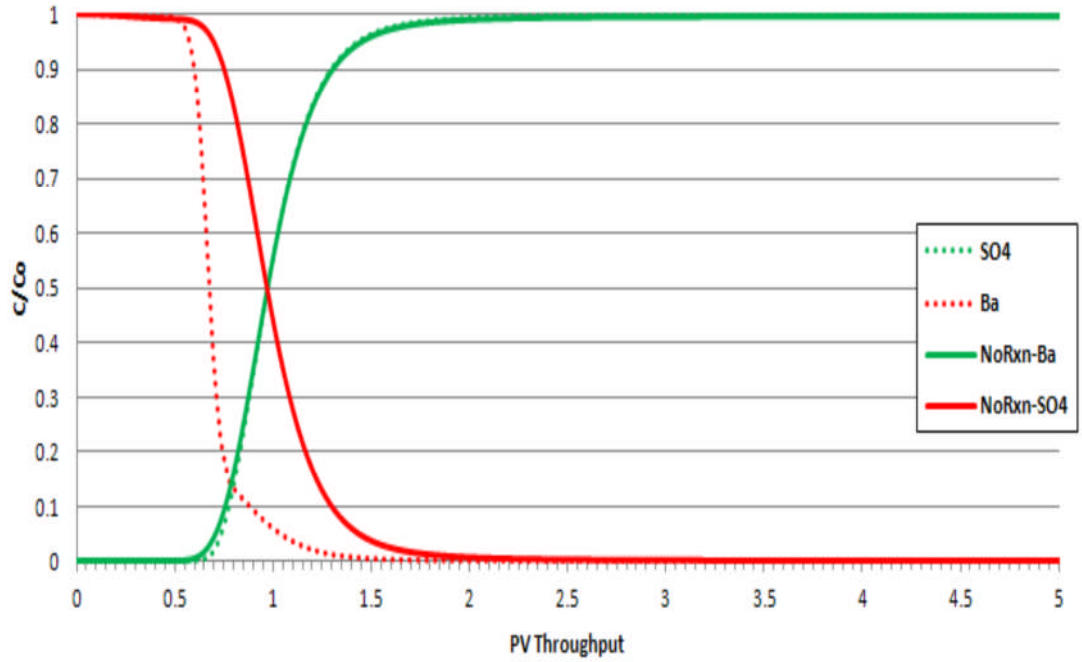

Figure 4-1 Effluent profile against pore volume throughput for 3,000 mg/L SO_4^{2-} and 200 mg/L Ba^{2+}

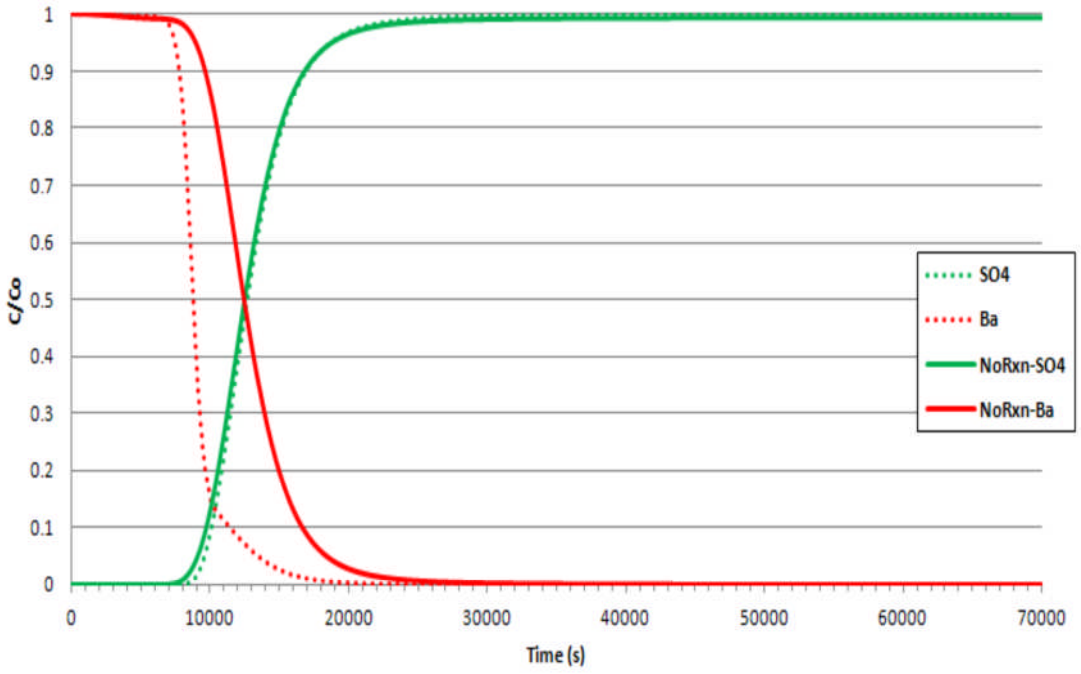

Figure 4-2 Effluent profile against time for 3,000 mg/L SO_4^{2-} and 200 mg/L Ba^{2+}

For the next case, we maintain the concentration of sulphate at 3,000 mg/L and increased the concentration of barium to 2,000 mg/L. We then analyse the effluent profile as before. The result (Figure 4-3 and Figure 4-4) shows stripping of barium and sulphate *in situ*. Sulphate break through is delayed to about 1,000s (Figure 4-4) or 0.75PV throughput (Figure 4-3). This suggests that if an adequate amount of barium is present in the formation water to react with sulphate, both ions will be consumed more or less evenly

within the reservoir. The consumption of sulphate within the reservoir will result in a further delay in breakthrough of the sulphate ions.

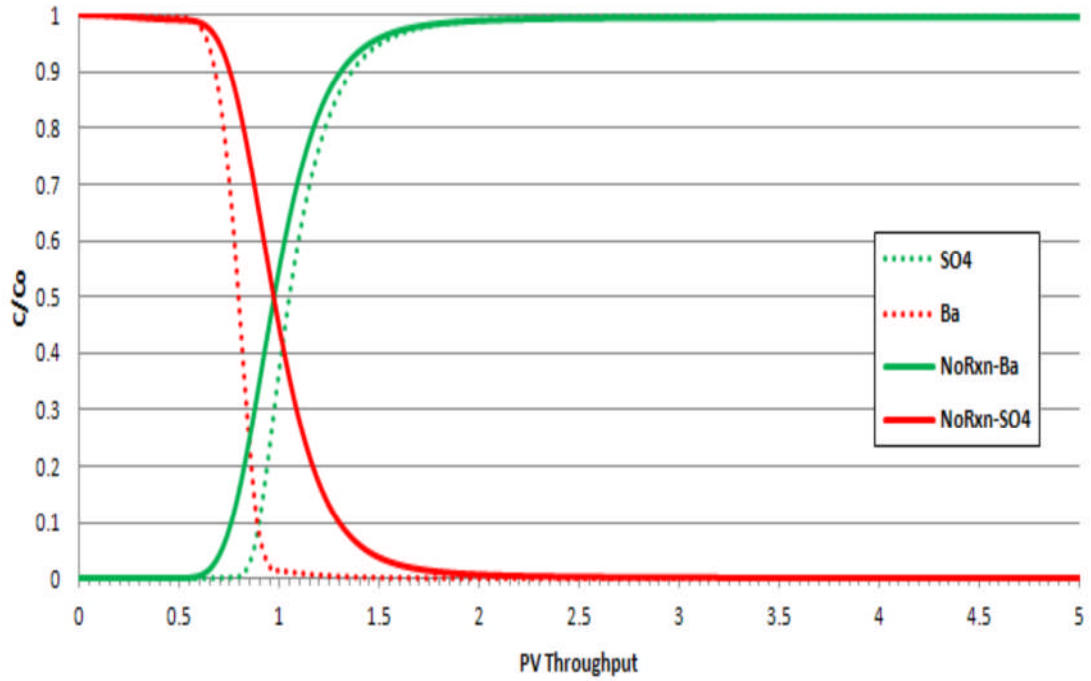

Figure 4-3 Effluent profile against pore volume throughput for 3,000 mg/L SO_4^{2-} and 2000 mg/L Ba^{2+}

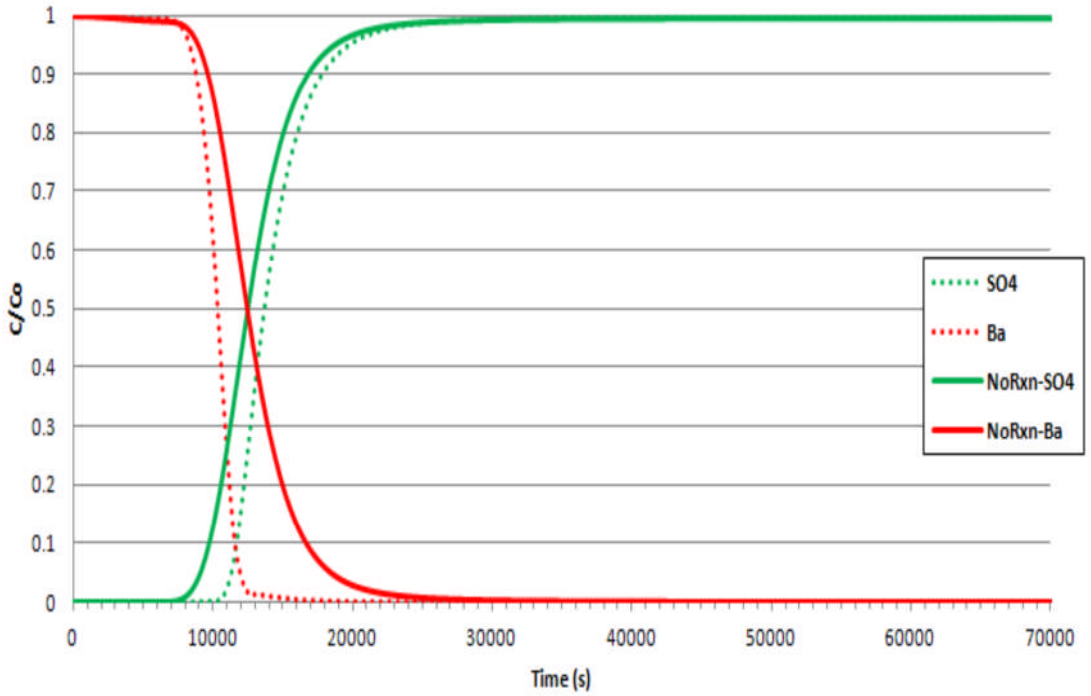

Figure 4-4 Effluent profile against time for 3,000 mg/L SO_4^{2-} and 2000 mg/L Ba^{2+}

Next, we consider the effluent profile of the de-sulphated water case at barium concentration of 200 mg/L. We observe that the sulphate breakthrough is delayed even

further to about 1,200 s or 1 PV throughput (see Figure 4-5 and Figure 4-6). This implies that the combined effects of desulphation and *in situ* reactions will result in a further delay in breakthrough of the sulphate-rich brine.

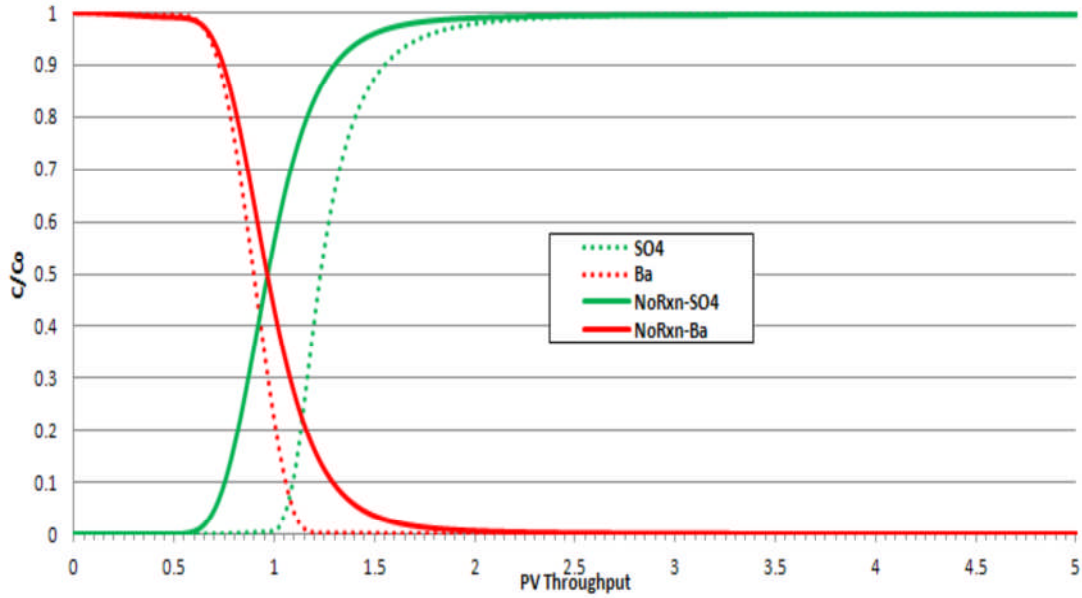

Figure 4-5 Effluent profile against pore volume throughput for 50 mg/L SO_4^{2-} and 200 mg/L Ba^{2+}

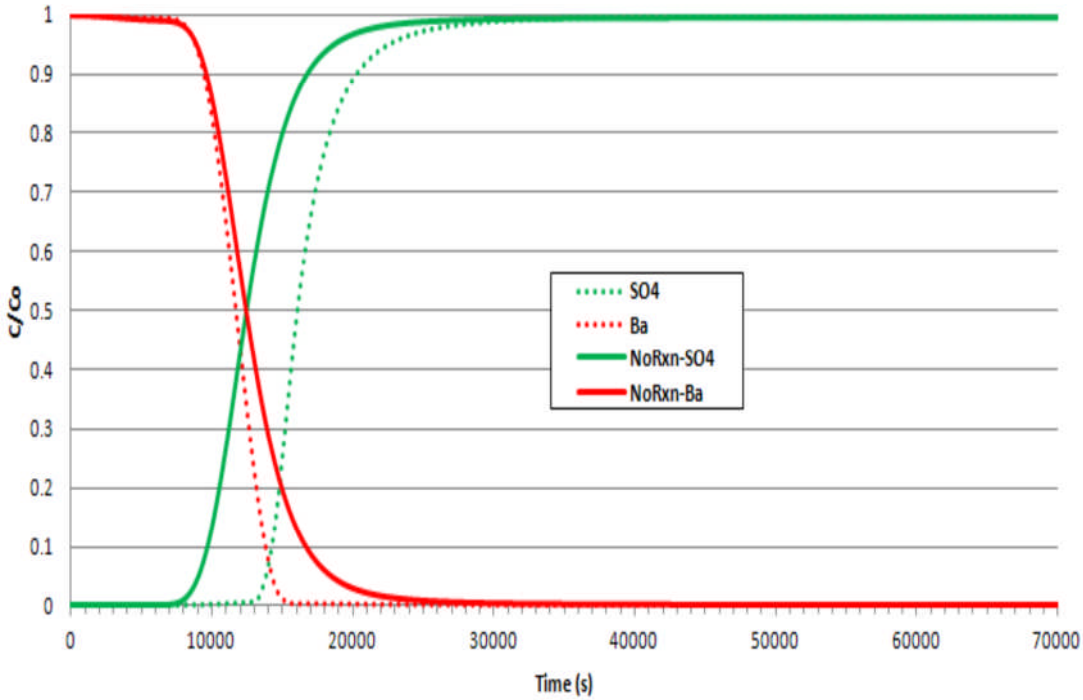

Figure 4-6 Effluent profile against time for 50 mg/L SO_4^{2-} and 200 mg/L Ba^{2+}

The delay in sulphate break through observed for desulphated brine is only possible when sufficient barium is available for *in situ* reactions. In order to demonstrate this, the

concentration of barium is reduced to 20 mg/L. The desulphated sea water injection at 50 mg/L is maintained. In this case, we observe earlier breakthrough of sulphate compared to the case of desulphated water with 200 mg/L barium (see Figure 4-7 and Figure 4-8). In other words, sea water desulphation helps reduces the severity of scaling in production tubing by retarding the breakthrough of sulphate-rich waters as well as by reducing the overall mass of sulphate available to react. However, this reduction is only effective if there is sufficient barium within the reservoir to strip these ions before the brine travels up to the tubing.

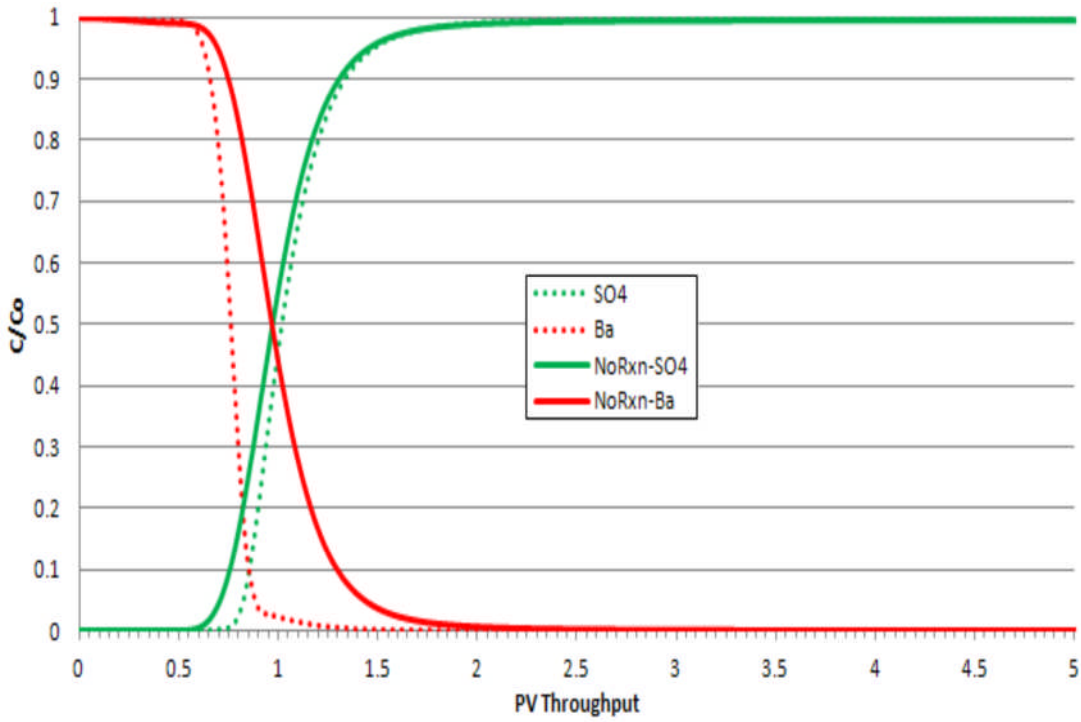

Figure 4-7 Effluent profile against pore volume throughput for 50 mg/L SO_4^{2-} and 20 mg/L Ba^{2+}

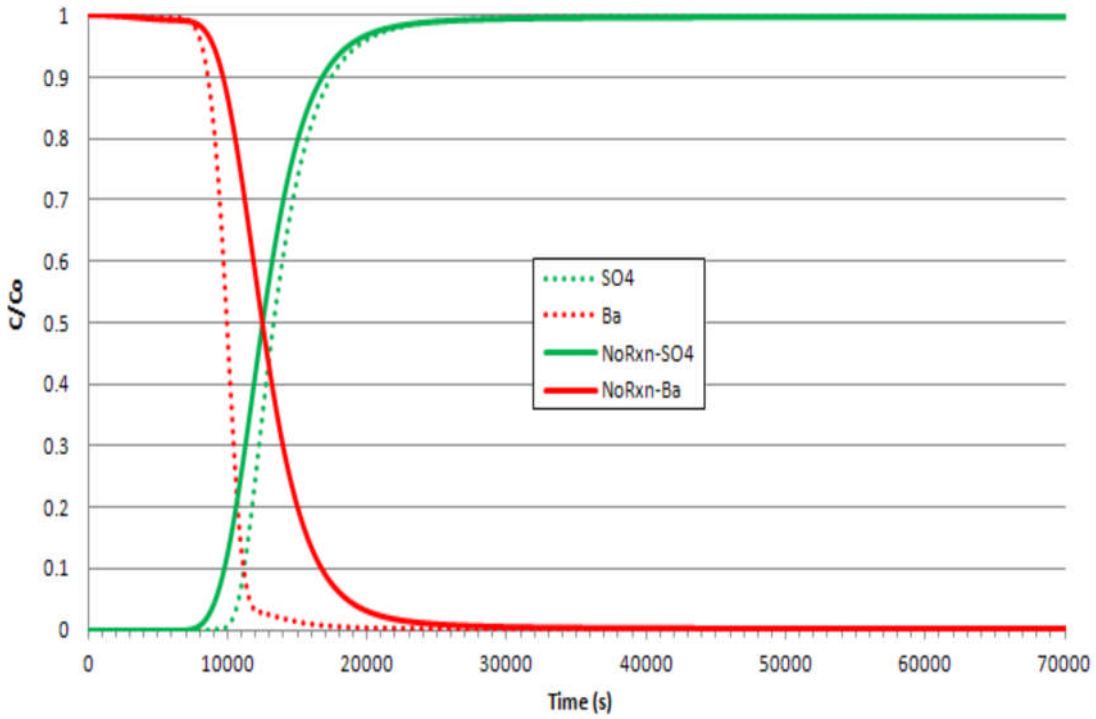

Figure 4-8 Effluent profile against time for 50 mg/L SO_4^{2-} and 20 mg/L Ba^{2+}

Thus sulphate is a poor choice of ion to identify seawater breakthrough. However, whether or not there are *in situ* reactions, the barium concentration will start to decline as soon as seawater breakthrough occurs, and so this is an excellent ion to use to detect seawater breakthrough, even if it cannot be used in isolation to *quantify* the seawater fraction.

Figure 4-9 summarises the findings in the *in situ* reaction study. The figure shows clearly that desulphation not only reduces the concentration of sulphate in the produced brine, but it also significantly delays the breakthrough of the sulphate ions relative to seawater breakthrough. This delayed breakthrough is enhanced when there is sufficient barium *in situ* to react with sulphate.

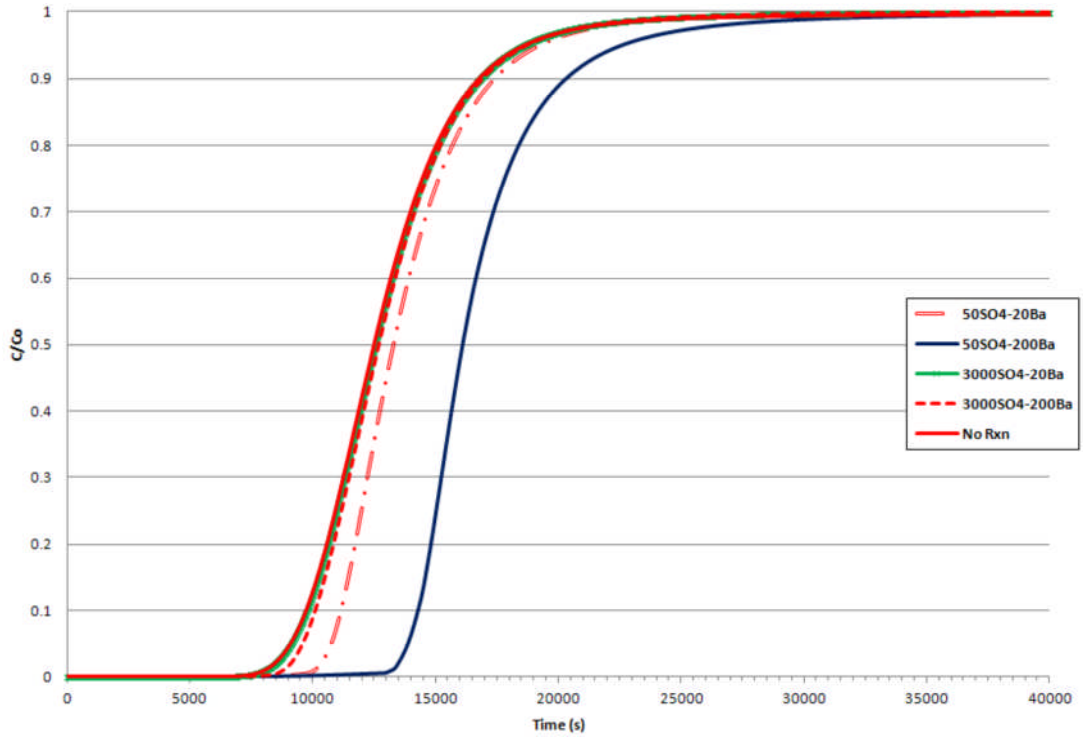

Figure 4-9 Summary on SO_4^{2-} retardation

4.1 Defining a Retardation Factor

We have demonstrated that the ions experience a delay in breakthrough due to the degree of reactions that might be taking place *in situ* (see Figure 4-9). We can infer that the retardation in the travel of the chemical species is somewhat related to the concentration of the component ions present *in situ*. In this section we seek to define a delay factor as a function of the concentration of the reacting ion concentration. The results of the *in situ* reaction studies have shown that the time of seawater breakthrough may not necessarily be the same as the time when sulphate ions break through if there is a reaction in the network. Therefore, deducing a delay factor (as a function of concentration) will be a valuable input for simulators used in modelling geochemical reactions under reservoir conditions.

Two methods have been adopted here in defining the delay factor. First, we consider the spread in the effluent concentration profiles between the cases where there is reaction and the cases of no reaction. We define different retardation factors for barium and sulphate as shown in equation 4-1 and 4-2 respectively.

$$DF_{Ba^{2+}} = NoRxnBa_{@0.5} - RxnBa_{@0.5} \quad \textbf{4-1}$$

$$DF_{SO_4^{2-}} = RxnSO_{4@0.5} - NoRxnSO_{4@0.5} \quad \textbf{4-2}$$

where $DF_{Ba^{2+}}$ and $DF_{SO_4^{2-}}$ are the delay factors of barium and sulphate ions, respectively. $NoRxnBa_{@0.5}$ and $NoRxnSO_{4@0.5}$ are the respective times taken to experience concentration values of 50% of input for barium and sulphate respectively (in a system where there *is no* reaction). $RxnBa_{@0.5}$ and $RxnSO_{4@0.5}$ are the respective time taken to experience concentration value of 50% of input for barium and sulphate respectively (in a system where there *are* reactions). Figure 4-10 below has been used to illustrate these terms

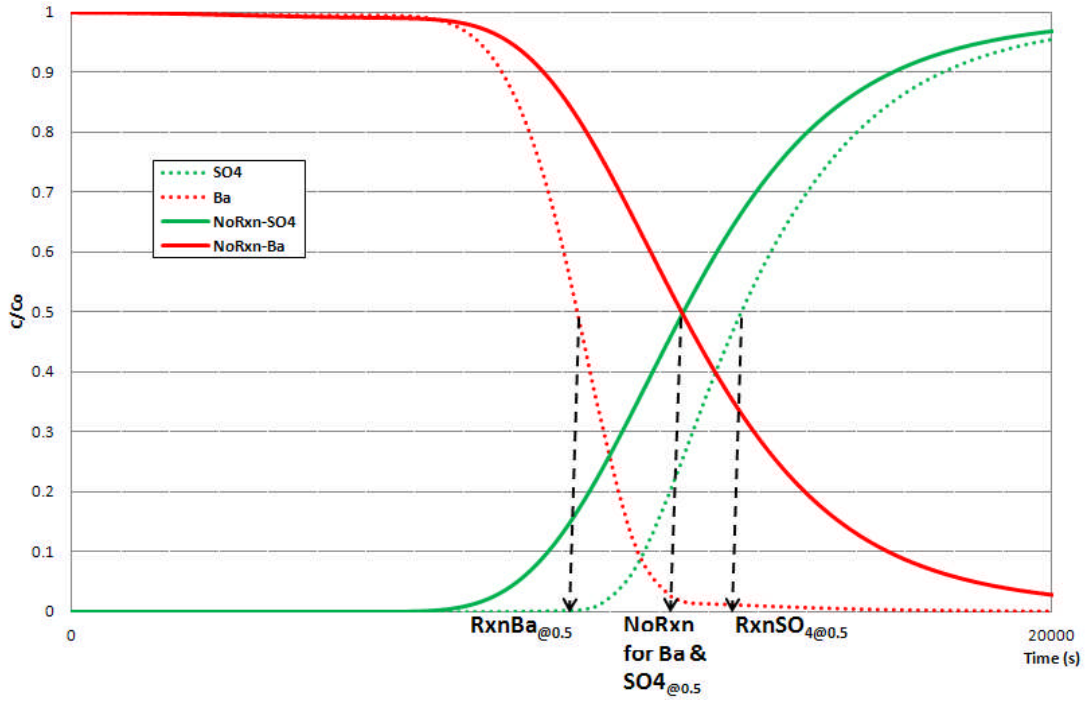

Figure 4-10 Illustrating the terms used to derive the delay factor.

Using equations 4-1 and 4-2 we derived the retardation factors for different scenarios involving displacement of barium with sulphate at different concentrations of both ions. These computed values have been plotted against the ratio of the normalised concentration of barium to normalised concentration of sulphate $[Ba]_n/[SO_4]_n$ (see Figure 4-11).

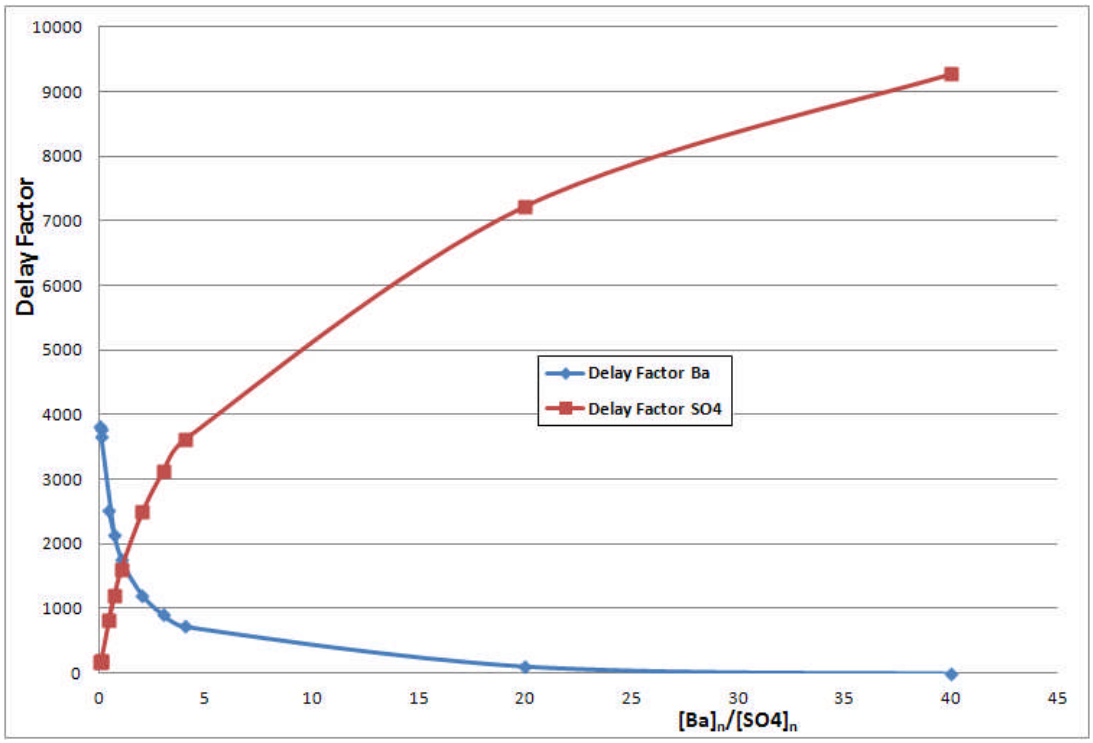

Figure 4-11 Delay factor against the normalised concentration ratio

In our second method of defining the retardation factor, we take the ratio of the terms instead of their differences. This is given in equations 4-3 and 4-4.

$$DF_{Ba^{2+}} = \frac{NoRxnBa_{@0.5}}{RxnBa_{@0.5}} \qquad \textbf{4-3}$$

$$DF_{SO_4^{2-}} = \frac{RxnSO_{4@0.5}}{NoRxnSO_{4@0.5}} \qquad \textbf{4-4}$$

where all the terms in the equations have been illustrated in Figure 4-10 and defined above.

Using Equations 4-3 and 4-4, we compute the respective delay factors of barium and sulphate as presented in Figure 4-12.

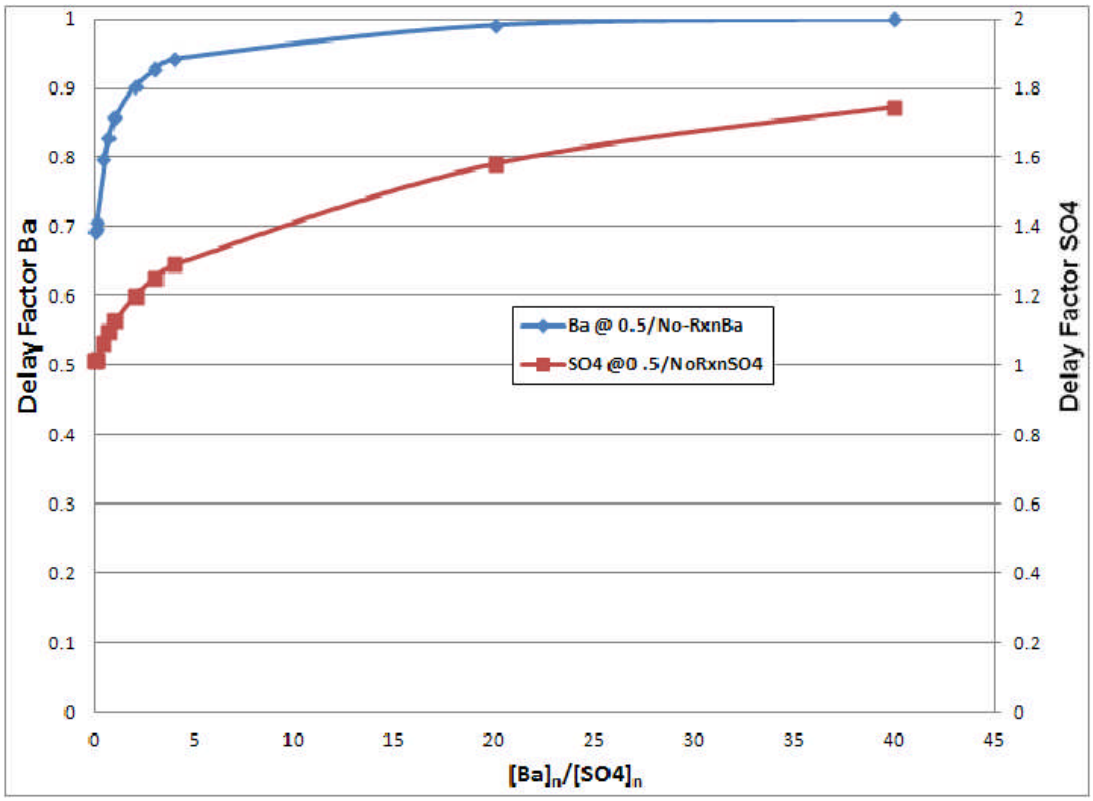

Figure 4-12 Delay factor based on equation 4-3 and 4-4

Both Figure 4-11 and Figure 4-12 indicate that as the barium concentration increases with respect to the sulphate, the barium is less retarded while the sulphate breakthrough is increasingly delayed.

4.2 Rock Properties and *In situ* Stripping

Reservoir rocks are known to have structural heterogeneity relating to pore connectivity and pore size distribution (PSD). This heterogeneity may impact on the processes of *in situ* reaction and mineral scale deposition. The extent to which they impact on *in situ* reactions has not been clearly understood. The degree of accuracy in scale prediction hinges partly on sound understanding of rock structural parameters and their corresponding controls on fluid flow.

In this section, we use a pore network model to assess the impact of rock properties (i.e. pore size distribution and pore connectivity) on *in situ* reactions. Network parameters such as coordination number and range of pore radii were used to model pore connectivity and PSD, respectively, to demonstrate the impact of reservoir heterogeneity on the scaling tendency at production wells. These two parameters are varied for different concentrations of barium and sulphate ions. We then conduct a comparative study of the

effluent profiles coming from the different cases simulated. We also analysed the saturation ratio for some of the scenarios we studied.

4.2.1 Coordination Number and Pore Size Distribution

Similar to the *in situ* reaction study presented earlier, we present a series of sensitivity calculations to ascertain the impact of network parameters (i.e. rock properties) on *in situ* stripping due to geochemical reactions. We set up the pore network to model equilibrium reactions of barium and sulphate components. A 3D network of 25x25x25 nodal dimension was used in all the cases presented in this report. In all cases also, we set the initial conditions of the model as follows:

1. All bonds contain brine rich in barium at uniform concentration.

2. Sulphate-rich brine is then continuously injected from the inlet bonds (at uniform concentration) to mix with and displace the barium-rich brine.

The concentrations of sulphate injected were varied between 50 mg/l and 3,000 mg/L. These sulphate concentrations represent de-sulphated and raw sea water concentrations respectively. For each of the 50 mg/l and 3,000 mg/l concentrations of sulphate, the barium concentration was increased from 20 mg/l to 200 mg/l to 2,000 mg/l. This gives six different scenarios, as shown in Table 3-1.

In order to assess the impact of pore connectivity, we varied a network parameter known as *coordination number* (discussed earlier in section 2.1 see Figure 2-1). A fully connected 3-D network will have a *coordination number*, z, of 6. When the value of z is less than 6 for a 3-D network, it indicates that the model is not fully connected.

In this study, we vary the coordination number from 6 to 4. For each scenario, we run the simulation using the suite of concentration values presented in Table 3-1 above.

Furthermore, pore size distribution from a real rock is extremely complicated to the point that one may wonder if there is any gain in analysing such structures with idealised geometries (such as cylindrical tubes) as is the norm in pore network modelling. However, in the bid to reconstruct the actual pore structures, the radii of the cylindrical tubes are assigned randomly from a realistic probability distribution function. This statistical distribution is defined for radius range Rmax and Rmin, and it could be likened to the fingerprints of different rock samples (see section 2.1).

In this study, we varied the minimum and maximum radii of the pore in order to assess the impact of pore size distribution.

In Table 4-1 below, we have summarized the network parameters we used in this study.

Table 4-1: Network Parameters

R_{min},R_{max} (µm)	10,90 30,70 & 49,51
Flow speed	1m/day
Nodal Dimensions	25 x 25 x 25
Bond Length (µm)	333 µm
Inlet Pressure (Pa)	1
Outlet Pressure (Pa)	0

4.2.2 Results and Discussion

In the different sensitivity scenarios, we simulate the displacement of barium-rich brine with sulphate. For each simulated case, we interrogate the effluent profile to deduce the extent of stripping taking place due to the *in situ* reactions as we vary the network parameters discussed in section 4.2.1. In order to ensure an effective comparative study among the different scenarios, we used a normalised value of the concentrations observed at the effluent (i.e. C/C_o). The value used to normalise the concentrations C_o is different for sulphate and barium. For sulphate, we normalised with the concentration value that is being injected (i.e. C_o = 3000 mg/L or 50 mg/L as the case may be). For barium we normalised with the maximum barium concentration value used to initialise the network (see Table 3-1).

4.2.2.1 Impact of Pore Connectivity and Pore Sizes on In situ Stripping

First we evaluate the impact of varying the coordination number with the R_{max} and R_{min} kept constant. The effluent profile against the pore volume throughput is presented in Figure 4-13. The figure depicts the impact of changing coordination number on network with high variance in pore sizes (i.e. R_{max} 90 µm and R_{min} 10 µm). Figure 4-13 shows that the curves for the three coordination numbers overlay each other. This suggests that in the cases with high variation in pore radii, the changes in coordination number have little or no impact on the geochemical reactions taking place *in situ*.

Figure 4-14 compares the observation for a narrow pore size distribution i.e. (R_{max} 49 µm and R_{min} 51 µm). In this case, separation of the effluent profile curves is clearly observed. The deduction that could be made here is that variation in coordination number may have some impact on the geochemical reactions taking place in the pores, if the pore sizes are homogeneous. That is to say that if the pores of a rock are about the same size, the degree of connectivity between the pores will impact the extent of incompatible brine mixing, and hence on the reactions taking place *in situ* as a result of this mixing.

The observation made here suggests that pore connectivity and pore size distribution have a combined control on the *in situ* reactions as opposed to isolated control. We observed that the extent of stripping is affected only when the two network parameters are acting together (and not acting separately).

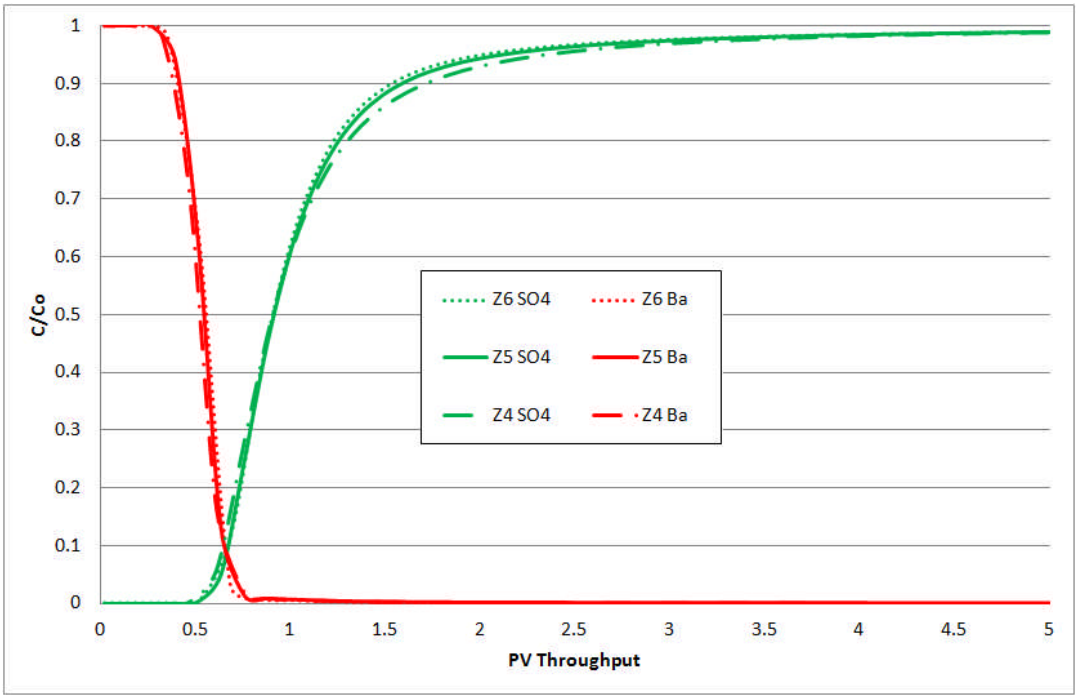

Figure 4-13 Effluent concentration profile for R_{min}, R_{max} of 10,90; 3,000 mg/l SO_4 and 2,000mg/l Ba

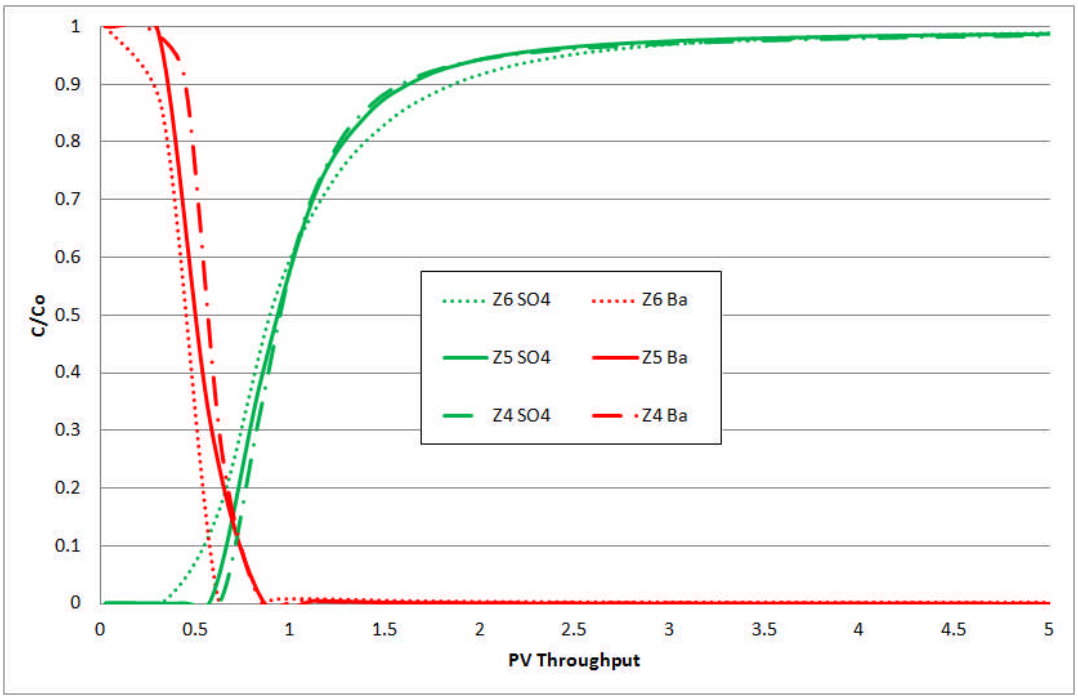

Figure 4-14 Effluent concentration profile for R_{min}, R_{max} of 49,51; 3,000 mg/l SO_4 and 2,000mg/l Ba

4.2.3 Permeability Heterogeneity and In situ Stripping

Finally, we introduce more heterogeneity into the network by creating two layers of different permeabilities (see Figure 4-15b). The upper 'high-permeability' layer consists of uniformly distributed bond radii with R_{min} and R_{max} of 50 µm to 90 µm. The bottom lower-perm layer consists of bond radii in the range of 10 µm to 50 µm. Thus, the entire network actually has a range of pore radii distribution of 10 µm to 90 µm. However, the bonds have been sorted into upper and lower parts to obtain high and low permeability layers. Just as before, we simulate the displacement of barium with sulphate (see Figure 4-16). All network parameters remain as given in Table 4-1 above.

It is evident that not only is displacement faster in the higher permeability upper layer, but there is a greater degree of mixing here, and hence of *in situ* deposition.

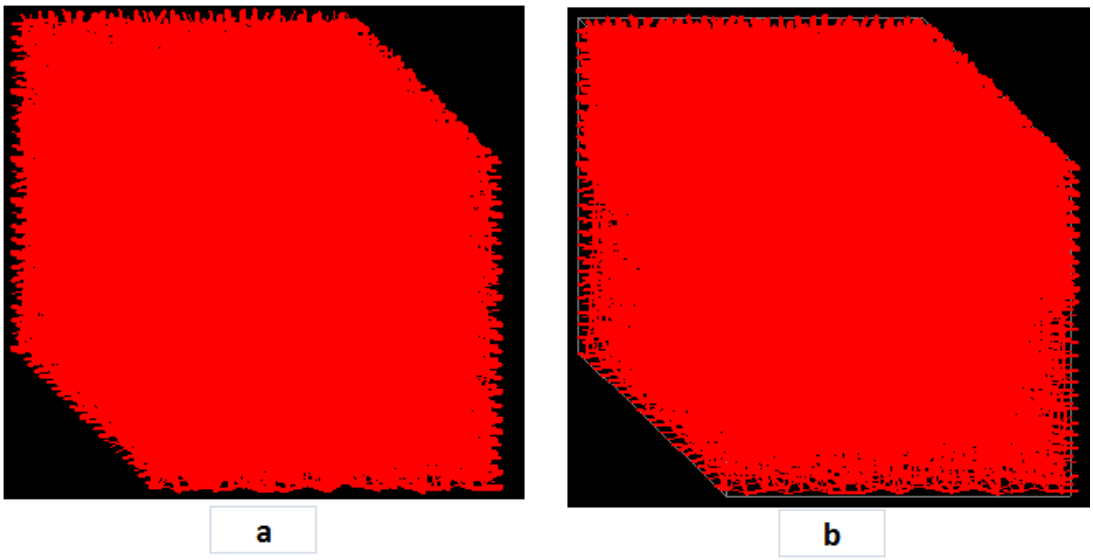

Figure 4-15 Network structure for homogeneous permeability (a) and 2-layer permeability (b) (Coordination numbers for both networks are Z=6 i.e. fully connected)

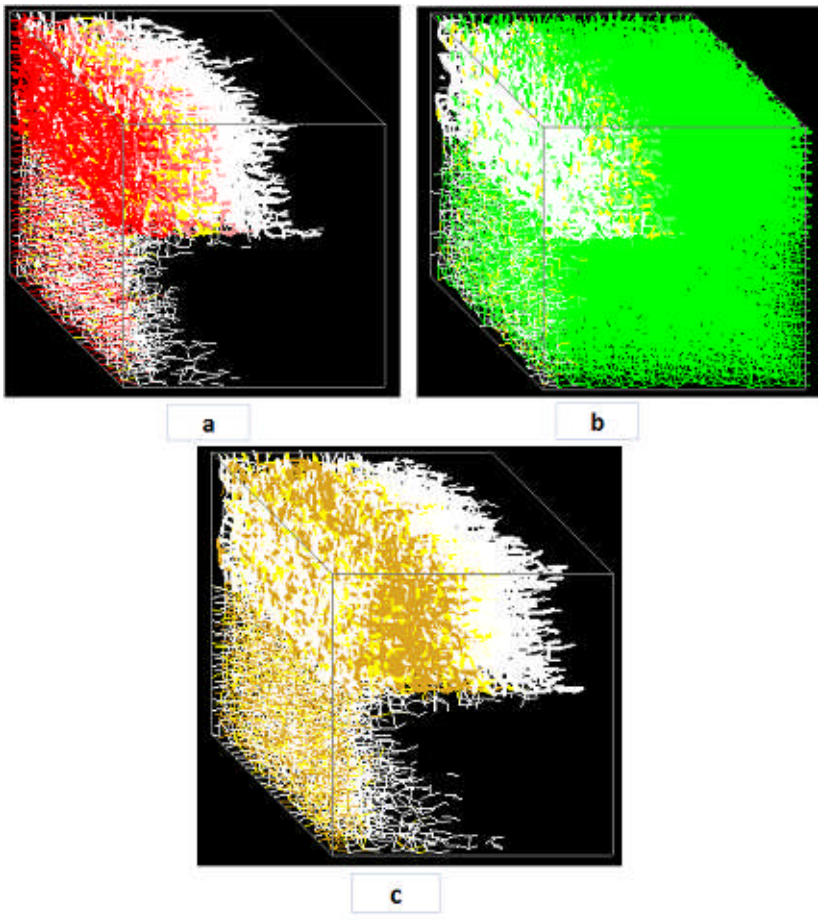

Figure 4-16 Migration of SO_4 (a); Ba (b) and $BaSO_4$ (c) for the 2-Layered Permeability Network after 0.2 PV throughput. (Coordination Z=6 and concentration are SO_4=3,000 mg/l & Ba=2,000 mg/l)

The result for the two-layer permeability is presented in Figure 4-17. The concentration observed at the effluent is similar for the three coordination numbers (i.e. Z=6, 5 and 4). As such, the curves overlay each other (Figure 4-17). This result is, at first glance, similar to that observed for the network with homogeneous permeability (Figure 4-13 above). However, we observe, in the two-permeability layer case, that barium is still being produced after 2 pore volume throughput. This is unlike the homogeneous permeability cases where there is rarely any barium produced after 1 pore volume throughput and none at all after 2 pore volume throughput (compare Figure 4-17 with Figure 4-13). This result suggests that the risk of downstream or wellbore scaling is higher in the heterogeneous network. Although the concentration of barium as observed in the layered permeability case is not very high (Figure 4-17), the risk of downstream scaling still exists nevertheless, and would need to be managed, albeit the concentrations of scale inhibitor chemical required to manage it would be low.

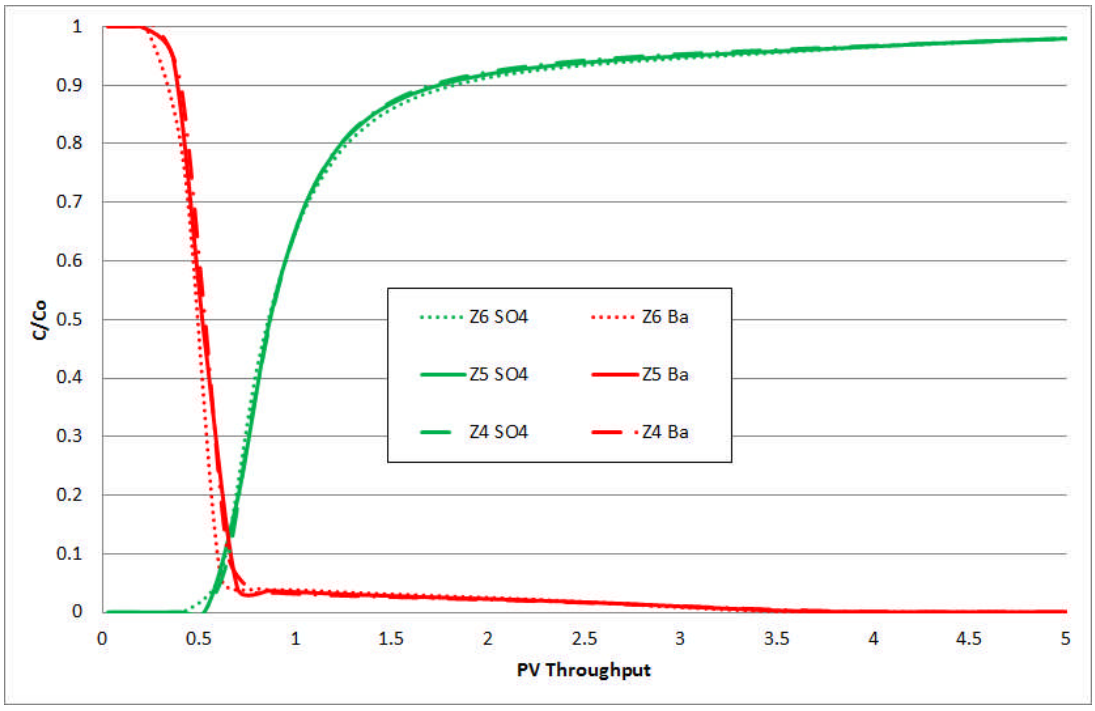

Figure 4-17 Effluent concentration profile for 2-layer permeability R_{min}, R_{max} of 10,90; 3,000 mg/l SO_4 and 2,000mg/l Ba

On comparing the saturation ratios calculated for the full mix of brines in the effluent of the single-perm layer network and the 2 layer network, we further confirm that the risk of scaling is higher for the system with heterogeneous permeability. We see in Figure 4-18 that the 2 layer network has a significantly higher SR relative to the single layer network. This indicates that not only would the scale inhibitor concentration required to prevent

damage to a production well be higher in a heterogeneous system, but that it would have to be applied for a longer period of time.

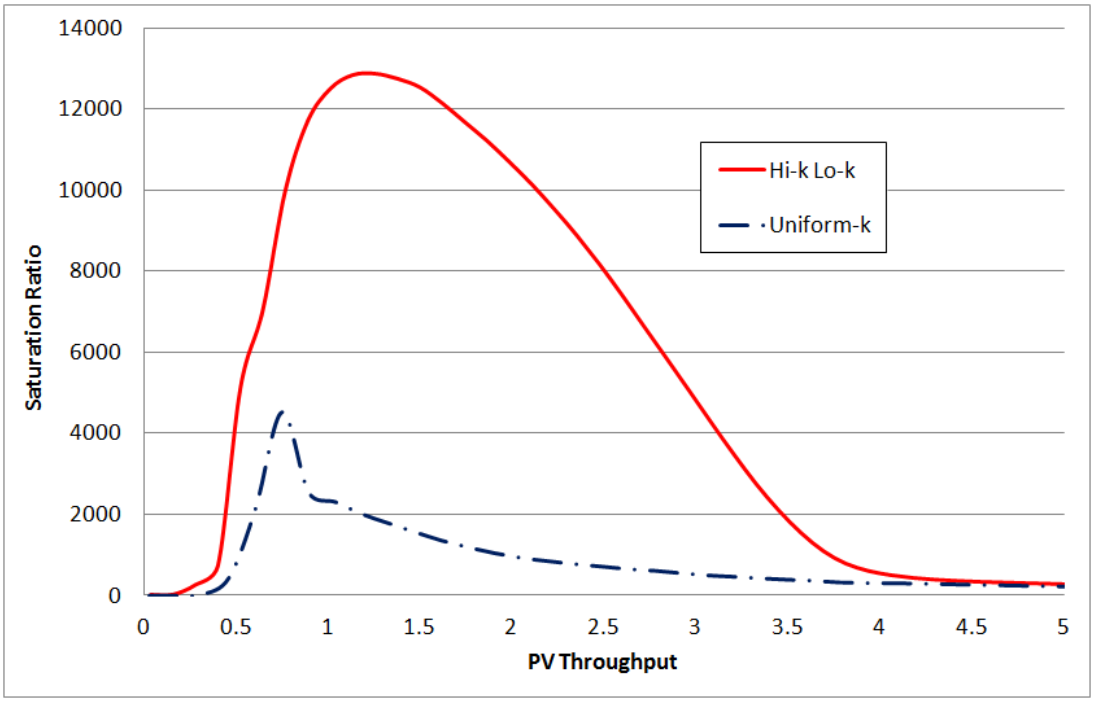

Figure 4-18 Comparing the saturation ratio in the effluent brine of the two-layer network with the homogeneous layer network (Concentration level: 3,000 mg/l SO_4 and 2,000 mg/l Ba)

Note that in the case illustrated in Figure 4-18 there are equal numbers of pores of each size, but that in the two layer system they are grouped, so that larger than average pores are in the upper half of the model, and smaller than average pores are in the lower half of the model. Also note that this example illustrates a relatively severe scaling scenario (concentration levels of 3,000 mg/l SO_4 and 2,000 mg/l Ba) which is why the Saturation Ratios are very high.

In Figure 4-19 we consider the same system, but with much lower concentrations of 50 mg/l SO_4 and 20 mg/l Ba, corresponding to injection of desulphated seawater in a lower scaling risk reservoir. Note that there is a residual scaling risk for the two layer system, which would require active scale management, but that for the homogenous case there is effectively no scaling tendency at the outlet – thorough mixing and *in situ* precipitation will have depleted most of the scaling ions.

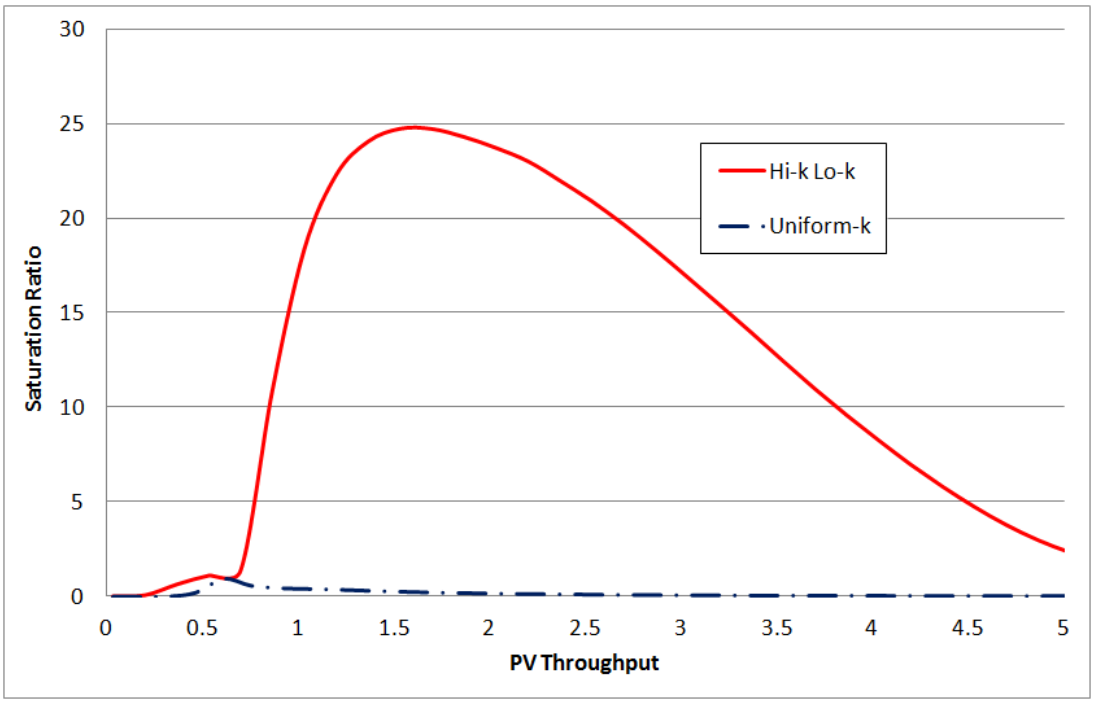

Figure 4-19 Comparing the saturation ratio in the effluent brine of the two-layer network with the homogeneous layer network (Concentration level: 50 mg/l SO_4 and 20 mg/l Ba)

4.3 Summary and Conclusions

Pore network modelling has been used to study the impact on effluent brine composition, of *in situ* reactions during mixing/displacement of incompatible brines. As mentioned in section 3.7, the objective is to demonstrate that the pore network model is a useful tool for investigating geochemical reaction processes and *in situ* stripping.

In the studies presented here, both 2D and 3D lattices were used for simulations. Various concentrations were used to ascertain the extent of retardation suffered by sulphate when it is partly consumed in reactions taking place within the reservoir.

Based on the results presented here, the following conclusions could are derived:

- For both desulphated and raw seawater injection, *in situ* reactions will lead to retardation in the breakthrough of sulphate into the production tubing provided there is a sufficient concentration of barium in the formation water in order not to limit the reaction. Indeed, the higher the formation water barium concentration, the greater the retardation.

- On comparing *in situ* reactions involving desulphated and raw seawater, desulphation of the seawater has shown to contribute to the greatest retardation in sulphate breakthrough. Hence it could be used as means of delaying or even eliminating scale formation in production tubing.

- In this chapter, we also considered the impact that coordination number has on the $BaSO_4$ scaling tendency, and identify that except for cases with very narrow pore size distributions, coordination numbers varying between 4 and 6 have little impact. Only for scenarios with a narrow pore size distribution, and hence a tendency for formation water to be stagnant in pores that are orientated at right angles to the principal flow direction, will a reduction in coordination number force more flow through these otherwise stagnant pores, and hence reduce the tendency for a delay in mixing.
- Of greater significance is the finding that a layered system will lead to longer period of coproduction of formation water (from the lower permeability layers) and injection water (from the higher permeability layers), leading to a longer period of scale risk, and greater scaling tendencies than for more homogenous systems. Thus the impact of *in situ* precipitation will be higher in layered systems, and so more chemical management will be required than in more homogeneous systems.

5 CONCLUSIONS AND RECOMMENDATIONS

5.1 Conclusions

Gaining detailed understanding of geochemical reaction *in situ* within the reservoir is partly dependent on the ability to adopt a technique that will reflect the porous network topology of the reservoir rock. Hence the use of pore-scale network models in investigating the physics and chemistry of geochemical reactions has merit. In this study, a pore-scale simulator was developed to help achieve this purpose. Sensitivity studies to validate the model were performed. Results of the study also give valuable insights on the transport of chemical species through the rock's pore spaces.

Further study of the precipitation / dissolution reaction taking place between the chemical species suggests that when one pore volume through-put is considered, the level of scale deposition is insignificant in terms of impact on permeability. Scaling due to *in situ* reaction could only lead to significant formation damage after hundreds (perhaps thousands) of pore volumes throughput have occurred. This corresponds to what occurs approaching production wells during seawater flood as flow streams converge. It also corresponds to the near injection well zone during co-injection sea water and produced water.

The literature review suggests that *in situ* formation damage and flow assurance issues are likely to be due to a combination of various processes, such as fines migration and entrapment, clay mineral expansion, scale deposition etc.

Interrogation of the effluent concentration profile shows that *in situ* reactions lead to retardation in breakthrough of sulphate ions into the production tubing. The extent of this delay is increased if the formation water contains high concentration of barium ions. Injecting desulphated water delays breakthrough of sulphate even further.

On the whole, pore-network modelling has proven to be a useful tool for studying geochemical reactions and mineral scale precipitation.

5.2 Recommendations for Future Work

The recommended areas for future work are listed below:

- In section 3.2.2 (p. 30), the precipitation-dissolution equation has been developed without accommodating the common ion effect. It will be desirable to account for common ion effects and other physico-chemical processes that are not modelled at this time.

- The bond blocking process in the model (Section 3.3) has assumed that the mineral precipitate from *in situ* reaction deposits evenly on the pore walls. In reality, scale might adhere randomly on the pore surfaces. Accounting for random scale deposition on the pores will be desirable.
- The studies presented in this thesis have been achieved with a simple equilibrium reaction model. The actual concentration of the species, rather than the activity of the species, has been used in the reaction model. The solubility product value used in the reaction is that of barite at room temperature. So the reaction model did not consider the pressure and temperature dependence of the solubility products. Extending the study to temperature and pressure dependence of solubility will also be useful.
- Scale prediction in this thesis has been restricted to $BaSO_4$. Another area for future work could be extending pore-scale prediction studies on carbonate scale.
- In addition, the studies presented in this are based on the simplest of pore size distributions; future work should consider the impact of other pore size distributions, including analytical forms such as Gaussian and Log-Normal distributions.
- An interesting future work will be to compare Darcy's scale simulations with the pore-scale simulations for the processes of geochemical reactions and mineral scale precipitations.

  In pore-scale network modelling we observe a clear delineation between the rock-matrix/grain (i.e. solids) on one hand and pores (i.e. void spaces) on the other hand (see Section 1.1 and Figure 1-1). We have also seen, in this thesis, the physico-chemical phenomena (e.g. mixing, scaling and deposition) taking place at the interface of pore-space and rock matrix. We have seen the strong effects of the local heterogeneous topologies on the flow pathways. Solving for flow at the pore scale involves direct input of pore space-rock matrix geometry. Direct Numerical Solution (DNS) may be needed when geometry/topology of the porous medium becomes complex. (Sorbie & Skauge, 2012) and (Jiang, et al., 2017) has described and demonstrated the ability to extract complex networks from high resolution digital images like CT scans.

  This approach of modelling, is of particular importance when studying natural porous media, however, it is not sustainable for larger domains. Imagine how difficult it is to extract exact pore network topology of say 50 m^3 of rock?

Darcy-scale simulation allows us to investigate (in larger domains) the physics of fluid flow through porous media. In this approach, control volumes (i.e. Representative Elementary Volumes REVs) are defined all over the domain and quantities averaged over these volumes are considered (see Figure 5-1).

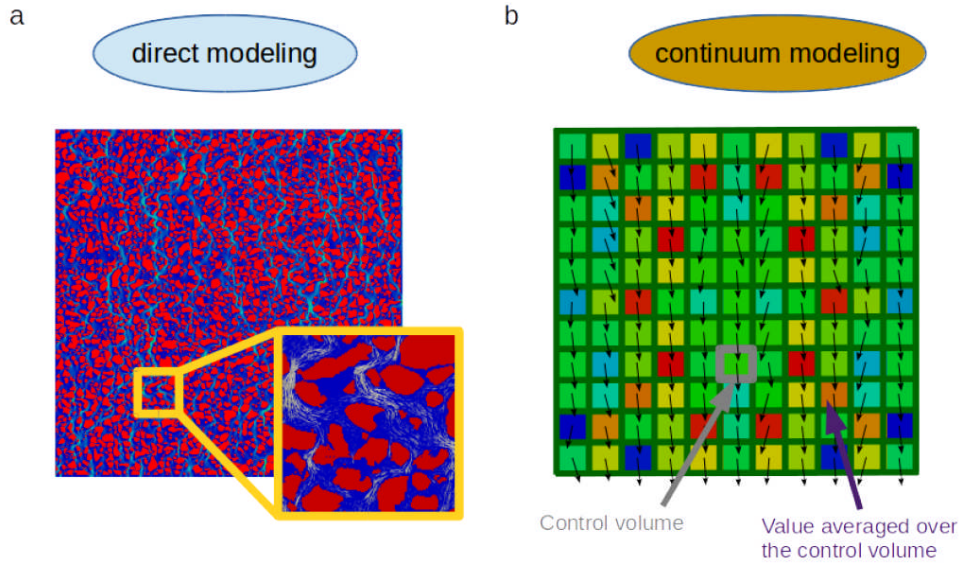

Figure 5-1: Two different representations of the physics of flow in porous media. The arrows represent the velocity vectors. (a) direct modelling or pore-scale approach where the solid is explicitly represented. (b) the continuum modelling or Darcy-scale where the physics is governed by quantities averaged over control volumes. The colour map represents the volume fraction of solid per control volume (Soulaine & Tchelepi, 2016).

The definition of the REV is a major challenge in Darcy-scale simulations. However, after the REV scale is defined, we can derive effective quantities averaged according to this control volume. In other words, the pore space-rock matrix parameters are not explicitly represented in Darcy-scale simulation. Given that the pore network structures are not explicitly represented, the fluid mechanics solution becomes invalid. Thus, in this approach, the derived averaged quantities are governed by Darcy's law.

Interesting part of the future work is to see how the results from this approach of modelling compares with that of pore-scale network modelling of geochemical processes presented in this thesis.

Ideally, these two representations of the underlying physics of flow should yield the same results (Soulaine & Tchelepi, 2016). However, both representations present some core differences in their approach. The pore-scale simulation has an explicit interface that delineates the matrix (solid) and the pore space and each distinct point of the model's domain contains either fluid or solid. On the other hand, each point of the domain in the Darcy-scale simulation contains both fluid

and solid (in the average sense). In the Darcy-scale model, the solid/fluid interfacial information is embedded in the derived effective properties.

- The impact of including an oil phase on mixing behaviours and flow redistribution would make an interesting study. With multi-phase condition existing *in-situ*, the concept of relative permeability and wettability could have significant effect on the rate of mixing and by extent on the amount of scaling taking place.

  There has been lot of activities in Pore Network Modelling (PNM) of two-phase (and even three-phase) flow phenomena in porous media. Evidence in literature shows great progress has been made in the application of PNM in understanding pore-scale processes involving multi-phase flow. Few examples include use of PNM: to explain/analyse hysteresis and the dispersion in two-phase flow experiments (Mohanty & Salter, 1982); to study the effects of wettability and model mixed wet systems (McDougall & Sorbie, 1995) and (Blunt, 1998); to study viscous pressure gradients during heavy oil depletion (Bondino, McDougall, & Hamon, 2005); to understand buoyancy-driven migration during depressurization of oil-saturated system (Ezeuko, McDougall, Bondino, & Hamon, 2010); to predict residual oil saturation based on oil layer drainage in mixed wet systems (Ryazanov, van Dijke, & Sorbie, 2010).

  However, (Sorbie & Skauge, 2012) has pointed out the inherent challenge of multi-phase flow study using a PNM. This challenge pertains to the accurate *a priori* prediction of two-phase petrophysical quantities i.e. relative permeability (K_r), capillary pressure (P_c) and residual oil saturation (S_{or}). In the course of making this *a priori* prediction, certain parameters need to be set or choices need to be made. As a result of these interventions, the two-phase flow functions may not be accurately predicted with PNM in a meaningful manner.

  Having said that, it is important to underscore that PNM could be used for wide range of useful purpose in multiphase petrophysics. One of such purpose is the explanation of global trends in multi-phase behaviour. Hence, in the case of *in-situ* mixing and scaling of multi-phase flow configurations, it will be interesting to see how much insight we could gain when PNM is used to study, the nature of impacts, the dynamics of aging, fractional wettability, contact angle re-distributions and interfacial tension has on *in-situ* mixing, reaction and scale deposition.

- Finally it will be useful to make a comparative lab/experimental study using 2D micromodels. Furthermore, pertinent experimental data where pore size

distributions had been measured were not available for comparison. It would be useful in the future to commission such experiments with detailed rock characterisation before and after the test and measurement of pressure differentials and effluent profiles during the test. An ideal experiment could be envisaged in which the porous medium is digitally printed. This means that for a single-phase flow, the characteristics would not need to be measured but would be determined *a priori*.

REFERENCES

Almon, W. R., & Davies, D. K. (1978). Clay Technology and Well Stimulation. *Golf Coast Geological Society*, 28(Part 1).

Bertero, L., Chierici, G. L., Gottardi, G., Mesini, E., & Mormino, G. (1988). Chemical Equilibruim Models: Their Use in Simulating the Injection of Incompatible Waters. *in SPE Intl Meeting on Petroleum Engineering*, (p. SPE 14126). Beijing.

Blunt, M. J. (1998). Physically-Based Network Modelling of Multiphase Flow in Intermediate-Wet Porous Media. *Journal of Petroleum Science and Engineering 20(3-4)*, 117-125.

Boak, L., AL-Mahrouqi, J., Mackay, E. J., Inches, C. E., Sorbie, K. S., Bezerra, M. C., & Motta, R. O. (2005). What Level of Sulphate Reduction is Required to Eliminate the Need for Scale-Inhibitor Squeezing. *in SPE International Symposium on Oilfield Scale*, (p. SPE 95089). Aberdeen, UK.

Bondino, I., McDougall, S. R., & Hamon, G. (2005). Pore Network Modelling of Heavy Oil Depressurisation: a Parametric Study of Factors Affecting Critical Gas Saturation and 3-Phase Relative Permeabilities. *SPE Journal*, 196-205.

Crabtree, M. (1999). *Fighting Scale - Removal and Prevention.* Autumn: pp. 30-45.

Daher, J. S., Gomes, J. A., Rosario, F. F., Bezerra, M. C., Mackay, E. J., & Sorbie, K. S. (2005). Evaluation of Inorganic Scale Deposition in an Unconsolidated Reservoir by Numerical Simulation. *in SPE International Symposium on Oilfield Scale.* Aberdeen.

Dawe, R. A., & Zhang, Y. (1997). Kinetics of Calcium Carbonate Scaling Using Observations from Glass Micromodels. *Journal of Petroleum Science and Engineering*, pp 179-187.

Donaldson, E. C., & Baker, B. A. (1977). Particle Transport in Sandstones. *in SPE-SIME 52nd Annual Fall Technical Conference and Exhibition.* Denver.

Ezeuko, C. C., McDougall, S. R., Bondino, I., & Hamon, G. (2010). Dynamic Pore-Network Simulator for Modeling Buoyancy-Driven Migration During Depressurization of Oil-Saturated Systems. *SPE Journal*, 912-922.

Frenier, W. W., & Ziauddin, M. (2008). *Formation, Removal and Inhibition of Inorganic Scale in the Oilfield Environment.*

Gabriel, G. A., & Inamdar, G. R. (1983). An Experimental Investigation of Fines Migration in Porous Media. *in 58th SPE Annual meeting.* San Francisco, CA.

Ghaderi, M. S. (2009). Experimental and Theoretical Study of Calcium Sulphate Precipitation in Porous Media Using Glass Micromodel. *Oil and Gas Technology*, pp 489-501.

Gray, D. H., & Rex, R. (1966). Formation Damage in Sandstone Caused by Clay Dispersion and Migration. *14th National Conference on Clays and Clay Minerals*, (pp. pp 355-366).

Gruesbeck, C., & Collins, R. E. (1982). Entrainment and Deposition of Fine Particles in Porous Media. *SPEJ*, 847.

Hertzig, J. P., Leclerc, D. M., & Le Goff, P. (1970). Flow of suspensions through porous media - application to deep filtration. *Ind. Engng Chem*, 62(8): pp 127-157.

Imdakm, A. O., & Sahimi, M. (1987). Transport of large particles in flow through porous media. *Physical Rev.*, 36(11): p. 5304-5309.

Ives, K. (1975). *Capture mechanisms in filtration.* Leyden, The Netherlands: Noordhoff International.

Jiang, Z., Van Dijke, M., Geiger, S., Ma, J., Couples, G., & Li, X. (2017). Pore Network Extraction for Fractured Porous Media. *Advances in Water Resources*.

Jones, F. (1965). Influence of Chemical Composition of Water on Clay Blocking of Permeability. *Jour. Pet. Tech.*

Khilar, K. (1981). *The Water Sensitivity of Sandstones.* University of Michigan: Ann Abor.

Khilar, K. C., & Fogler, H. S. (1983). Water Sensitivity of Sandstone. *SPEJ*, 55.

Khilar, K. C., & Fogler, H. S. (1984). The Existence of Critical Salt Concentrationfor Particle Release. *J. Colloid Int. Sci.*, 101(214).

Lake, L. W. (1989). *Enhanced Oil Recovery.* Prentice Hall.

Mackay, E. J., Jordan, M. M., Feasey, N. D., Shah, D., Kumar, P., & Ali, S. A. (2005). Integrated Risk Analysis for Scale Management in Deepwater Developments. *in SPE International Symposium on Oilfield Scale*, (p. SPE 87459). Aberdeen.

Mackay, E., Sorbie, K. S., Kavle, V., Sørhaug, E., Melvin, K., Sjursæther, K., & Jordan, M. (2006). Impact of In Situ Sulphate Stripping on Scale Management in the Gyda Field. *in International Oilfield Scale Symposium*, (p. SPE 100516). Aberdeen.

Maly, G. (1976). Close attention to the smallest job details vital for minimizing formation damage.

Marathon Oil, & Dow Chemical Company. (n.d.). *Patent No. U.K.N. 2221700.* Preventing Plugging by Insoluble Salts in Hydro-Carbon Bearing Formations and Associated Wells U.S.

McDougall, S. (1994). The Application of Network Modelling Techniques to Steady- and Unsteady-State Multiphase Flow in porous Media. *in Institute of Petroleum Engineering.* Edinburgh: Heriot Watt Universit.

McDougall, S. R., & Sorbie, K. S. (1995). The Impact of Wettability on Waterflooding: Pore-Scale Simulation. *SPE Reservoir Engineering 10(3)*, 208-213.

McElhiney, J. E., Sydansk, R. D., Lintelmann, K. A., Benzel, W. M., & Davidson, K. B. (2001). Determination of In-Situ Precipitation of Barium Sulphate During Coreflooding. *in 3rd Internation Symposium on Oilfield Scale*, (p. SPE 68309). Aberdeen.

Mohanty, K. K., & Salter, S. J. (1982). Multiphase Flow in Porous Media: II. Pore-level Modeling. *SPE Annual Technical Conference and Exhibition.* New Orleans, Louisiana: SPE-11018.

Muecke, T. (1979). Formation Fines and Factors Controlling Their Movement in Porous Media. *Journal of Petroleum Technology*.

Mungan, N. (1965). Permeability Reduction through Changes in pH and Salinity.

Nancollas, G. H. (1985). Oilfield Scale - Physical Chemical Studies of its Formation and Prevention. *Chemicals in the Oil Industry*, pp 143-164.

Naono, H. (1967). The Effect of Triphosphate on the Crystallization of Strontium Sulphate. *Bull. Chem. Soc. Japan*, p. 1104.

Ochi, J., & Vernoux, J.-F. (1995). A Two-Dimensional Network Model for Simulating Permeability Decrease During Fluid Injection into Aquifers. *in Groundwater Quality: Remediation and Protection.* Prague.

Read, P. A., & Ringen, J. K. (1982). The Use of Laboratory Tests to Evaluate Scaling Problems during Water Injection. *SPE 10593, SPE Oilfield and Geothermal Chemistry Symposium.* Dallas, texas.

Rege, S. D., & Fogler, H. S. (1987). Network model for straining dominated particle entrapment in porous media. *Chetn Engng Sci*, 42(1553-1564).

Ryazanov, A. V., van Dijke, M. I., & Sorbie, K. S. (2010). Pore-network Prediction of Residual Oil Saturation Based on Oil Layer Drainage in Mixed-wet Systems. *Improved Oil Recovery Symposium.* Tulsa Oklahoma: 129919.

Sahimi, M. (1994). *Applications of Percolation Theory.* London: Taylor and Francis Limited.

Sharma, M. M., & Yortsos, Y. C. (1986). Permeability Impairment Due to Fines Migration in Sandstones. *in Seventh SPE Symposium on Formation Damage Control*, (p. SPE 14819). Lafayette, IA,.

Sorbie, K. S., & Skauge, A. (2012). Can Network Modeling Predict Two-Phase Functions. *Petrophysics (53)*, 401-409.

Soulaine, C., & Tchelepi, H. (2016). *Pore-scale Modeling and Simulation of Flow in Complex Porous Formation.* California.

Todd, A. C., Somerville, J. E., & Scott, G. (1984). The application of depth of formation damage measurements in predicting water injectivity decline. *in SPE Formation Damage Control Symposium*, (p. SPE12498). Bakersfield, USA.

Vu, V. K., Latapie, D., & Davis, R. A. (1999). Barite Scale Prevention for Elf Angola's Girassol Field Using Sulphate Removal Technology. *in Deep Offshore Technology Conference.* Stavanger, Norway.

Wang, Z., & Others. (2005). How and Why Does Scale Stick-Can the Surface Be Engineered to Decrease Scale formation and Adhesion. *SPE 94993.* Aberdeen: Paper presented at the SPE International Symposium on Oilfield Scale held in Aberdeen, UK.

Yuan, M. (1989). *Prediction of Sulphate Scaling Tendency and Investigation of Barium and Strontium Sulphate Solid Solution Scale Formation.*

Yuan, M. (1994). Sulphate scale precipitation arising from seawater injection: A Prediction Study. *Marine and Petroleum Engineering 11 (1)*, pp24-30.

Zemel, B. (1995). *Tracers in the Oilfield.* Elsevier.

Zhang, Y., & others. (2001). The Kinetics of Carbonate Scaling–Application for the Prediction of Downhole Carbonate Scaling. *Journal of Petroleum Science and Engineering*, pp85-95.